

## Geochemistry, Geophysics, Geosystems

### RESEARCH ARTICLE

10.1002/2014GC005407

**Key Points:**

- A data set of ~22,500 horizontal geodetic velocities is compiled
- Geodetic plate motions for 36 plates are estimated
- A new velocity gradient tensor field for plate boundary zones is modeled

**Supporting Information:**

- Readme
- Figures S1–S14
- Tables S1–S2

**Correspondence to:**

C. Kreemer,  
kreemer@unr.edu

**Citation:**

Kreemer, C., G. Blewitt, and E. C. Klein (2014), A geodetic plate motion and Global Strain Rate Model, *Geochem. Geophys. Geosyst.*, 15, 3849–3889, doi:10.1002/2014GC005407.

Received 9 MAY 2014

Accepted 21 AUG 2014

Accepted article online 30 AUG 2014

Published online 21 OCT 2014

### A geodetic plate motion and Global Strain Rate Model

Corné Kreemer<sup>1,2</sup>, Geoffrey Blewitt<sup>1,2</sup>, and Elliot C. Klein<sup>1,3</sup>

<sup>1</sup>Nevada Bureau of Mines and Geology, University of Nevada, Reno, Nevada, USA, <sup>2</sup>Nevada Seismological Laboratory, University of Nevada, Reno, Nevada, USA, <sup>3</sup>Now at AIR-Worldwide, Boston, Massachusetts, USA

**Abstract** We present a new global model of plate motions and strain rates in plate boundary zones constrained by horizontal geodetic velocities. This Global Strain Rate Model (GSRM v.2.1) is a vast improvement over its predecessor both in terms of amount of data input as in an increase in spatial model resolution by factor of ~2.5 in areas with dense data coverage. We determined 6739 velocities from time series of (mostly) continuous GPS measurements; i.e., by far the largest global velocity solution to date. We transformed 15,772 velocities from 233 (mostly) published studies onto our core solution to obtain 22,511 velocities in the same reference frame. Care is taken to not use velocities from stations (or time periods) that are affected by transient phenomena; i.e., this data set consists of velocities best representing the interseismic plate velocity. About 14% of the Earth is allowed to deform in 145,086 deforming grid cells (0.25° longitude by 0.2° latitude in dimension). The remainder of the Earth's surface is modeled as rigid spherical caps representing 50 tectonic plates. For 36 plates we present new GPS-derived angular velocities. For all the plates that can be compared with the most recent geologic plate motion model, we find that the difference in angular velocity is significant. The rigid-body rotations are used as boundary conditions in the strain rate calculations. The strain rate field is modeled using the Haines and Holt method, which uses splines to obtain an self-consistent interpolated velocity gradient tensor field, from which strain rates, vorticity rates, and expected velocities are derived. We also present expected faulting orientations in areas with significant vorticity, and update the no-net rotation reference frame associated with our global velocity gradient field. Finally, we present a global map of recurrence times for  $M_w=7.5$  characteristic earthquakes.

### 1. Introduction

Given the global distribution of shallow seismicity and active faulting, the classical description of plate tectonics (i.e., the motions of a set of rigid plates separated by narrow boundaries) does not hold for ~15% of the Earth's surface [Gordon and Stein, 1992]. Over the last two decades, velocities from space-geodetic data have provided direct constraints on crustal motions in those deforming zones. Based on those data, the Global Strain Rate Model (GSRM) has included velocity gradients inside the (wide) plate boundaries into a self-consistent description of the surface kinematics of the entire world [Kreemer et al., 2000, 2003; Holt et al., 2005]. The last GSRM version (v.1.2) stems from 2004 and used geodetic, geologic, and seismologic data to constrain the rigid-body rotations of 25 spherical caps (i.e., tectonic plates) and the velocity gradient tensor field between them.

Thus far, GSRM results have been used in a wide range of studies. Besides GSRM's use in numerous regional studies and in the definition of relative plate motion across plate boundaries, one strength of the GSRM has been in providing a global model of crustal motion and strain rates. The global strain rate field has been used to constrain mantle [Yoshida, 2010; Alisic et al., 2012; Ghosh and Holt, 2012] and subduction zone dynamics [Husson, 2012]; to find correlations with seismic structure [Zhu and Tromp, 2013] and attenuation [Mitchell et al., 2008]; to constrain the forces acting on the lithosphere [Ghosh et al., 2009]; and to find correlations with earthquake populations [Kreemer et al., 2002] and make subsequent forecasts [Bird et al., 2010]. The GSRM surface velocity field has been used to constrain mantle [Becker, 2006] and subduction zone dynamics [Schellart et al., 2008; Long and Silver, 2009], to find correlations with seismic structure [French et al., 2013] and anisotropy [Hammond et al., 2005; Kang and Shin, 2009; Kaviani et al., 2009; Wang et al., 2013], and to estimate surface motions relative to the subasthenospheric mantle [Kreemer, 2009]. The GSRM surface velocity field is often used in a no-net rotation (NNR) reference frame, which is constrained by the global velocity gradient field [Kreemer and Holt, 2001; Kreemer et al., 2003, 2006].

**Table 1.** Differences Between GSRM v.1.2 and v.2.1

GSRM	v.1.2 (2004)	v.2.1 (2014)
Number of velocities	5170	22,415
Number of locations	4281	18,356
Number of studies	86	233
Number of plates	25	50
Number of grid cells	22,310	145,086
Cell dimension (Lon. × Lat.)	0.6° × 0.5°	0.25° × 0.2°

Here we present an update to GSRM v.1.2. The new model, commissioned by the Global Earthquake Model (GEM) foundation is named the GEM Strain Rate Model, and version 2.1 is presented here (v.2.0 was released to GEM in 2013). The new GSRM is a large improvement on its predecessor, mostly because of the enormous increase in data. The data increase is large enough that the new model is exclusively based on the geodetic data (except for some geologic plate motion estimates), whereas the older model used Quaternary faulting information and earthquake focal mechanisms as additional constraints. The data increase is due to two reasons: (1) we benefited from the proliferation of continuous GPS (CGPS) stations around the world and analyzed all available raw data ourselves to obtain a unique consistent set of horizontal velocities, and (2) a large number of studies with geodetic velocities have been published since 2004. Table 1 lists the differences between GSRM v1.2 and v2.1. Because of GEM's need for a purely geodetic model as an objective addition to the use of faulting and seismicity data in seismic hazard studies, Quaternary faulting information and earthquake focal mechanisms were not incorporated for GSRM v2.1.

We focus here on modeling the deformation field inside plate boundary zones, not on the description of relative motions between plates in terms of relative angular velocities. Nevertheless, we do provide for the first time geodetically constrained rotations of a number of smaller plates (e.g., Shetland, micro-plates in the Ryukyu back arc) and greatly expand the number of geodetically constrained plates in a global framework. We are also able to better constrain the motion of some plates (e.g., Caribbean, Nazca) than previous geodetic plate motion models because of our much larger data set that allows for a better geometric coverage.

In order for the velocity gradient field inside the plate boundaries to be self-consistent with the rigid plate motions, our description of plate motion can differ from recent studies [Kogan and Steblow, 2008; Argus *et al.*, 2010; Altamimi *et al.*, 2012]. Our aim is to determine plate motions that are most consistent with velocities within adjacent plate boundary zones considering the wide range effect of postseismic transients and Glacial Isostatic Adjustment (GIA). We will present and discuss the difference between our angular velocities and those of previous studies.

## 2. GPS Data Analysis

We analyzed all available GPS data (i.e., daily RINEX files) from around the world. Most data come from public online archives, but some come from archives for which we have been given specific access (see Acknowledgements). Most data come from CGPS stations, but we also analyzed data for stations for which data are recorded intermittently at a stable monument (e.g., MAGNET in Nevada, USA [Blewitt *et al.*, 2009; Hammond *et al.*, 2011], CBN network, Canada [Henton *et al.*, 2006], and Jura, France [Walpersdorf *et al.*, 2006a]). Furthermore, some data come from CGPS stations for which only data for a few days per year are available (e.g., APRGP) [Dawson *et al.*, 2004].

For the data analysis, we use the GIPSY-OASIS II software package from the Jet Propulsion Laboratory (JPL) as well as JPL's final fiducial-free GPS orbit products. Station coordinates were estimated every 24 h by applying the Precise Point Positioning method to ionospheric-free carrier phase and pseudo-range data [Zumberge *et al.*, 1997]. Data initially at the 15 or 30 s data intervals were automatically edited using the TurboEdit algorithm, and carrier phase data were decimated and pseudo-range carrier-smoothed to obtain the ionosphere-free combinations of carrier phase and pseudorange every 5 min [Blewitt, 1990]. The observable model includes (1) ocean tidal loading and companion tides [Scherneck, 1991] using the FES2004 ocean tidal model [Lyard *et al.*, 2006], (2) estimation of wet zenith troposphere and two gradient parameters every 5 min as a random walk process [Bar-Sever *et al.*, 1998] using the Global Mapping Function (GMF) [Boehm *et al.*, 2006], (3) antenna calibrations for ground receivers and satellite transmitters [Schmid *et al.*, 2007], and (4) estimation of station clocks as a white-noise process. Finally, ambiguity resolution was applied to double differences of the estimated one-way bias parameters [Blewitt, 1989], using the wide lane and phase bias (WLPB) method, which phase-connects individual stations to IGS stations in common view [Bertiger *et al.*, 2010]. Resolving ambiguities significantly reduces the scatter in mostly the east component time series.

Satellite orbit and clock parameters were provided by JPL, who determine them in a global fiducial-free analysis using a subset of the available IGS core stations as tracking sites. The fiducial-free daily GPS solutions are aligned to IGS08 [Rebischung *et al.*, 2012] by applying a daily seven-parameter Helmert transformation (three rotations, three translations, and a scale component) obtained from JPL [Bertiger *et al.*, 2010]. IGS08 is a frame that is derived from ITRF2008 [Altamimi *et al.*, 2011] and consists of 232 globally distributed IGS stations. The data processing system includes quality control, such as iterative outlier detection of the input observations, and rejecting output coordinates if the data fail to meet certain criteria such as number of unresolved cycle slips, fraction of the day spanned by the data, and formal errors.

We considered all data between 1 January 1996 and 31 December 2013, but only derive velocities from time series that are at least 2.5 years long, so as to reduce the effect of seasonal cycles on velocity biases [Blewitt and Lavallée, 2002]. In some cases, time series for (near) collocated stations are concatenated to extend their length and/or to derive a single velocity for two stations that operated consecutively. Because we are interested in capturing the “secular,” or interseismic, velocity, we exclude parts of the time series that show significant transient motion. These transients are often due to postseismic deformation or slow-slip events (where the excluded part of the time series is replaced with an offset). In the extreme, the exclusion could be for periods >10 years, sometimes at stations as far as several thousands kilometers from the largest earthquakes [Reddy *et al.*, 2010; Baek *et al.*, 2012; Shestakov *et al.*, 2012; Tregoning *et al.*, 2013]. An exception is made for stations on the Indian plate, explained in section 4.1. We list the time periods for which data are excluded in the supporting information.

Postseismic transients related to earthquakes that occurred before 1996 are not considered, with the exception of the 1960 Great Chile earthquake, in which case we simply excluded all stations (particularly from the literature, see below) that are located in the apparently affected area [Klotz *et al.*, 2001; Wang *et al.*, 2007]. If we would leave those observations in, we would create some spurious results along strike of the margin. A couple noteworthy cases that we did not consider, and for which thus a transient strain rate signal remains in the model, are: (1) the 20th century earthquakes in central Nevada, USA [Hetland and Hager, 2003; Gourmelen and Amelung, 2005; Hammond *et al.*, 2009, 2012], and (2) the 1964 great Alaskan earthquake [Zweck *et al.*, 2002; Cohen and Freymueller, 2004; Sauber *et al.*, 2006; Suito and Freymueller, 2009]. While it is possible to correct for the observations using appropriate models, we chose not to do so. For one, because that would introduce a lot of model dependencies, but also because some would argue that a significant component of most observed velocities can be explained by relaxation [Pollitz *et al.*, 2008], in which case this becomes an impossible task, at least globally.

We modeled the time series as an intersect + trend (i.e., velocity) + annual cycle + semiannual cycle + offsets. Offsets could come from equipment changes, earthquakes, or unknown reasons discovered in the analysis. A list of offsets for each station is listed in the supporting information. Some stations only have intermittent data limiting our ability to model the seasonal terms, which could bias the velocity estimate. We therefore obtain the model parameters in a damped inversion, which ensures that the amplitude of the seasonal cycles remains small in those cases where data are only available for short periods year(s) apart. The velocities uncertainties are not adopted from this inversion, because it is well known that those are too small due to the time correlation of the errors [e.g., Langbein and Johnson, 1997; Zhang *et al.*, 1997; Mao *et al.*, 1999; Santamaría-Gómez *et al.*, 2011]. Instead, we used the CATS software [Williams, 2008] to calculate velocity uncertainties under the assumption that the error model consists of flicker-noise plus white-noise [e.g., Mao *et al.*, 1999; Williams *et al.*, 2004; Amiri-Simkooei *et al.*, 2007]. We then multiplied the standard deviations with a factor of 2.0 so that the reduced  $\chi^2$  misfit for fitting rigid-body rotations to velocities on stable plates is generally closer to 1.0 per plate (Table 2). That the chosen noise-model may still underestimate the true velocity by a factor of 2 requires more study, but is in line with some recent findings. Langbein [2012] found that velocity uncertainties can be underestimated by a factor of 2 when random-walk in the time series is unaccounted for or incorrectly modeled, and this factor is also in the right ballpark of the maximum of  $0.35\text{--}0.5 \text{ mm yr}^{-1/2}$  of random walk that King and Williams [2009] found from studying short baselines. The factor of 2 increase is assumed in the remainder of the paper and in the supporting information.

Stations for which the time series indicated rapid (i.e.,  $>3 \text{ mm yr}^{-1}$ ) subsidence, unexplained transients (i.e., those not associated with postseismic deformation or slow-slip event, and/or whereby it is not clear what

**Table 2.** Euler Pole Location and Rate, Relative to Pacific, for All Rigid Plates in Model<sup>a</sup>

Latitude (°N)	Longitude (°E)	Rate (°Myr <sup>-1</sup> )	Semimajor (°)	Seminor (°)	Azi. Major (°)	Red. $\chi^2$	Plate Abbreviation	Plate Name
59.12	-73.31	0.942	0.2	0.1	103	1.1	AF	Africa
63.38	-79.90	0.943	4.6	0.4	162	0.1	AM	Amur
64.08	-83.70	0.882	0.2	0.1	131	1.3	AN	Antarctica
60.57	-45.94	1.112	2.2	0.1	72	2.6	AR	Arabia
73.53	-35.98	0.812	8.4	0.2	107	2.0	AS	Aegean Sea
60.56	3.67	1.082	0.3	0.1	72	1.0	AU	Australia
33.68	-1.67	0.037	99.4	9.0	124	4.4	BC	Baja California
34.35	-62.81	0.663	22.1	1.2	151	0.0	BG	Bering
8.89	-75.51	2.667					BU	Burma*
56.17	-81.64	0.926	1.9	0.4	163	0.3	CA	Caribbean
10.13	-45.57	0.309					CL	Caroline <sup>#</sup>
42.20	-112.80	1.676					CO	Cocos <sup>#</sup>
62.30	-10.10	1.139					CP	Capricorn <sup>#</sup>
33.99	28.71	2.716	2.3	0.1	147	2.2	DA	Danakil
28.30	66.40	11.400					EA	Easter*
61.38	-78.79	0.927	0.2	0.1	41	6.1	EU	Eurasia
9.40	79.69	5.275					GP	Galapagos*
47.06	-78.95	1.071	9.2	0.2	177	1.5	GV	Góname
61.62	-37.54	1.134	9.6	0.3	61	0.3	IN	India
-0.60	37.80	0.625					JF	Juan de Fuca <sup>#</sup>
35.91	70.17	22.520					JZ	Juan Fernandez*
60.00	-66.90	0.932					LW	Lwandle <sup>#</sup>
28.29	147.83	2.135	6.3	0.3	9	1.1	MA	Mariana
49.30	-76.01	0.791	0.1	0.1	90	25.2	NA	North America
-0.94	144.91	0.778	1.6	0.6	112	0.5	NB	North Bismarck
6.87	-168.87	3.255					NI	Niuafou <sup>*</sup>
57.36	-88.59	1.250	1.2	0.2	1	0.2	NZ	Nazca
55.47	-78.14	0.840	13.6	0.7	153	0.7	OK	Okhotsk
60.10	158.24	1.673	10.6	0.2	46	2.1	ON	Okinawa
0.00	0.00	0.000	0.0	0.0	0.0	0.3	PA	Pacific
31.26	-81.76	1.904	4.2	0.2	175	5.3	PM	Panama
48.11	-77.02	1.109	9.9	0.2	160	0.4	PR	Puerto Rico
-3.95	-41.86	0.864	0.5	0.3	23	1.6	PS	Philippine Sea
25.70	-104.80	4.966					RI	Rivera <sup>#</sup>
59.81	-70.19	0.929	27.2	0.3	81	0.1	RO	Rovuma
55.15	-83.39	0.684	0.9	0.2	144	0.5	SA	South America
11.49	-33.95	6.995	3.2	0.5	141	0.0	SB	South Bismarck
57.80	-78.00	0.755					SC	Scotia <sup>#</sup>
62.90	-39.78	1.093	8.5	0.2	87	0.4	SI	Sinai
32.53	129.60	7.194	4.3	0.1	31	0.4	SK	Sakishima
78.48	150.44	2.198	3.9	0.1	46	18.8	SL	Shetland
58.35	-80.84	0.994	1.3	0.3	61	0.8	SO	Somalia
19.53	135.02	1.478					SS	Solomon Sea*
48.65	139.00	3.052	20.6	0.3	24	6.9	ST	Satunam
59.39	-79.39	1.004	1.8	0.2	176	0.8	SU	Sunda
-3.80	-42.40	1.444					SW	Sandwich <sup>#</sup>
29.44	2.20	9.206	0.6	0.1	162	0.6	TO	Tonga
58.09	-84.24	0.971	8.2	0.3	69	1.0	VI	Victoria
17.69	134.30	1.763	10.1	0.9	147	1.9	WL	Woodlark
64.56	-82.47	0.987	2.8	0.3	164	1.4	YA	Yangtze

<sup>a</sup>All results are derived by us, except \* is from Bird [2003] and # is from DeMets et al. [2010]. For our estimates we also present error ellipse of 95% confidence interval as well as reduced  $\chi^2$  misfit.

the secular rate is), or for which the velocities were significantly different than nearby stations, were mostly excluded. We also excluded any station near volcanic activity.

In total, we derived 6739 horizontal velocities. For the strain rate modeling we removed 34 velocities for stations within 22 km of the creeping section of the San Andreas Fault. The reason for this is that the velocity profile across this fault is a step-function, which causes artifacts in the model, i.e., the spline function that we fit to the data will contain “overshoots” [Kreemer et al., 2012]. Removal of the data points close to the fault allows us to model the step-function while reducing “overshoots.” Another solution, that should be considered for a future model, is to locally decrease the size of the grid cells. We did not find other places where a combination of dense GPS coverage and creep (or shallow locking depth) caused similar overshoots.

### 3. Synthesis of Published Velocities

We included additional velocities from 233 other studies, which are mostly published (Appendix A) but includes seven unpublished studies made available through Personal Communications. The majority of geodetic velocities found in the literature is based on campaign-style measurements. In other cases, publications report velocities for CGPS stations for which data are not publicly available. A very small minority of publications also report velocities derived from non-GPS techniques, such as DORIS [Bettinelli *et al.*, 2006; Ader *et al.*, 2012; Saria *et al.*, 2013], VLBI [Shen *et al.*, 2011], or trilateration [Shen *et al.*, 2011; Weber *et al.*, 2011]. For several studies researchers supplied us with additional information such as station coordinates or velocities at nearby IGS sites. For the first time, we included a handful of velocity estimates from submarine markers, offshore Peru [Gagnon *et al.*, 2005] (used through the compilation of Chlieh *et al.* [2011]) and Japan [Tadokoro *et al.*, 2012; Sato *et al.*, 2013].

We included several studies focused exclusively on intraplate areas even though we do not solve for the strain rates there. The reason for this is that these studies could provide useful data in the future, when strain rates in plate interior will be modeled, and it would be useful to already have them in the velocity compilation. We included studies that put constraints on either the strain rates due to GIA [Mazzotti *et al.*, 2005; Lidberg *et al.*, 2010; Kierulf *et al.*, 2013] or on a known seismically active intraplate area such as the Carpathian Mountains [van der Hoeven *et al.*, 2005].

Where strain rates due to GIA coexist with tectonic strain rates, such as in southeast Alaska, and where the effects have been separated by the original studies, we include GPS velocities that have been corrected for GIA [Elliott *et al.*, 2010, 2013].

We applied the following criteria to decide whether data should be included:

a. studies were excluded when the velocity field was entirely based on publicly available data from (semi-) CGPS stations already analyzed for the core solution. Some examples since 2004 are:

[Niemi *et al.*, 2004; Prawirodirdjo and Bock, 2004; Wdowinski *et al.*, 2004; D'Agostino and Selvaggi, 2004; Hill and Blewitt, 2006; Walpersdorf *et al.*, 2006a; Calais *et al.*, 2006b; Fernandes *et al.*, 2007; Kogan and Steblow, 2008; Teferle *et al.*, 2009; Bechtold *et al.*, 2009; Argus *et al.*, 2010; Kreemer *et al.*, 2010a, 2010b; Le Pichon and Kreemer, 2010; Hammond *et al.*, 2011; Asensio *et al.*, 2012; Nocquet, 2012; ten Brink and López-Venegas, 2012; Berglund *et al.*, 2012; Malservisi *et al.*, 2013; de Lis Mancilla *et al.*, 2013; Ganis *et al.*, 2013]; Those studies all provided valuable data and interpretations, but we analyze the same stations, with typically (much) longer time series than available in those original studies.

b. if study A clearly superseded study B, then only results from study A were used. When in doubt, both were included;

c. clear outlier velocities (determined through visual inspection) were removed, including those affected by volcanic deformation;

d. results reflecting postseismic deformation were not included;

e. only velocities derived from  $\geq 2.5$  years (but sometimes just  $\geq 2$  years) time series were included;

f. any station that was also excluded from the core solution;

g. velocities for 62 stations near the creeping portion of the San Andreas Fault (see section 2.1), but only after all data are combined (see below).

Standard deviations in published velocities were occasionally increased, in particular for some earlier studies who did not account for time-correlated noise and thus gave standard deviations that could be too small by as much as an order of magnitude. If we inflated the standard deviations, we mention this in the original data files, which we have added to the supporting information.

Next, we performed one large inversion in which we solve for, and apply, a translation rate and rotation rate that transform all results into the IGS08 reference frame of our core solution. The model parameters are obtained by minimizing velocity differences at collocated sites (within  $\sim 1\text{ km}$ , short enough to avoid combining stations on opposite sides of the creeping section of the San Andreas Fault). We use the sum of squares of the standard deviations in the velocities at each collocated site to weight the inversion. We do

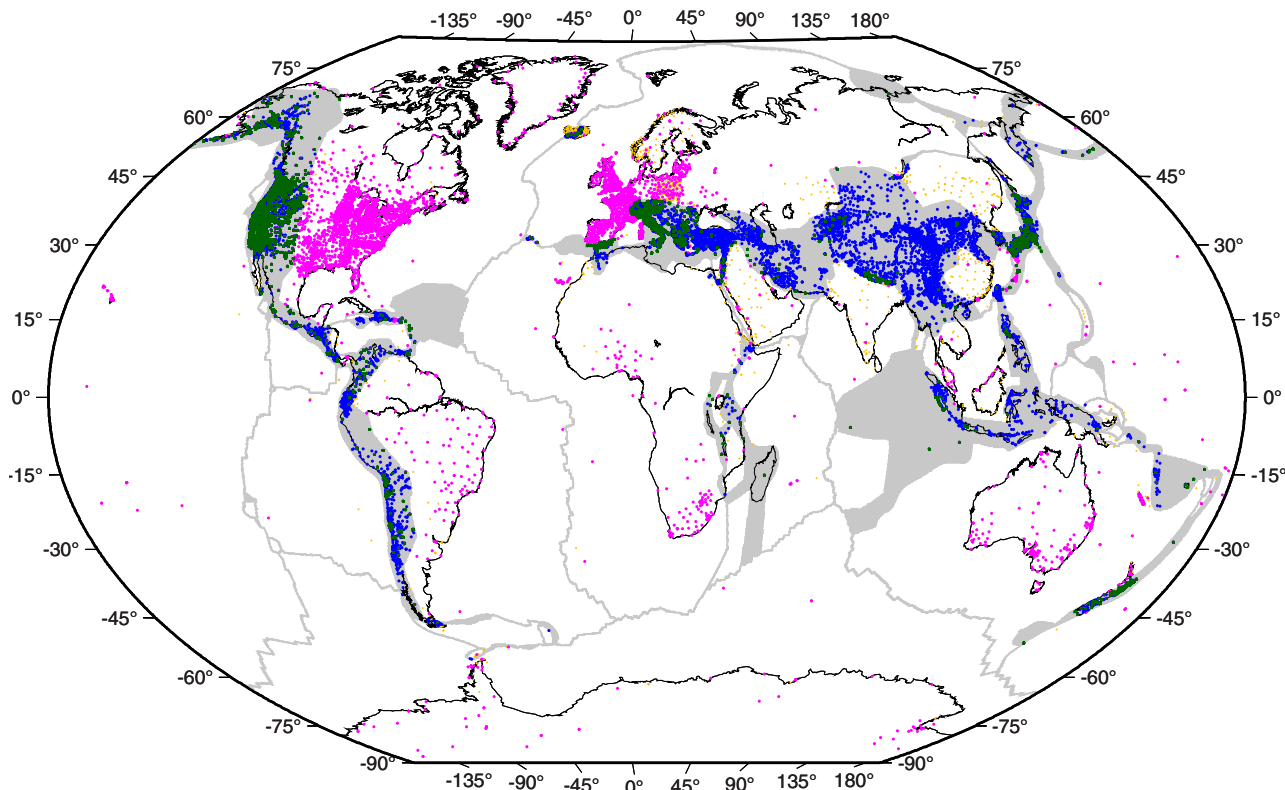


**Figure 1.** Gray shading is outline of all areas allowed to deform. White areas comprise of 50 assumed rigid plates. Purple and green dots are for GPS stations on rigid plates or in deforming zones, respectively, for which we derived a velocity. Yellow and blue dots are for GPS stations on rigid plates or in deforming zones, respectively, for which we took the velocity from the literature.

this analysis for all studies simultaneously, because study *A*, for example, may not have any collocated sites with the core solution, but has collocations with study *B*, which does have collocated sites with the core solution. Any velocity for a site collocated with the core solution will be removed, under the assumption that the velocity of the core solution is superior (e.g., it is typically derived from longer time series and we checked for offsets and transients ourselves). At least three collocated sites are needed to solve for a translation and rotation rate. If only two collocated sites are present, we only solve for a rotation rate. To avoid solving for a large translation rate when the geographic footprint is small (in which case there may be a trade-off between translation and rotation rate), we down-weight the translation rate parameters in the inversion. In the few cases where study *A* mostly supersedes study *B*, but some velocities from study *B* are not in study *A*, we first translate study *B* onto study *A* before we perform the global transformation. In those cases we do not duplicate the velocities at the collocated sites. The supporting information lists the misfit velocities (weighted and unweighted) for any collocated station.

Thirteen studies could not directly be transformed, because they had less than two data points collocated with the other studies. Of those studies, those that were presented in an ITRF-flavor reference frame were assumed to be in our IGS08 frame, and those studies that were relative to a stable plate were fixed to the respective plates in our model. This leaves seven studies which were then rotated into the model reference frame (i.e., Pacific) as part of modeling the velocity gradient tensor field while minimizing misfits between observed and model velocities.

The procedure described above is an improvement on that followed in the previous GSRM in which the transformation (i.e., rotation) of each study was determined in the modeling of the strain rates. The new approach is superior in that (except for the few exceptions mentioned above) the data are independent of the strain rate model.

In the end, we included 15,710 velocities from 233 studies (mostly) in the literature. Together with the core solution, there are 22,415 velocity data at 18,356 unique locations available for the modeling. The site locations are shown in Figure 1. For comparison, the previous model used 5170 velocities from 86 studies.

All velocities (including those excluded near the creeping San Andreas Fault) are provided in the supporting information in many different reference frames.

#### 4. Mesh Definition

We completely redefined the mesh for the modeling compared to what was used for the previous model. We consider the whole globe between 87.5°S and 87.5°N, which includes all data points, and the mesh is continuous in longitudinal direction. Individual grid cells are 0.2° (latitudinal) by 0.25° (longitudinal) in dimension, a decrease of a factor of ~2.5 in size compared to the previous model's cell sizes of 0.5° by 0.6°. To determine which cells should be allowed to deform (i.e., cover the plate boundaries) and which not (i.e., move with a rigid plate), we started with the plate definitions of the PB2002 model of *Bird* [2003]. For each node of the mesh, it was determined whether or not it was within the polygon of a plate (and which plate). As a result, for plate boundary zones that are defined by a single "line," such as oceanic ridge-transform systems, the boundary consist of a single grid cell, of which four corner nodes are typically divided over two plates. The definition of the diffuse zones in PB2002 was augmented by the boundary definitions of *Chamot-Rooke and Rabaute* [2006]. We made numerous adjustments to these definitions, mostly guided by the information from the GPS data that areas originally considered part of a rigid plate should be considered part of a deforming zone. In total, the model contains 145,086 deforming cells, compared to 22,310 cells in the previous model. The deforming cells are shown in Figure 1 as well as in the supporting information. Of the total 22,415 velocities, 17,567 are inside the deforming cells.

One notable place where we adjusted previous definitions of plate boundary zones was for the Tyrrhenian Sea area. *Bird* [2003] included this area, as well as Corsica and Sardinia, into his definition of the Alpine deformation zone, *Chamot-Rooke and Rabaute* [2006] did not. We, and most previous studies [e.g., *Nocquet and Calais*, 2003; *Serpelloni et al.*, 2005; *Nocquet*, 2012], found that GPS stations on Corsica and Sardinia clearly move with other stations in western Europe. However, we also noted, as some previous studies [*Serpelloni et al.*, 2005; *Nocquet*, 2012], that GPS stations along the western side of the Italian Peninsula have a NW-NNW motion of 1–1.5 mm yr<sup>-1</sup> relative to western Europe. While this motion remains unexplained, it does suggest that rigid Eurasia likely does not extend to Italy's western margin. We therefore included the area between Corsica-Sardinia and the Italian Peninsula in the definition of the deforming zone, allowing the relative motion between west-central Italy and stable western Europe to be accommodated across the Tyrrhenian Sea.

Another significant adjustment in the plate boundary definition is that we included the Canadian Cordillera, which both *Bird* [2003] and *Chamot-Rooke and Rabaute* [2006] excluded. *Kreemer et al.* [2003] excluded this area as well. In our new definition we essentially connect the broad boundary zone in the American Southwest to the one in Alaska. Our choice is based on evidence from both GPS data and seismicity that this area is deforming [e.g., *Mazzotti et al.*, 2008].

A number of micro-plates defined in PB2002 were allowed to deform in our model, typically in areas of diffuse deformation in a subduction back arc such as Southeast Asia or the Andes. The rationale for this is that these micro-plates are typically in areas of large and complex deformation. If the micro-plates are covered by GPS stations, their velocities do often not reflect long-term motion as a result of elastic strain buildup along its margin (e.g., the Altiplano plate) or, if they have no GPS coverage, the motion defined in PB2002 may not be compatible with nearby GPS data, causing spurious strain rates along the plates' edges. This is not to say that no rigid micro-plates exist in continental back arcs [*Brooks et al.*, 2003; *Wallace et al.*, 2004b; *Chlieh et al.*, 2011; *McCaffrey et al.*, 2013], but that it is not possible to properly model the surface deformation (i.e., rigid plate motion with localized high strain rates along its edges) without correcting/modeling for elastic strain accumulation. Such exercise was beyond the scope of this work and beyond GEM's requirement.

Our model contains 50 rigid plates and micro-plates, compared to the 25 plates assumed in the previous model. We added a number of micro-plates that were not in PB2002. All these additional plates have been shown to exist in the literature and, with two exceptions (Capricorn and Lwandle), we were able to constrain their rigid-body rotations by the GPS data (see section 4.2). The new micro-plates, with selected references arguing for their existence, are: Bering [e.g., *Mackey et al.*, 1997; *Cross and Freymueller*, 2008], Baja California [e.g., *Umhoefer and Dorsey*, 1997; *Plattner et al.*, 2007], Capricorn [e.g., *Royer and Gordon*, 1997;

Conder and Forsyth, 2001], Danakil [McClusky et al., 2010], Gônave [e.g., Mann et al., 1995; Benford et al., 2012], Lwandle [e.g., Hartnady, 2002; Horner-Johnson et al., 2007], Puerto Rico [e.g., McCann, 1985; Jansma et al., 2000; Manaker et al., 2008], Rovuma [e.g., Hartnady, 2002; Calais et al., 2006b], Sakishima [Nishimura et al., 2004], Satunam [Nishimura et al., 2004], Sinai [Masle et al., 2000; Salamon et al., 2003; Mahmoud et al., 2005], Victoria [e.g., Hartnady, 2002; Calais et al., 2006b].

The Sakishima and Satunam micro-plates are subplates of PB2002's Okinawa micro-plate and named here for the first time. In our model the Okinawa micro-plate is limited to only the central portion of the plate defined in PB2002, with Sakishima to its south and Satunam to its north.

The Bering, Capricorn, Lwandle are part of the MORVEL plate motion model [DeMets et al., 2010], although MORVEL did not have a rotation rate for Bering, which we estimated from the GPS data.

Compared to the previous strain rate model, other new plates in the model are (from PB2002): Aegean Sea, Burma, Easter, Galapagos, Juan Fernandez, Mariana, Niuafo'ou, North Bismarck, Okinawa, Panama, Shetland, Sandwich, Solomon Sea, South Bismarck, Tonga, Woodlark. For some of these micro-plates (Aegean Sea, Mariana, Okinawa, Panama, Shetland, South Bismarck, Tonga, Woodlark) we were able to estimate the rigid-body rotation from the GPS data (see section 5) and thus replace the rotation given by PB2002.

Two plates that existed in the previous GSRM are now part of a deforming zone. One is the Anatolia micro-plate, which also exists in PB2002. While it has long been considered as a rigid micro-plate [McKenzie, 1970; McClusky et al., 2000], it is now evident from a new dense GPS network that there is significant internal deformation within Anatolia [Aktuğ et al., 2013a]. The other plate is Tarim. While it may indeed be a rigid micro-plate [Avouac et al., 1993; Shen et al., 2001; Meade, 2007; Zhang and Gan, 2008], there is now significant GPS coverage to constrain the Tarim area as having low strain rates within the greater India-Eurasia subduction zone. Because of there being ample geodetic data present to describe some micro-plates simply as low straining areas, we also do not consider, for example, a central Iranian micro-plate [Jackson and McKenzie, 1984; Vernant et al., 2004a], a Sierra Nevada-Great Valley micro-plate in the western United States [Argus and Gordon, 1991a; Dixon et al., 2000; McCaffrey, 2005], or an Adria and/or Apulia micro-plate(s) between Italy and the Balkans [e.g., Anderson and Jackson, 1987; Ward, 1994; Battaglia et al., 2004; D'Agostino et al., 2008].

Polygon coordinates of all 50 plates/are provided in the supporting information and plate identifiers are shown together with the deforming mesh in supporting information Figure S1.

## 5. Rigid-Body Rotations

In Table 2, we list the angular velocities (in terms of the corresponding Euler pole and rotation rate) for all assumed rigid plates included in the model. They are listed relative to the Pacific plate, which is the model's reference plate. Euler poles and full covariance matrices for the IGS08 reference frame are in supporting information Table S2. Of the 50 plates, 36 angular velocities were estimated from the GPS velocities in our compilation (mostly ones derived by ourselves), 6 were taken from PB2002 [Bird, 2003] and 8 were taken from MORVEL [DeMets et al., 2010].

Supporting information Table S1 contains the IGS08-velocities used to constrain the plate motions, their residuals, and the study from which the velocity was taken.

We chose to not use every GPS velocity on each rigid plate to estimate the angular velocities. Typically we would only use the longest-running stations with low RMS scatter from our own analysis. In some cases, there were insufficient stations from our own analysis (or a sufficient number was not well distributed across the plate) to estimate the angular velocity. In those cases we also used velocities from the literature synthesis. In general, we follow the guidelines set forth by Argus and Gordon [1996] and omit stations near plate boundaries, mainly because those may be affected by elastic strain accumulation along active faults. A more detailed discussion is warranted for a subset of the plates:

- 1) Baja California: We estimate an Euler pole for Baja California relative to the Pacific plate at almost 90° away from the micro-plate, suggesting a quasi translational nature of its motion. The predicted motion relative to the Pacific plate is  $\sim 4.0 \text{ mm yr}^{-1}$  to S40°E. A GPS station near Cabo San Lázaro [Plattner et al., 2007], moves at  $\sim 2.2 \text{ mm yr}^{-1}$  to S51°E, suggesting that the boundary between the Pacific plate and the Baja

California micro-plate is likely accommodated across a broad zone along the western margin of the Baja Peninsula. However, without any other information we define the boundary between Baja California and the Pacific plate as a discrete boundary.

2) Caribbean: We estimate the angular velocity for the Caribbean plate by using our velocity estimates for San Andres Island and Grenada and the additional estimate for Aves Island from *Weber et al.* [2001]. Most studies have considered station CRO1 on Saint Croix, U.S. Virgin Islands, to be part of the Caribbean plate [e.g., *Sella et al.*, 2002; *Prawirodirdjo and Bock*, 2004; *Altamimi et al.*, 2012]. In our analysis, CRO1 and nearby station VIKH move to the SSW at  $0.4\text{--}1.3 \text{ mm yr}^{-1}$  relative to the Caribbean plate, possibly suggesting that the Muertos Trough is active as far east as south of the U.S. Virgin Islands [McCann, 1985].

3) Cocos: We used the MORVEL angular velocity for Cocos [DeMets *et al.*, 2010]. Cocos Island is the only sub-aerial site on this plate and has two closely located geodetic sites. We find that the residual velocity for campaign station COCO, recently remeasured by *Protti et al.* [2012], has a residual velocity of  $2.6 \text{ mm yr}^{-1}$  to the east and  $2.4 \text{ mm yr}^{-1}$  to the north. For the new CGPS station ISCO that we analyzed, we find a residual velocity of  $0.9 \text{ mm yr}^{-1}$  to the east and  $2.2 \text{ mm yr}^{-1}$  to the north (which include solving for a coseismic offset due to the 2012  $M_w=7.6$  Nicoya earthquake). However, we also observe a slight velocity change at the time of the earthquake. If we account for that velocity change, the residual velocity reduces to  $0.2 \text{ mm yr}^{-1}$  to the east and  $1.5 \text{ mm yr}^{-1}$  to the north. This very closely confirms the MORVEL prediction. The velocity change at the time of the event is  $2 \text{ mm yr}^{-1}$  to the NE, probably due to visco-elastic postseismic relaxation.

4) Eurasia: The station coverage for the Eurasian plate is highly biased toward western Europe. To estimate the angular velocity, we used our velocity estimates from ten long-running CGPS sites that are roughly equally distributed across the plate. We excluded stations in Scandinavia, where velocities are affected by GIA [Lidberg *et al.*, 2010; Kierulf *et al.*, 2013]. The areas in the farfield from the former Fennoscandian ice sheet may be moving toward the ice sheet, but by picking stations equally covered over the plate, that effect is down-weighted (see discussion North American plate below). We did not find significant motion across the Pyrenees, as was reported by *Asensio et al.* [2012], and most of Iberia (except for the Betics in the south) [Pérez-Peña *et al.*, 2010; Koulali *et al.*, 2011; de Lis Mancilla *et al.*, 2013; Echeverria *et al.*, 2013] thus moves with Eurasia. Although we formally include the Alps in the deforming zones, it is worth mentioning that we see no significant motion across the western Alps, as was reported earlier by *Calais et al.* [2002]. Our finding of no-significant motion across the Pyrenees or western Alps agrees with the latest findings of *Nocquet* [2012], and the disagreement with the aforementioned studies may lie in reference frame definition, choice of noise model, or insufficient time series length.

5) India: Like *Reddy et al.* [2010], we observe a change (i.e., speed-up) of  $1.3 \text{ mm yr}^{-1}$  toward the SE of the long-running station at Bangalore (IISC) at the time of the 26 December, 2004,  $M_w=9.15$ , Sumatra earthquake. Even though this station is  $>2000 \text{ km}$  from the epicenter, it is likely that this velocity change is due to visco-elastic postseismic relaxation. Similar far-field effects are seen in stations in SE Australia after the 23 December 2004,  $M_w=8.1$ , Macquarie Ridge earthquake [Tregoning *et al.*, 2013] and in east Asia after the 11 March 2011,  $M_w=9.0$  Tohoku-Oki event [Baek *et al.*, 2012; Shestakov *et al.*, 2012]. However, unlike *Reddy et al.* [2010], we do not see an east-ward speed-up for the CGPS station in Hyderabad, 500 km north of Bangalore. Many of the studies we use in this area have velocities based on data (partially) from after the 2004 earthquake. Estimating India's rigid-body rotation from data before the 2004 earthquake would cause undesired strain rate estimates along the boundaries of the rigid plate. We therefore estimate Indian plate motion from data after the 2004 earthquake, and understand that this may not truly be the plate's present-day steady motion.

6) Mariana: For the Mariana plate we used our CGPS velocity on Mariana Island (CNM0, formed by concatenating the time series of CNMI and CNMR) and three additional velocities from *Kato et al.* [2003] along the central Mariana Islands. Like *Kato et al.* [2003], we do not correct for any possible elastic strain accumulation along the Marianas trench. We find a significant N-to-S increase in the back-arc spreading rate, but overall  $3\text{--}8 \text{ mm yr}^{-1}$  slower than predicted by *Kato et al.* [2003].

7) Nazca: It has been shown that significant deformation near Easter Island affects the GPS station there [*Kendrick et al.*, 2003] (ISP0, formed by concatenating the time series of EISL and ISPA). We therefore add to the single CGPS station on the Galapagos Islands (GLP0, formed by concatenating the time series of GALA and GLPS), the two velocities on San Felix and Robinson Crusoe Islands originally presented by *Kendrick*

*et al.* [2003], but taken from *Wang et al.* [2007]. ISPO moves  $2.8 \text{ mm yr}^{-1}$  toward S52°E relative to our definition of stable Nazca.

8) North America: Most previous studies of the motion of the North American plate only considered stations south of the former ice sheet [e.g., *Sella et al.*, 2007; *Argus et al.*, 2010; *Altamimi et al.*, 2012; *Blewitt et al.*, 2013]. However, most of the latest GIA models predict a significant far-field motion toward the former ice sheet [*Latychev et al.*, 2005; *Sella et al.*, 2007; *Peltier and Drummond*, 2008]. If we were only to choose GPS stations south of the ice sheet to estimate the plate's angular velocity, the assumed rigid-body motion of the northern part of the plate will be biased. We therefore chose 10 long-running stations that covered the entire plate roughly uniformly. Unfortunately, this still causes a small problem; we find artificially elevated strain rates along the eastern edge of the Pacific-North America plate boundary in the western United States, because of the northerly oriented velocities ( $1\text{--}1.5 \text{ mm yr}^{-1}$ ) of the numerous stations in the eastern end of the boundary (due to GIA) relative to the (artificially) fixed plate interior. For future models, to avoid this artifact, all of the North American plate should be allowed to deform. Then, the strain rates due to GIA would be correctly found around the former ice sheet.

9) Okhotsk: It is difficult to estimate an angular velocity for the Okhotsk plate, because GPS can only be found along its margins, where velocities may be affected by elastic loading (for which we do not account). Nevertheless, we are fairly confident about our results, which predict (relative to Amur plate)  $\sim 8 \text{ mm yr}^{-1}$  WSW directed shortening across the island of Sakhalin and  $\sim 2 \text{ mm yr}^{-1}$  NE directed motion relative to North America across the Chersky Range. Both results are, at least in direction, consistent with regional focal mechanisms, with the motion across the Chersky Range being partitioned between E-W directed left-lateral strike-slip and N-S shortening [e.g., *Cook et al.*, 1986; *Riegel et al.*, 1993].

10) Pacific: Our definition of a stable Pacific plate includes the first global use of velocities at two stations (Kiritimati (KRTM), Kiribati Islands, and Gambie Island (GAMB), French Polynesia) for which data were collected by the Asia Pacific Crustal Monitoring System [*Harada*, 2000; *Munekane and Fukuzaki*, 2006], which allows for a better geometric spread of stable stations. Although the station on Guadalupe Island (GUAX), southwest of Baja California, would provide an important geometric constrain in the rotation estimation, the suggestion of thermal contraction in the young oceanic lithosphere precludes us from using it [*Kumar and Gordon*, 2009; *Kreemer and Gordon*, 2014]. Indeed, GUAX moves at  $\sim 1.2 \text{ mm yr}^{-1}$  toward S27°E. For similar reasons, we also exclude the IGS stations on Chatham Island, east of New Zealand.

11) Philippine Sea: There are a couple of islands with GPS stations on this oceanic plate. The data from station G140 on Okino Torishima (also called Parece Vela) near the center of the Philippine Sea plate are noisy and are not used in the angular velocity estimation. To avoid a geometric bias, we used only one of the two velocities on the Daito Islands, namely on Kita Daito (J746), and combine it with the velocity for Koro, Palau Islands (PAL0, concatenated from PAL1 and PALA). In this definition G140 moves  $\sim 0.8 \text{ mm yr}^{-1}$  toward the NNE.

12) Scotia: There is only one GPS site (ORNO) located on the very western side of the plate away from the SC-SA plate boundary [*Smalley et al.*, 2003, 2007], such that it is not possible to estimate the angular velocity. We therefore adopted the rotation from MORVEL [*DeMets et al.*, 2010]. Our velocity for ORNO (after transformation) is  $6.8\text{--}7.0 \text{ mm yr}^{-1}$  eastward, while our SC-SA prediction for that location is  $7.7 \text{ mm yr}^{-1}$  S60°E.

13) Shetland: We combined data for various studies to present the first angular velocity estimate for the small Shetland micro-plate (see supporting information), which is almost entirely surrounded by the Antarctic plate. The pole of rotation of the micro-plate relative to Antarctica is near Gibbs Island. The result predicts northward directed shortening across the South Shetland Trench, from  $6 \text{ mm yr}^{-1}$  in the east to  $12 \text{ mm yr}^{-1}$  in the west, and a maximum of  $9 \text{ mm yr}^{-1}$  NNE directed extension across the Bransfield Rift System near Deception Island.

14) Tonga: As for the Mariana micro-plate, we assume that the three velocities we use to estimate the angular velocity of the Tonga micro-plate are not affected by elastic loading along the subduction interface.

## 6. Strain Rate Model

As for previous GSRM versions, we used the method of Haines and Holt [e.g., *Haines and Holt*, 1993; *Holt et al.*, 2000; *Beavan and Haines*, 2001] to model the strain rate field. Given the specific nature of inferring a

continuous strain rate field from irregularly spaced geodetic observations, several strain rate modeling techniques have been put forward [e.g., *Shen et al.*, 1996; *Kahle et al.*, 2000; *Spakman and Nyst*, 2002; *Cardozo and Allmendinger*, 2009; *Hackl et al.*, 2009; *Tape et al.*, 2009; *Wu et al.*, 2011; *Masson et al.*, 2014]. Here we use the Haines and Holt method because (1) it is in spherical coordinates, (2) it allows for the model to wrap around the Earth in longitudinal direction, and (3) it allows for a straightforward manipulation of *a priori* assumptions about the level and style of strain rate. The Haines and Holt method can also incorporate strain rate “observations” from seismology or geology, but that feature is not implemented for this version of GSRM. The Haines and Holt method uses bicubic splines to obtain a continuous velocity gradient tensor field in the plate boundary zones. The rigid-body rotations listed above are applied as *a priori* boundary conditions, relative to the Pacific plate, which is the reference plate in the model. More details are in Appendix B.

### 6.1. A Priori Strain Rate Variances

Following a Bayesian philosophy, the method requires us to assign *a priori* strain rate (co)variances to each deforming grid cell. In order to properly fit the velocity gradient field in areas of high and low strain rates, and to avoid under or overfitting the geodetic velocities, respectively, we prefer to assign *a priori* variances that reflect the actual expected strain rates. To accomplish this, we decided on a two-step approach, modeling the strain rate field twice. In the first step, we assign the same standard deviations of  $10^{-8} \text{ yr}^{-1}$  for  $\dot{\varepsilon}_{\varphi\varphi}$  and  $\dot{\varepsilon}_{\theta\theta}$ , and  $1/\sqrt{2} 10^{-8} \text{ yr}^{-1}$  for  $\dot{\varepsilon}_{\varphi\theta}$  to each cell, with zero covariances (i.e., assumed isotropy). However, if we would assign the same *a priori* variances to each grid cell, we would create some erroneous results in the diffuse oceanic areas, where GPS data are largely absent. For instance, we can assume that in the Indian Ocean the majority of the deformation occurs along the spreading centers and not in the diffuse zone between the India, Capricorn and Australian plates. If we assign the same *a priori* variances to all grid cells, relatively high strain rates due to the relative plate motions will spread into the diffuse zone. To remedy this, we give all cells with transform and ridge segments very large *a priori* variances. We do the same for the part of the Sunda subduction zone that borders the Indian Ocean diffuse deformation area. We follow a similar approach for the diffuse oceanic areas between the New Hebrides and Fiji, the one between the North and South America plates, and in the “armpit” of the easternmost Aleutian/Alaska subduction zone. For the diffuse boundary between Africa and Eurasia, south west of Portugal (as defined by *Chamot-Rooke and Rabaute* [2006]), the PB2002 boundary segments run through the middle of the diffuse zone and we set very high variances for the cells containing the PB2002 boundary segments. The second invariant of the strain rate model resulting from step 1 are shown in supporting information Figure S2.

In the second step, we take the modeled strain rate field from the first step and used it to constrain the *a priori* standard deviations. For this, we did not take over the style or covariances but set the *a priori* standard deviation of  $\dot{\varepsilon}_{\varphi\varphi}$  and  $\dot{\varepsilon}_{\theta\theta}$  equal to the second invariant of the tensor modeled in step 1 (i.e.,

$\sqrt{\dot{\varepsilon}_{\varphi\varphi}^2 + \dot{\varepsilon}_{\theta\theta}^2 + 2\dot{\varepsilon}_{\varphi\theta}^2}$ , and  $\dot{\varepsilon}_{\varphi\theta}$  to the second invariant divided by the square-root of 2. An exception was given to the Colorado Plateau area in the western United States. Because of how we define stable North America, we would obtain a band of elevated strain rates on the eastern edge of the Pacific-North America plate boundary zone (see discussion on the definition of the North America rotation vector in section 5) when following the procedure above. To avoid most of this artifact, we set the *a priori* strain rates in the second step to  $3 \times 10^{-9} \text{ yr}^{-1}$  for the area between  $26^\circ$ – $44^\circ\text{N}$  and  $110^\circ$ – $102^\circ\text{W}$  in order to damp the model there.

### 6.2. Results

The second invariant of strain rate of GSRM v.2.1 is shown in Figure 2. The second invariant is defined above, and is equivalent to the total strain rate:  $\sqrt{\dot{\varepsilon}_1^2 + \dot{\varepsilon}_2^2}$  where  $\dot{\varepsilon}_1$  and  $\dot{\varepsilon}_2$  are the largest and smallest eigenvalue, respectively. Note that the color scale is nonlinear and that the high values are saturated. Strain rates in most oceanic boundaries are exclusively constrained by the imposed relative plate motions. Some of the highest values can be found there due to the narrow definition of the boundary across spreading ridges and transforms. For example the strain rates along the East Pacific Rise are up to  $4.5 \times 10^{-6}/\text{yr}$ , which merely reflects the creation of new crust rather than actual extensional deformation of this magnitude.

We also estimated the standard deviation in the second invariant and used it to divide the second invariant to create a signal-to-noise (SNR) map (Figure 3). It is important to note that the formal standard errors are indicative for uncertainty of the model at the scale of the  $0.2^\circ$  by  $0.25^\circ$  large cells. Because station spacing is for many areas (much) larger than the grid dimension, model uncertainties are correspondingly large, and

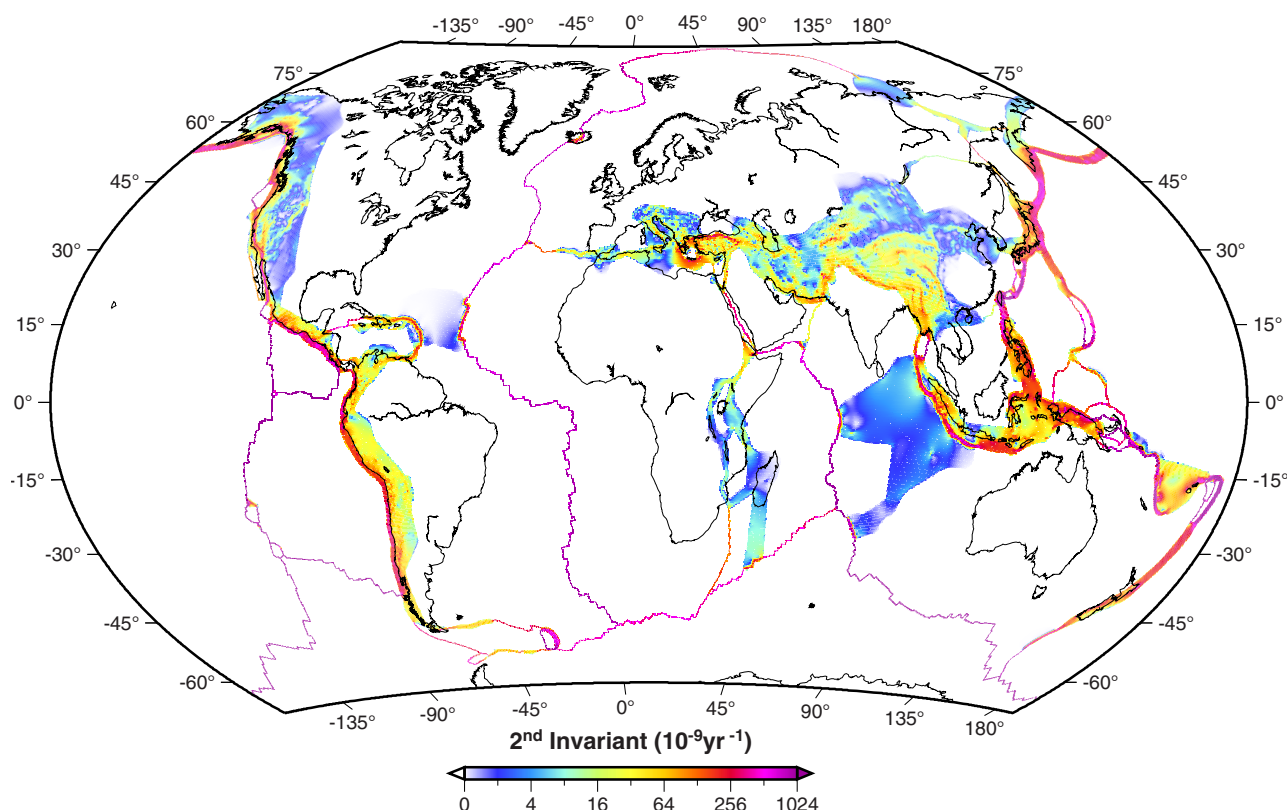


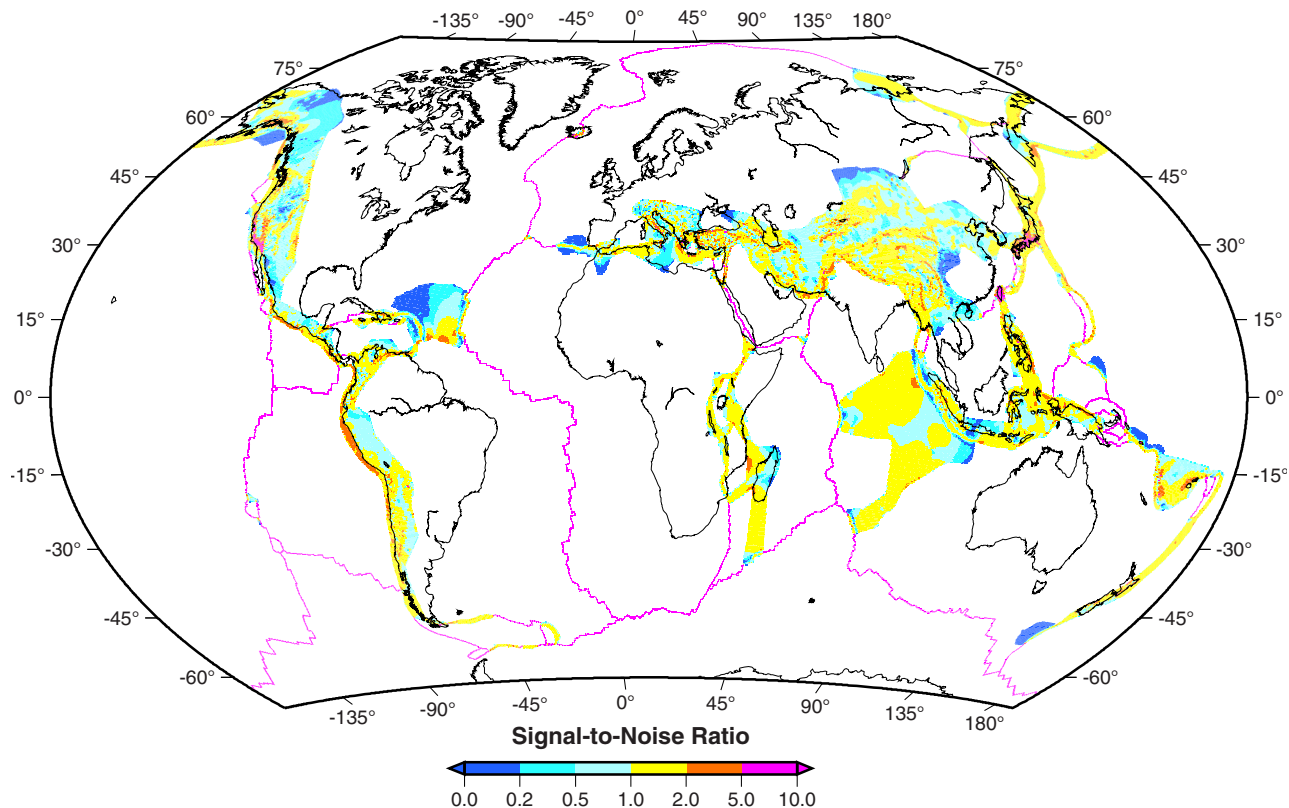
**Figure 2.** Contours of the second invariant of the model strain rate field. Color scale is not linear and saturated at high values. White areas were assumed to be rigid plates and no strain rates were calculated there. Instead, the rigid body rotation of these plates was imposed as boundary condition when solving for plate boundary strain rates from the geodetic velocities.

SNR thus low. Also note that the strain rate uncertainties are zero for most spreading ridges and transform, because the deforming grid is only one grid cell wide, and thus the average model strain rates for those cells are exact. Consequently we used maximum saturated SNR values for those boundaries. The SNR map largely reflects the spatial density of the geodetic stations but the imposition of plate motions as boundary conditions also contributes to the result (e.g., diffuse boundary in Indian Ocean). Supporting information Figure S3 shows a measure of variance reduction for a case with uniform *a priori* variances and it is thus another measure of where the model is well resolved (given the grid cell size) due to sufficiently dense geodetic coverage.

Figure 4 shows the dilatational component of the strain rate tensor. It highlights a first-order dichotomy: positive dilatation (i.e., extension) is mostly constrained to the narrow mid-oceanic boundaries and negative dilatation (i.e., contraction) mostly occurs on continental margins. Well-known exceptions are the continental extension found in the Basin and Range province in the western United States, central Italy, the Aegean, the East African Rift, and parts of Tibet. Overall, 72% of the plate boundary zones have a component of contraction, while 28% of the boundaries have a component of extension. When summed together the global net dilatation is zero, as required kinematically.

Figure 5 shows a measure of the style tensor, defined as  $(\dot{\epsilon}_1 + \dot{\epsilon}_2)/\max(|\dot{\epsilon}_1|, |\dot{\epsilon}_2|)$ . In case both eigenvalues have a similar sign, we saturate the definition at 1.0 or -1.0 when both values are positive or negative, respectively. Increasing positive (negative) values imply an increasing component of extension (contraction).

Figure 6 shows the vorticity rate. Positive (negative) vorticity implies anticlockwise (clockwise) rotation around a vertical axis. While the vorticity rate in the deforming zones is essentially reference frame independent, a reference frame needs to be chosen for the display of vorticity for the rigid plates. For this, we choose the reference frame of Kreemer [2009] which is relative to the subasthenospheric mantle. Because Euler poles in this frame can be  $>90^\circ$  from the plate, some plates show internal changes from positive to negative vorticity (e.g., Pacific, Australia).



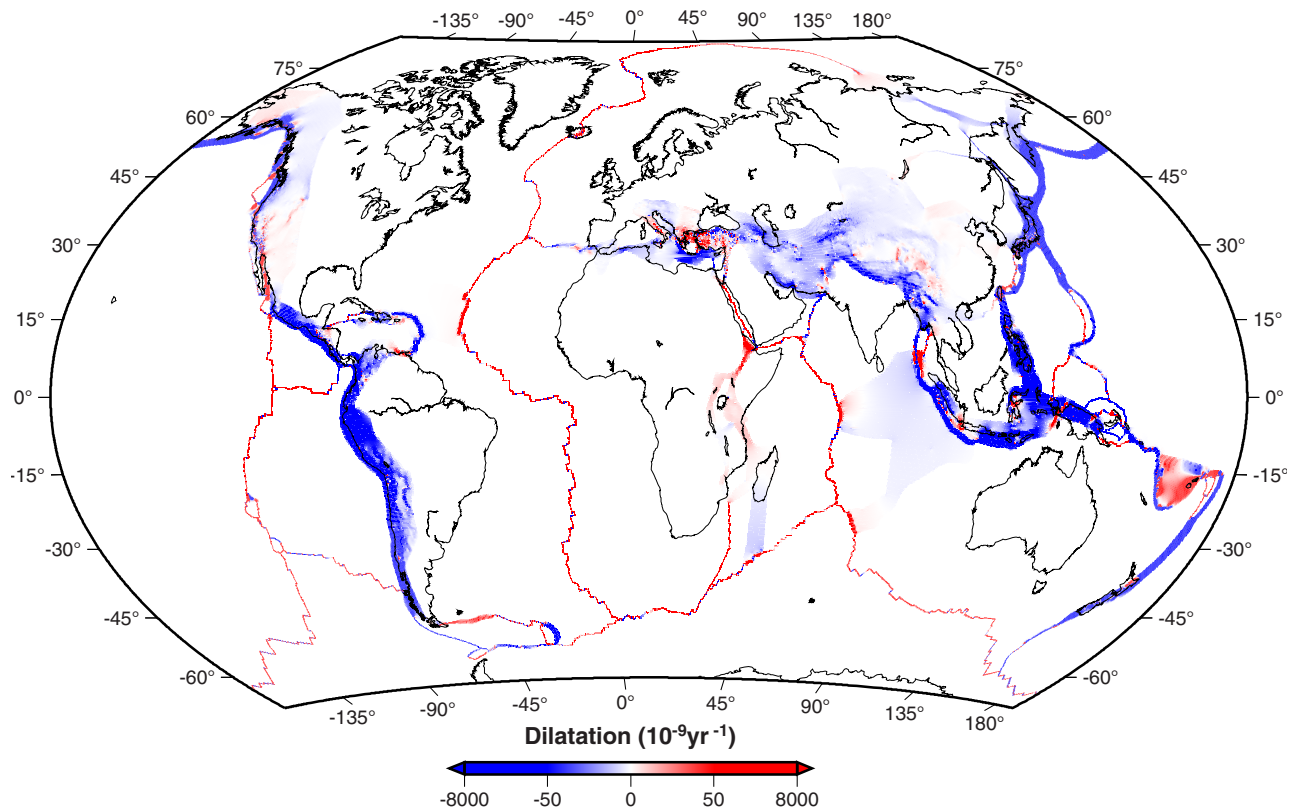
**Figure 3.** Signal-to-noise ratio of the second invariant of the modeled strain rates (i.e., second invariant divided by the standard deviation in the second invariant).

Figure 7 shows close-ups of some areas of diffuse continental deformation: Italy, Aegean, Persia, western and eastern Tibet, and western United States. The figures show the locations of the data points. All figures show contours of the second invariant at the same scale as those in Figure 2. The figures also show the principal axes for every other grid cell (normalized to the largest absolute eigenvalue of the two), with the result being the average of neighboring grid cells (up to two cells away). These results are only shown where the model is well resolved, as defined by places where the reduction in the variance (*a priori* and *a posteriori* standard deviations) in all three strain rate components is larger or equal to  $1 - \sqrt{2}/2$ , or, where that is not the case, the SNR of the second invariant is larger than  $\sqrt{2}$ . (These limits were chosen subjectively.) For the same places we also show the two orientations for the expected shear planes (i.e., orientations of no-length change), but these can only be defined when the two eigenvalues have opposite sign [Holt and Haines, 1993]. The two orientations are distinct, unless one of the two principal axes is zero, and correspond to a component of either left or right-lateral slip. We show both orientations but at places emphasize the more likely one. The more likely orientation can in most cases be inferred from the local sense of vorticity (i.e., right-lateral slip for negative vorticity, and vice versa). We only show the likely orientation when the absolute value of vorticity is larger or equal to  $0.8^\circ \text{ Myr}^{-1}$ . The color of the preferred orientation reflects the style of the strain rate tensor (same definition and color scale as in Figure 5), but that should also be evident from the principal axes. We believe this is the first time a study has used the local vorticity in differentiating the likely fault plane orientation from the auxiliary orientation implied by the strain rate tensor.

ASCII files of the strain rate results (both for grid-cell average and  $0.1^\circ$  grid) are available in the supporting information. Predicted velocities on a  $0.1^\circ$  grid in any reference frame are also given in the supporting information.

## 7. No-Net Rotation Reference Frame

A spin-off from previous GSRM versions has been to calculate a NNR reference frame [Kreemer and Holt, 2001; Kreemer *et al.*, 2003, 2006]. The definition of such frame requires knowing the horizontal velocity



**Figure 4.** Dilatational component of the modeled strain rates ( $\dot{\varepsilon}_{\phi\phi} + \dot{\varepsilon}_{\theta\theta}$ ). Extension (contraction) is positive (negative). Highest values are saturated.

anywhere on Earth. We showed earlier that NNR models can be significantly biased if they ignore that a significant portion of the Earth's surface does not move as/with a rigid plate.

We recalculated the NNR frame (GSRM-NNR-2.1) and list NNR Euler poles of all plates in the supporting information Table S2. We find that NNR angular velocities differ significantly from those estimated in IGS08, which, through ITRF, has the NNR condition built in using the NNR-NUVEL-1A model [DeMets *et al.*, 1990, 1994; Argus and Gordon, 1991b; Altamimi *et al.*, 2007]. To rotate from the velocity field in our IGS08 frame to the NNR frame requires a rate of  $0.0202^\circ \text{ Myr}^{-1}$  around a pole located at  $41.6^\circ\text{N}$  and  $47.7^\circ\text{W}$ . The corresponding maximum velocity difference is  $2.25 \text{ mm yr}^{-1}$ . Previous analyses [Kreemer and Holt, 2001; Kreemer *et al.*, 2006] show that this difference is in part due to nonplate-like velocity fields in the deformation zones and the use of geologic instead of geodetic plate motions in the NNR-NUVEL-1A model. The maximum velocity difference between the NNR model derived from GSRM v.1.2 and ITRF2000 was  $3.1 \text{ mm yr}^{-1}$  [Kreemer *et al.*, 2006]. Additional study is required to assess the source of the reduction.

We will present a detailed comparison between our new NNR model and previous ones [e.g., Kreemer *et al.*, 2006; Argus *et al.*, 2011] in a future study. We note, however, that there is a significant difference between our model and the model by Argus *et al.* [2011] (NNR-MORVEL-56), because (1) NNR-MORVEL-56 has most of the relative surface motion described by MORVEL (the remainder surface area is covered by small plates for which angular velocities come from Bird [2003] and is a mixture of geologic and geodetic estimates) and we show below that geologic and geodetic motions differ significantly, and (2) NNR-MORVEL-56 ignores the velocity gradients within the diffuse plate boundary zones.

## 8. Discussion

### 8.1. Angular Velocities

We compare our angular velocities relative to the Pacific plate with previous geodetic estimates that provided a full covariance matrix (GEODVEL [Argus *et al.*, 2010], ITRF2008 [Altamimi *et al.*, 2012], GSRM1[Kreemer

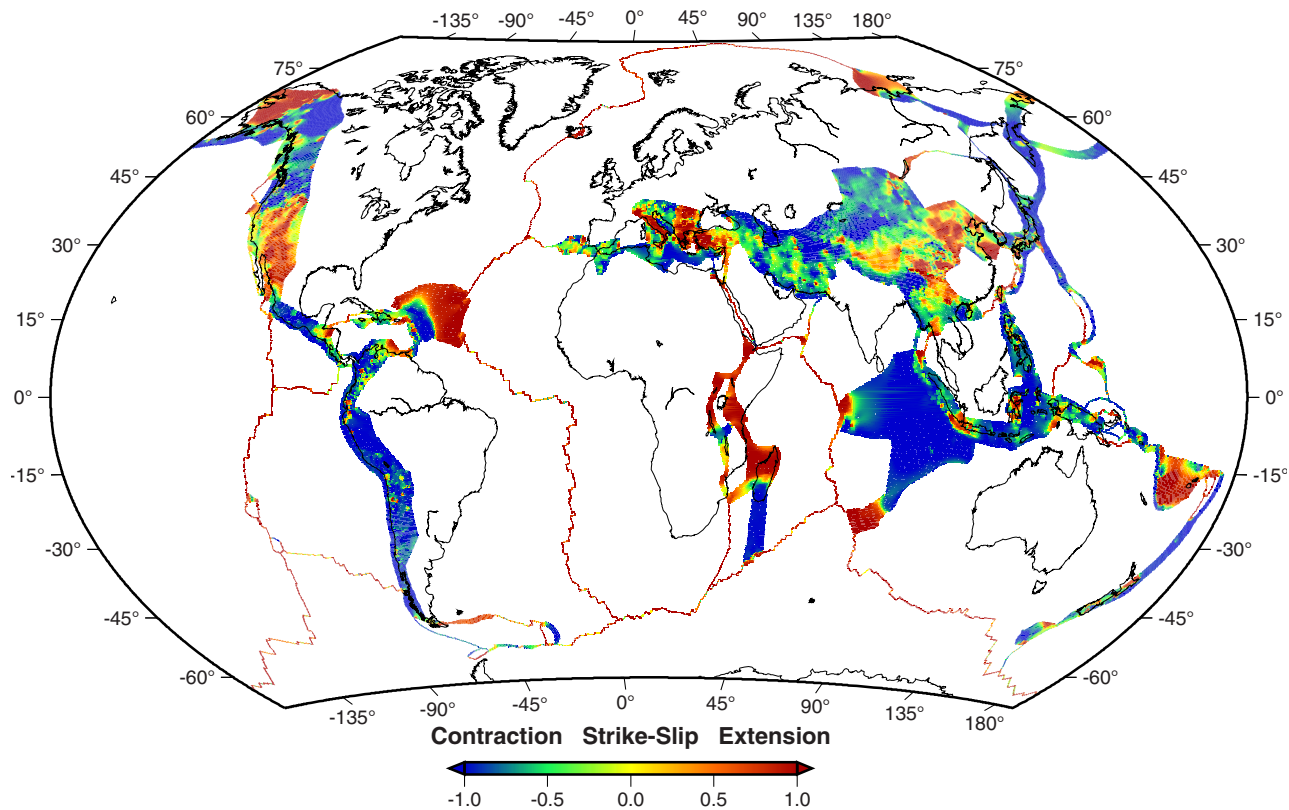


**Figure 5.** A measure of the style of the strain rate tensor, after averaging the grid-averaged strain rate values over an area up to two cells away from the cell considered. The style is defined as  $(\dot{\varepsilon}_1 + \dot{\varepsilon}_2)/\max(|\dot{\varepsilon}_1|, |\dot{\varepsilon}_2|)$ , with  $\dot{\varepsilon}_1$  and  $\dot{\varepsilon}_2$  the largest and smallest eigenvalue, respectively.

et al., 2003]) and with the latest geologic model (MORVEL [DeMets et al., 2010]). Results are shown in the supporting information Figure S4.

There are three reasons for expected differences between our plate motion estimates and the most recent geodetic studies [Argus et al., 2010; Altamimi et al., 2012]. First, those studies estimated a translation rate of the reference frame origin while estimating plate motions. The reason for this practice is the uncertainty in the actual translation rate of the origin of recent ITRF models. In ITRF the origin is defined as the center of mass of the Earth, oceans, and atmosphere as estimated by satellite laser ranging (SLR), which is not only uncertain but is also inconsistent with the idea that surface motions should be referenced relative to the center of mass of the solid Earth [Argus, 2007; Argus et al., 2010]. While the estimation of the translation rate in plate motion studies is important in a holistic view of global kinematics and in studies reliant on vertical motion estimates (e.g., GIA and sea-level rise), it does not affect relative plate motions or the plate boundary velocity gradient field in the same way as it affects individual plate motions in a global reference frame [Argus et al., 2010]. Ignoring the translational frame velocity will add uncertainty to our angular plate velocities but not to the strain rate field.

The second reason why our and previous plate motion estimates may differ is that previous studies typically exclude stations in the near-field of the GIA signal while ignoring the fact that stations in the farfield may be affected by a GIA-related translation. This practice may lead to anomalous velocity gradients between the rigid plate's motion and its plate-bounding deforming zones (see discussion of North American plate section 5). The third reason for differences is that previous studies may have ignored observations that stations in the farfield of large earthquakes may be affected by postseismic deformation (see e.g., discussion of Indian plate in section 5).

For some of the plates unaffected by GIA or long-ranging far-field postseismic effects, i.e., Australia, Africa, and Antarctica, our angular velocities (relative to Pacific) are consistent with previous geodetic estimates. To a lesser extent this is also true for Somalia and South America, for which our pole location is a few degrees southward from previous geodetic estimates. We also find agreement for Eurasia, because our data coverage (for estimating the angular velocity) is generally the same as in prior studies and away from

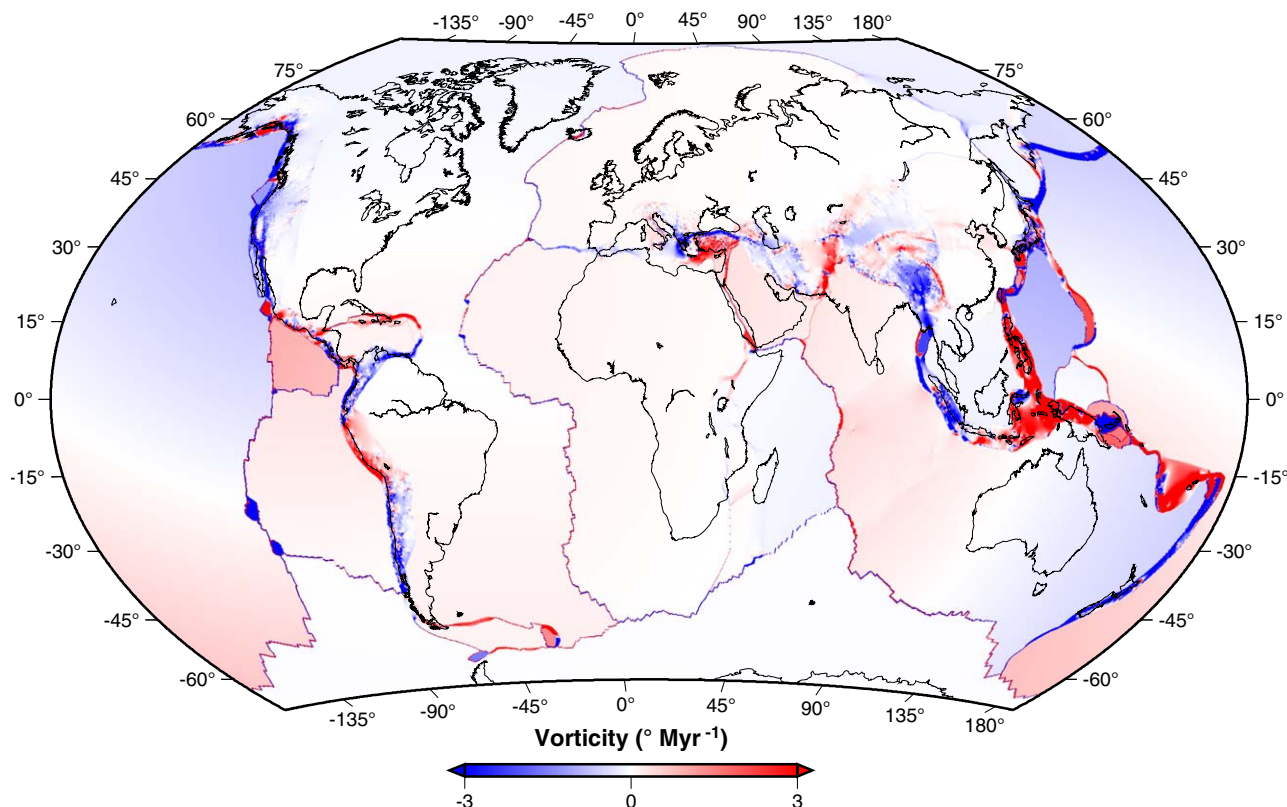


**Figure 6.** Vorticity associated with the velocity gradient tensor field (positive is counterclockwise). To also show the vorticity associated with rigid-body rotations, we chose the reference frame of Kreemer [2009] relative to the subasthenospheric mantle. Scale is saturated.

Fennoscandia. Our result for Amur agrees with the official ITRF2008 estimate [Altamimi *et al.*, 2012]. Any differences for most of the other plates can likely be ascribed to how we handle the effect of GIA (North America (see section 5)) and postseismic transients (Sunda), and/or due to inferior prior data coverage (Arabia, Caribbean, Sunda). Statistically, our estimate for India matches previous geodetic estimates, but our estimate is systematically offset. As discussed in section 5, for Nazca we do not use the velocity for Easter Island and instead include the campaign velocities on San Felix and Robinson Crusoe islands. As result, our angular velocity is systematically different from previous geodetic studies.

Compared to the MORVEL geologic model, our angular velocities relative to Pacific differ significantly for all plates for which MORVEL did only use geologic data. This finding resonates the conclusion of Argus *et al.* [2010] that geodetic estimates differ significantly from the NUVEL-1A geologic model [DeMets *et al.*, 1994]. Our result suggests that the large improvement of MORVEL over NUVEL-1A (including the use of the 0.78 Ma anomaly over the 3.16 Ma anomaly where possible) does not alter the observation that present-day motions differ from those over the most recent geologic time. The only two plates for which our estimate match the MORVEL result are the Philippines Sea and Yangtze, which were based on GPS data in MORVEL. For the two other plates for which MORVEL used GPS data (Amur and Sunda), our result is close to be consistent. Our rotation rate for Nazca is significantly slower than the MORVEL estimate, indicating the continued slow-down of the Nazca plate since 0.78 Ma [DeMets *et al.*, 2010]. The Euler pole for Eurasia is consistent with MORVEL's pole, but MORVEL's rate is  $>0.05^\circ \text{ Myr}^{-1}$  slower.

The fact that we find geodetic plate angular velocities to differ from the MORVEL geologic model feeds a persistent question: How constant are plate motions? Much of MORVEL was model based on sea-floor spreading data using the 0.78 Ma magnetic anomaly. Recently, Iaffaldano [2014] found that typically at least 1 Myr needs to pass for plate motions to change significantly due to a torque change. A possible explanation why the present-day and 0.78 Ma averaged angular velocities differ despite Iaffaldano's findings was already offered by himself: that there is significant internal plate deformation that would particularly affect plate-pairs involving long plate circuits. Indeed, DeMets *et al.* [2010] found significant nonclosure for a

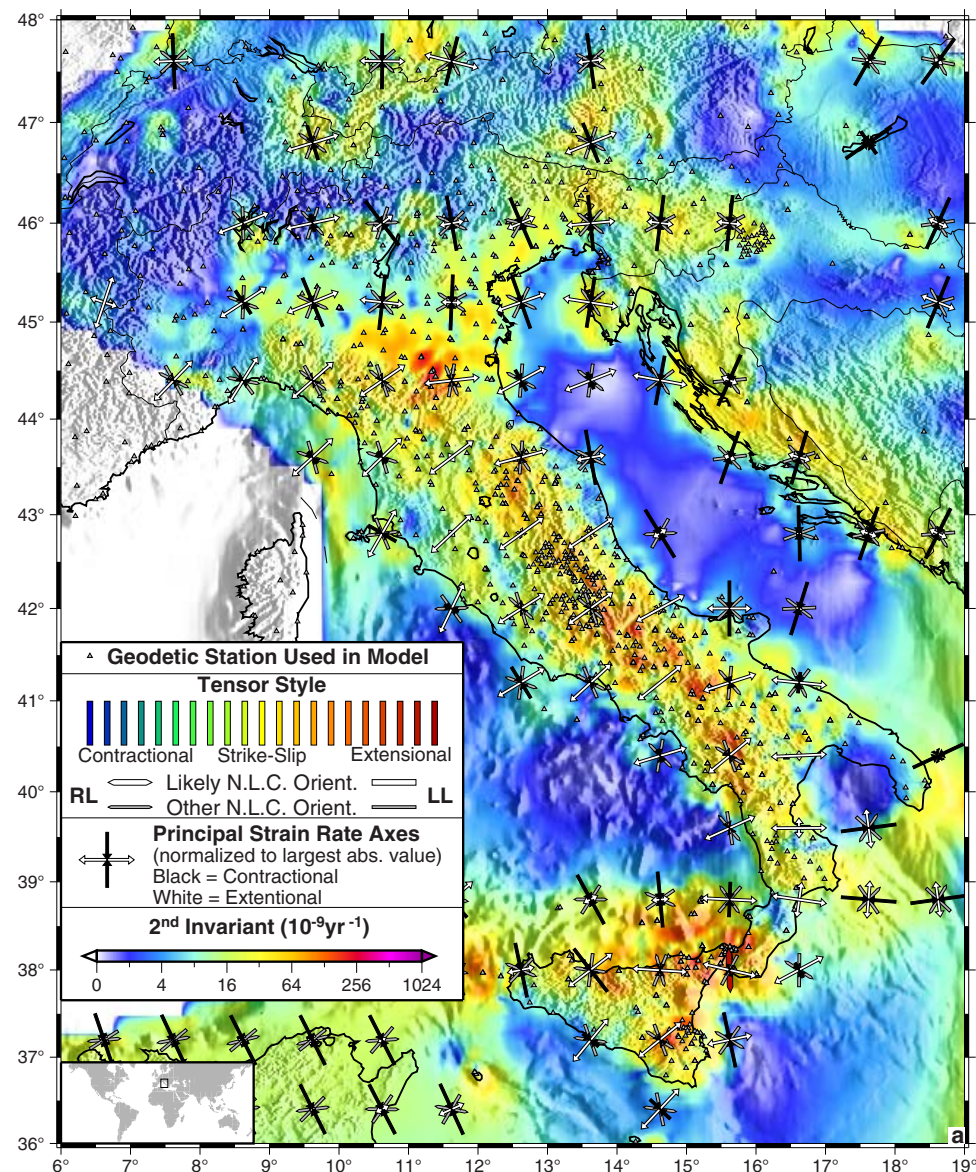


**Figure 7.** Close up results for regions of distributed deformation: (a) Italy, (b) Aegean, (c) Persia, (d) West Tibet, (e) East Tibet, and (f) western United States. A caption is provided in 7a. NLC = no-length-change, RL = right-lateral, LL = left-lateral. Refer to text for more details on what is plotted.

couple of plate-circuits compared to direct observations. A glimpse of the magnitude of internal deformation was recently offered by Kreemer and Gordon [2014] who found that, based on the process of horizontal thermal contraction in the Pacific plate, differential motion between the Pacific-Antarctic Rise and offshore California could be up to  $2.2 \text{ mm yr}^{-1}$ .

### 8.2. Strain Rates

Looking at the second invariant of the GSRM v2.1 globally (Figure 2), there are some obvious differences and similarities when compared to the same quantity for GSRM v1 [Kreemer et al., 2003]. Because of the way we constrain the strain rates to the plate boundaries, the 1st order pattern is the same. Strain rates in the new model along the oceanic ridge-transform systems are, however, considerably higher in the new model, simply because those boundaries are defined more narrowly now (previously they were manually outlined to encompass the seismicity there and now they follow the discrete boundaries of Bird [2003]). Other differences can be ascribed to the introduction of new (micro-)plates. For instance, the strain rate field is now much more

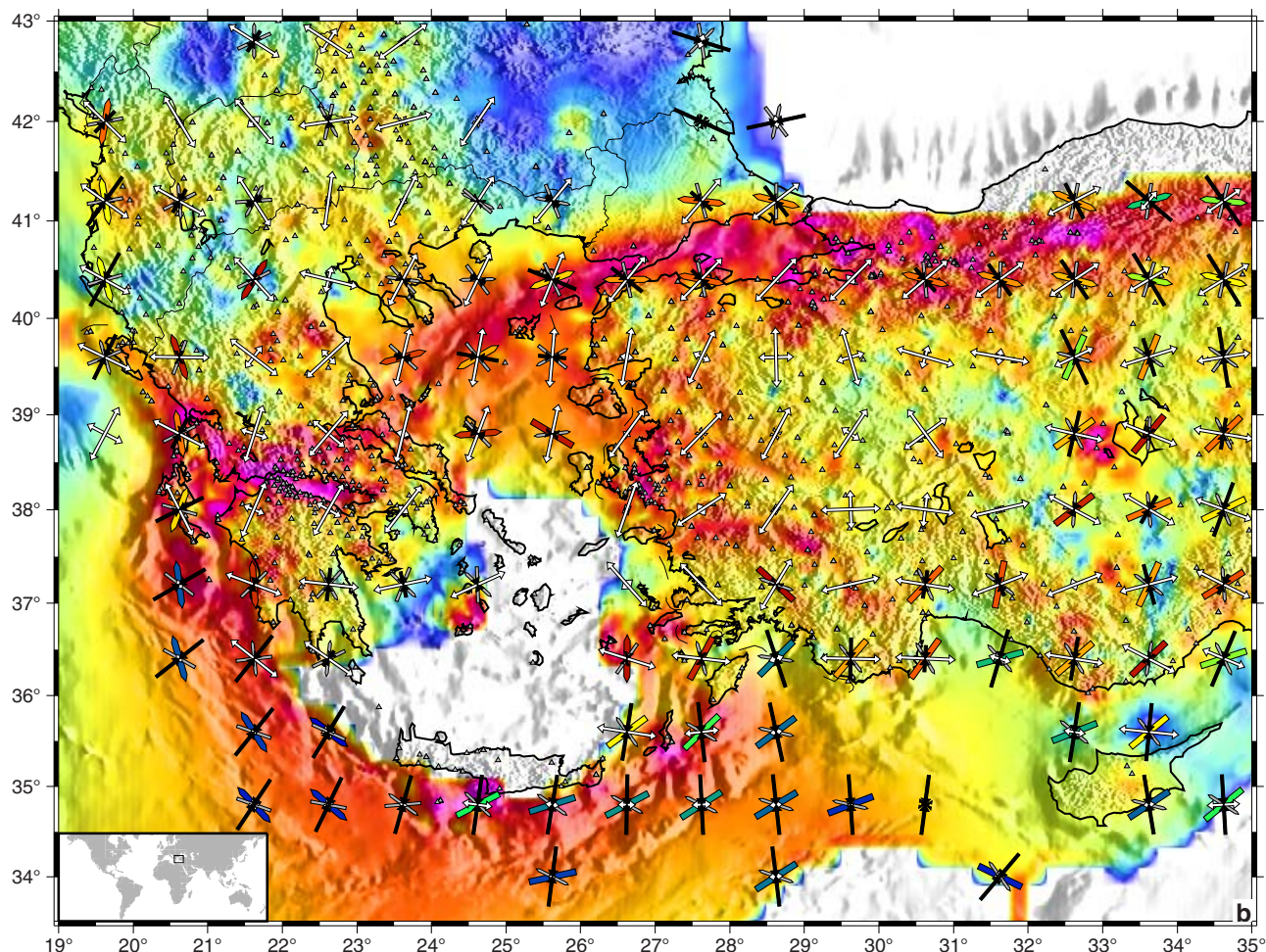


Figure 7. Continued

nuanced along the Africa-Somalia boundary, because of the introduction of several micro-blocks that force the strain rate to be localized along their edges. For subduction zones, such as the Chili Trench, previously strain rates were distributed linearly across the entire Nazca-South America plate boundary, because of the lack of data along most of its boundary. Now with there being many GPS data near the coast, the highest strain rates are clearly constrained to the offshore areas. While much of the onshore strain rates may still be elastically recovered in a future earthquake, the strain rate distribution in the new GSRM much better follows the observed distribution of seismicity.

The previous GSRM included Quaternary fault slip rates for central and east Asia in order to add more constraints on the distribution/localization of strain rate, which was otherwise ill-constrained by the relatively few GPS velocities there. Here without those constraints, GSRM v.2.1 clearly delineates zones of high strain rates along the area's major faults (Figures 2, 7d, and 7e): Main Boundary Thrust, Altyn-Tagh, Haiyan, Xian-shuihe/Xiaojiang, Kunlun, and Sagaing faults. Away from the Himalayas, the area with highest strain rates in Asia is around the Pamir, due to localized shortening [Mohadjer *et al.*, 2010; Ischuk *et al.*, 2013]. Earlier models of strain rate from an already rather dense GPS velocity field in Asia [e.g., Zhu *et al.*, 2006; Gan *et al.*, 2007; Wu *et al.*, 2011; Zhu and Shi, 2011] had limited resolution and did not necessarily identify all (if any) of the strain features described above. A shortcoming of those models was that they were exclusively limited to the territory of China and did not consider any data collected by scientists from outside China. Large areas in and around Tibet still suffer from relatively low data coverage and thus poor model resolution at the spatial resolution GSRM v.2.1 aims for. Future measurements could make a profound impact there. Nevertheless, for those areas in Tibet that are reasonably well covered, the strain rate seems to be distributed rather evenly and transtensional in style (with the extensional axes oriented ESE) (Figure 5 and 7e).

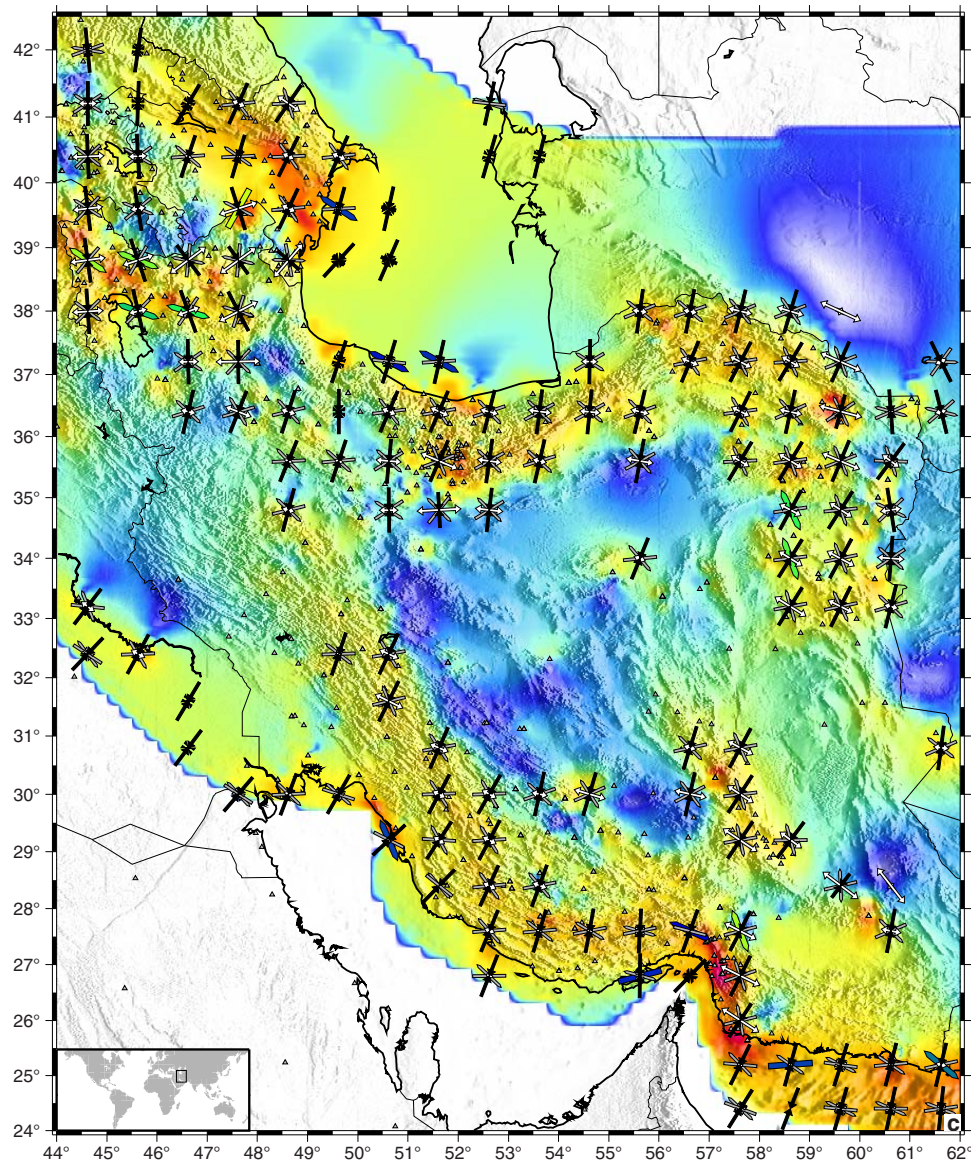


Figure 7. Continued

One area where strain rates are now much better resolved compared to the previous GSRM is Iran. This can be attributed to the large number of GPS campaigns performed by French and Iranian scientists ([Tatar *et al.*, 2002; Nilforoushan *et al.*, 2003; Vernant *et al.*, 2004a, 2004b; Bayer *et al.*, 2006; Masson *et al.*, 2007] in addition to the more recent studies listed in Appendix A). The strain rate field in Iran (Figure 7c) clearly shows that strain is localized in the north and south, with very low strain rates in central Iran. A similar result was found in a recent model by Masson *et al.* [2014], based on fewer data (from Nocquet [2012]). A main difference between the two models is that we also found elevated strain rates in eastern part of the country because of the new data there [Mousavi *et al.*, 2013; Walpersdorf *et al.*, 2014]. We found significant strain localization across the North Tabriz Fault in northwestern Iran, consistent with previous geodetic studies [Djamour *et al.*, 2011; Karimzadeh *et al.*, 2013], and the Minab-Zendan-Palami fault zone in the southeast [Peyret *et al.*, 2009]. Just to the north of Iran, in Azerbaijan, high strain accumulation occurs across the West Caspian Fault, based on the original findings by Aktuğ *et al.* [2013b] and Kadirov *et al.* [2012].

Another area that really benefited from an enormous increase in GPS measurements over the last decade is Italy (Figure 7a). In contrast to the previous GSRM, a zone of NE-SW oriented extension along the Apennines is now a prominent feature. While previous studies have used the new GPS data to estimate strain rates for

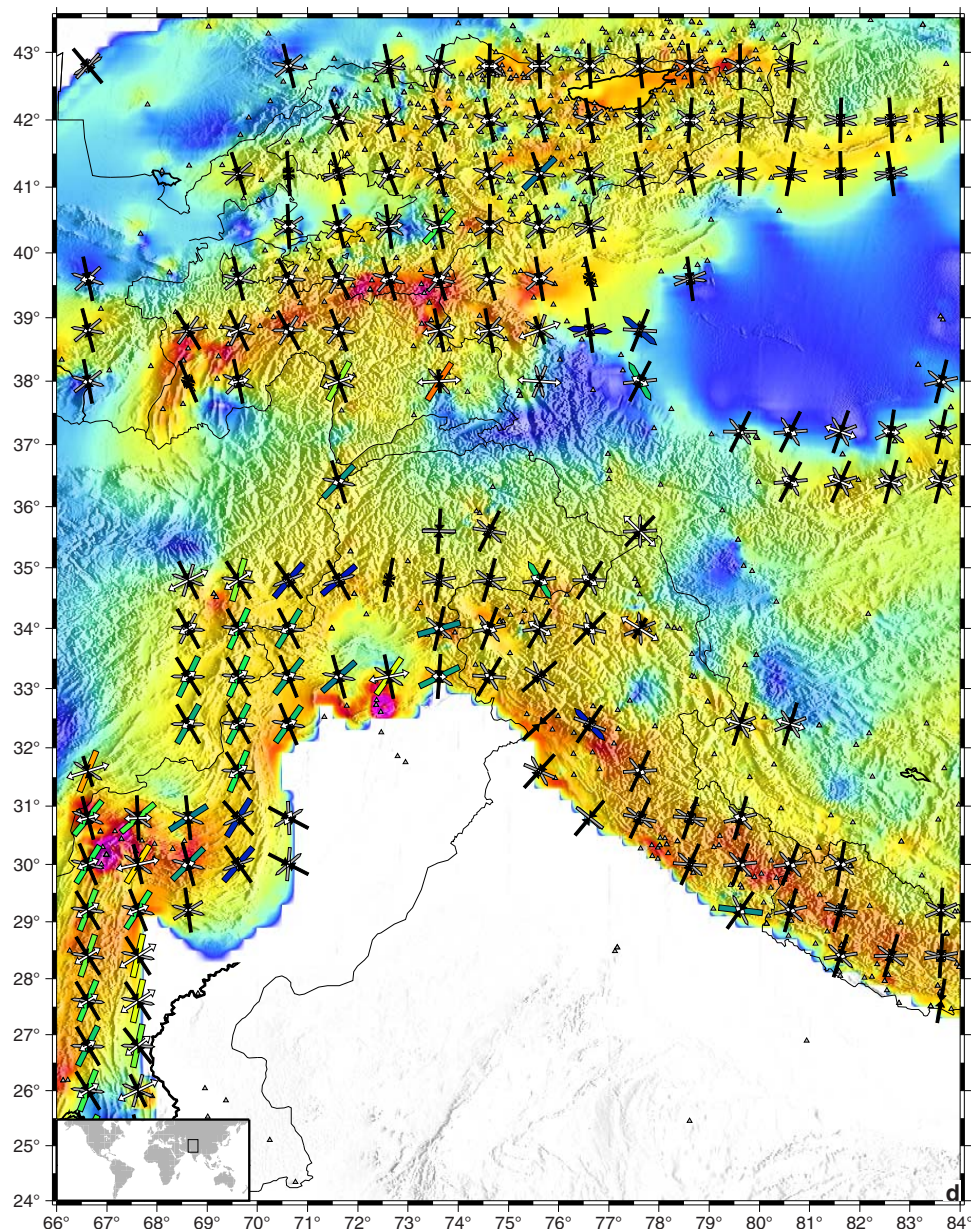


Figure 7. Continued

smaller regions [Pesci *et al.*, 2010; Serpelloni *et al.*, 2010; D'Agostino *et al.*, 2011a; Cenni *et al.*, 2012; Galvani *et al.*, 2012; Palano *et al.*, 2012; D'Agostino, 2014], our model is the first to show the deformation field across the entire peninsula in a comprehensive manner, adding much more detail to the earlier models by Devoti *et al.* [2011] and Caporali *et al.* [2009]. The counterpart to the extensional zone along the Apennines is the consistent zone of NNE-to-N oriented shortening from the Dinarides to northeastern Italy. Both features can be explained by the motion of Adria, which appears as a very low straining area. Extensional strain rates in southern Italy, along the Calabrian Arc, are oriented east-west, presumably due to the retreat of the Ionian subduction zone to its southeast [D'Agostino *et al.*, 2011b; Palano *et al.*, 2012].

### 8.3. Dilatational Strain Rates

The total area growth for our model is  $0.1038 \text{ m}^2 \text{ s}^{-1}$ , while it is only  $0.0987 \text{ m}^2 \text{ s}^{-1}$  for a strain rate model that is entirely based on the boundary conditions imposed by rigid plate motions. Also, the latter model predicts only 22% of the surface area of plate boundary zones to have a positive dilatation, compared to

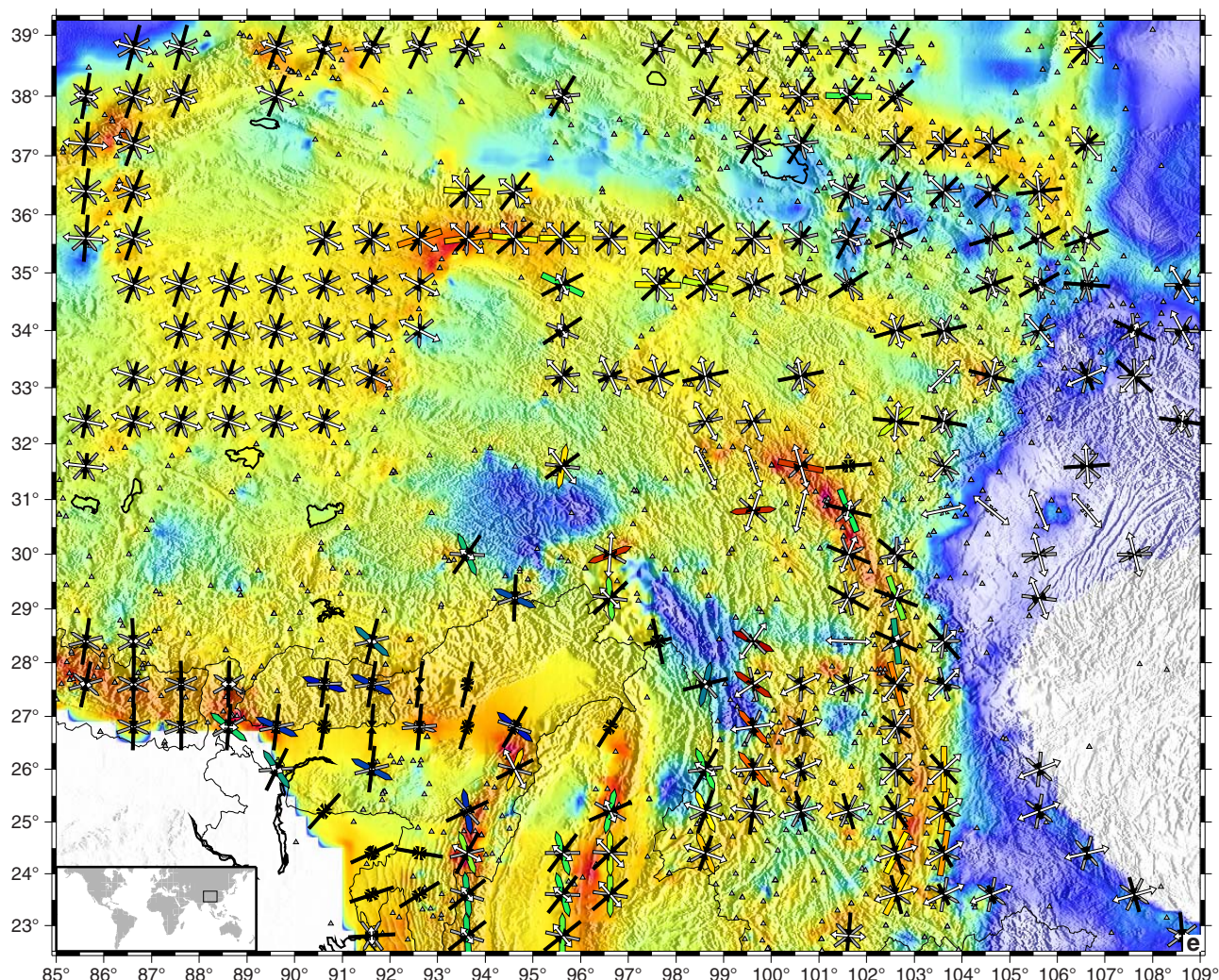


Figure 7. Continued

the 28% of our model. For comparison, *Bird* [2003] calculated an areal growth of  $0.1079 \text{ m}^2 \text{ s}^{-1}$ , which is substantially larger than our estimate (for a case when just using the relative motion between rigid plates only, as he did). This can be explained by the fact that we excluded several of the fast moving micro-plates that were in the model by *Bird* [2003]. Our model indicates that  $0.014 \text{ m}^2 \text{ s}^{-1}$  of areal growth cannot be explained by plate motions. This area growth, about 1 percent of the global total, occurs in zones of continental extension (e.g., in Tibet, Aegean, and Basin and Range of western United States). This number should, however, be considered an upper-bound as the model also contains zones of artificial dilatation (in a spatially rapidly alternating pattern of positive and negative dilation) along strike-slip zones. This pattern can be ascribed as an artifact of inferring the strain rate field from a heterogeneous GPS station network [*Baxter et al.*, 2011; *Titus et al.*, 2011].

#### 8.4. Vorticity Rates

We present the first global vorticity rate map (Figure 6). Vorticity rate patterns within the deforming zones highlight several previously documented along-strike rotation reversals along subduction margins: Ecuador [*Nocquet et al.*, 2014], Arica Bend in Bolivia [*Allmendinger et al.*, 2005], and Hellenic Arc [*Duermeijer et al.*, 2000]. Because positive (negative) vorticity corresponds directly to sinistral (dextral) shear, an along-strike vorticity change in many (if not all) cases may reflect a simple change in the sense of strain partitioning due to the change in orientation of the margin. Other clear examples of this effect are the Caribbean, Sunda, and South Sandwich Arcs.

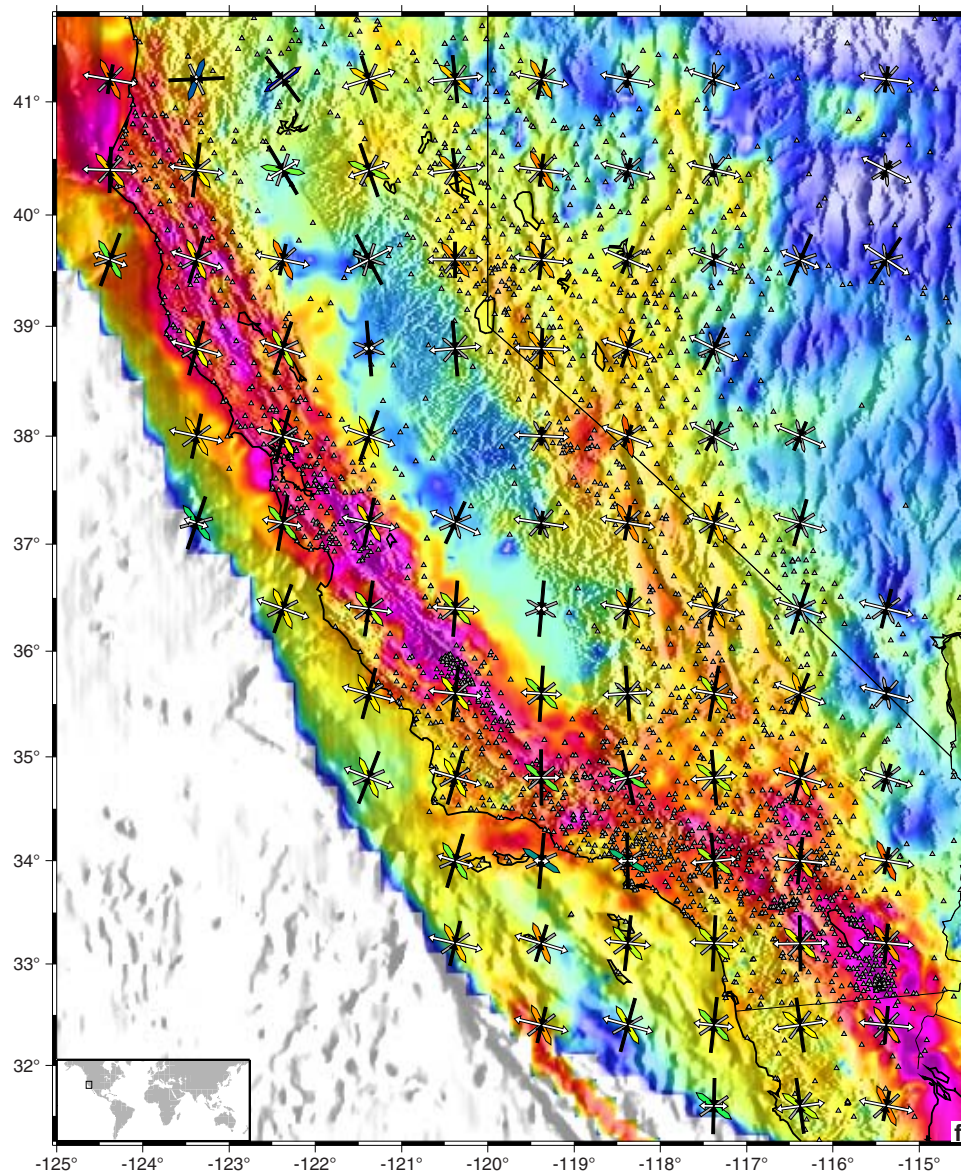


Figure 7. Continued

Within zones of distributed deformation, the vorticity pattern shows the clear differentiation between the anticlockwise rotation around the western Himalayan Syntaxis and the clockwise rotation around the eastern Himalayan Syntaxis. In southeast Asia, the northern arm of Sulawesi shows a distinct clockwise rotation in a region that is otherwise dominated by anticlockwise rotations.

Where a rapidly rotating area is bounded by an area that is nearly fixed, we see a shear zone with an opposite sense of rotation; i.e., The North Anatolian Fault between Anatolia and Eurasia, and the Xianshuihe/Xiaojiang Fault between the eastern Himalayan Syntaxis and the Yangtze micro-plate.

### 8.5. Geodetic Moment Rates

From a hazard perspective, the strain rates provide an important constraint on expected seismic activity, but only after the strain rates are converted to appropriate ('tectonic' or 'geodetic') moment rates. The largest uncertainties in this conversion are in the associated seismogenic thickness and in the 'coupling', that is the percentage of the geodetic strain rates that will be released seismically. *Bird and Kagan [2004]* determined the combined average value of those two factors for all areas of a similar tectonic regime and termed it the "average coupled thickness."

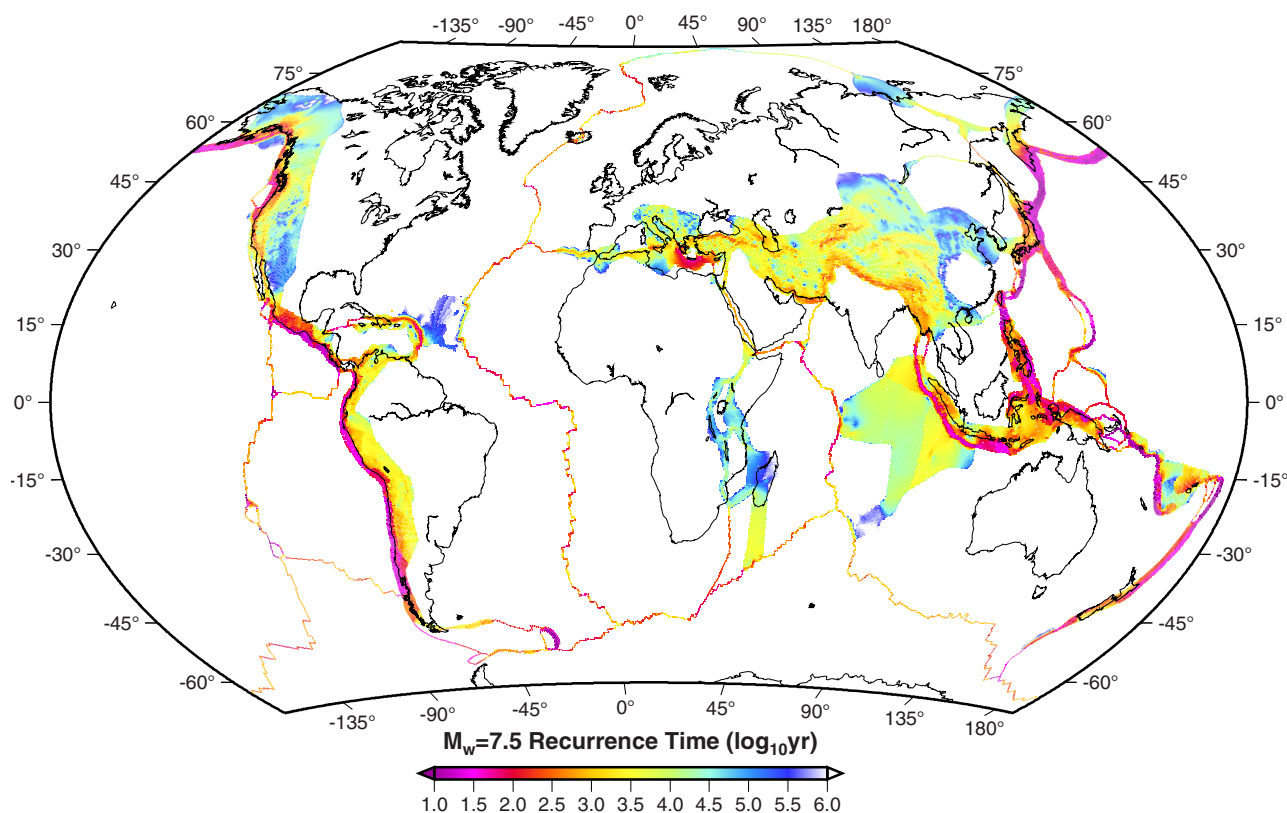


**Figure 8.** Log<sub>10</sub> of the recurrence time of an  $M_w = 7.5$  earthquake, when the geodetic moment is released by a single ("characteristic") event, but considering an average seismic coupling for the appropriate plate boundary type (through the use of an "effective averaged coupled thickness" in the strain rate to moment rate conversion). See text for more explanation.

Depending on whether seismic moment release follows a Gutenberg-Richter relationship or is concentrated in a single characteristic earthquake, the tectonic moment rate can be converted to a forecast of number of events above a certain moment or to a recurrence time for a certain characteristic moment, respectively. The former analysis was performed by *Bird et al.* [2010] and an update using the results of GSRM v.2.1 has been submitted for publication (P. Bird and C. Kreemer, Revised tectonic forecast of global shallow seismicity based on version 2.1 of the Global Strain Rate Map, submitted to *Bulletin of the Seismological Society of America*, 2014) and testing. To fit the number of observed events in a test period, empirical factors were introduced for different tectonic regime, and those factors are incorporated into an 'effective' averaged coupled thickness.

Here we present the recurrence time of a characteristic earthquake with chosen  $M_w = 7.5$  (Figure 8). To convert the strain rates to tectonic moment rates, we use the effective averaged coupled thickness values of *Bird and Kreemer* (submitted manuscript, 2014) (P. Bird, personal communication, 2014) (supporting information Figure S5), as well as a shear modulus specific to the tectonic regime. The style of the strain rate tensor was used to come up with a weighted effective averaged coupled thickness given any mixture of tectonic regimes expressed in the tensor. Because the length of a fault hosting an  $M_w = 7.5$  does not fit in any of our grid cells, the moment was calculated for an enlarged area that fits such fault length. While we acknowledge the wide range in magnitude-scaling relationships [*Stirling et al.*, 2013], for the purpose of this exercise we used those of *Leonard* [2010]. Although we distinguished between relationships for strike-slip and dip-slip events, we found this to make insignificant difference for our result.

Any location in some subduction zones would have  $M_w = 7.5$  recurrence times of approximately 1 year. This being unobserved, a characteristic earthquake, if present, would likely be larger there. For most other areas the recurrence time is longer than the recorded seismic history. The significance of this is that, unless we can convincingly accept Gutenberg-Richter relationship for any of the slowly deforming areas, a large earthquake with a (very) long return time cannot be dismissed. An example of this may be the southern Basin and Range Province of northern Sonora (Mexico) and southern Arizona (USA). An  $M_w = 7.5$  event occurred

there in 1887, in an area that has otherwise extremely low seismicity (with the exception of some ongoing aftershocks) [Castro *et al.*, 2010; Lockridge *et al.*, 2012]. We find the recurrence time in this area to range from 100 to 200 kyr, which happens to be same time period as has been found between the 1887 event and the penultimate event on the same fault [Bull and Pearthree, 1988].

## 9. Conclusion

GSRM v.2.1 is a vast improvement over GSRM v.1.2 in terms of data input and in a factor of ~2.5 increase in spatial model resolution in areas with dense data coverage. The recent surge in GPS data densification is likely to continue. About half of all studies included in our compilation were published since 2010 and the time series of thousands of additional CGPS stations will mature over the next few years. However, only at a few places is the data input sufficient to obtain well-constrained strain rates at the resolution of the underlying grid. In the future we are considering to use a dynamic grid that has the grid size adjusted to the station spacing, so that no computational power is wasted and no high-resolution model is presented at places where the data are insufficient. Given the increasing coverage of CGPS stations on some rigid plates (mainly due to Continuously Operating Reference Station (CORS) deployment by commercial and governmental agencies), it is inevitable that those areas will be included in future iterations of the GSRM. The strain rates there are expected to be at or below the uncertainty in the GPS velocity data and these areas will thus require special treatment.

## Appendix A: Studies Used in GPS Compilation and the Region Concerned

- Ader *et al.* [2012]—Nepal, Himalayas, northern India, southern Tibet  
Aktuğ and Kılıçoglu [2006]—western Turkey, Karaburun Peninsula  
Aktuğ *et al.* [2009]—western Turkey  
Aktuğ *et al.* [2013a]—central Turkey, Anatolian plate  
Aktuğ *et al.* [2013b]—Azerbaijan, Caucasus  
Aktuğ *et al.* [2013c]—Eastern Turkey, North and East Anatolian faults  
Almuselmani *et al.* [2008]—Saudi Arabia  
Alvarado *et al.* [2011]—El Salvador, Honduras, Nicaragua  
Alvarado *et al.* [2014]—Ecuador, Quito  
Antonelis *et al.* [1999]—Baja California, Mexico  
Apel *et al.* [2006]—eastern Siberia, Kamchatka, Amurian plate  
Árnadóttir *et al.* [2006]—southwest Iceland, Reykjanes Peninsula  
Árnadóttir *et al.* [2009]—Iceland  
Ashurkov *et al.* [2011]—eastern Siberia, Amurian plate  
Aurelio [2001]—Mindanao, southern Philippines  
Avallone *et al.* [2004]—central Greece, Corinth Gulf  
Avé Lallement and Oldow [2000]—Aleutian Arc  
Ayhan *et al.* [2002]—northwestern Turkey, Marmara Sea  
Bacolcol *et al.* [2005]—Masbate Island, central Philippines, Philippine Fault  
Banerjee *et al.* [2008]—India, southern Tibet, Himalayas  
Beavan *et al.* [1999]—central Southern Alps, New Zealand, Alpine Fault  
Beavan and Haines [2001]—New Zealand  
Béjar-Pizarro *et al.* [2013]—northern Chile  
Benford *et al.* [2012]—Jamaica, Gôname microplate  
R. Bennett (personal communication, 2013)—Italy, Dinarides, Serbia  
Bennett *et al.* [2012]—Italy, northern Apennines  
Bergeot *et al.* [2009]—New Hebrides, Vanuatu  
Bettinelli *et al.* [2006]—Nepal, Himalayas, southern Tibet  
Bock *et al.* [2003]—Indonesia  
J. Bogusz (personal communication, 2012)—Poland  
Brooks *et al.* [2003]—central Chile, Andes  
Brooks *et al.* [2011]—Bolivia, Andes, Altiplano  
Calais *et al.* [2006a]—Central Asia, Baikal rift, Amurian plate  
Calais *et al.* [2010]—Hispaniola, Haiti, Dominican Republic

- Calmant et al.* [2003]—New Hebrides, Vanuatu  
*Caporali et al.* [2009]—Italy, Alpes, Dinarides, Pannonian Basin  
*Catherine et al.* [2014]—Andaman Islands  
*Cenni et al.* [2012]—central and northern Italy  
*Chalouan et al.* [2014]—Morocco, southern Rif Cordillera  
*Chang et al.* [2006]—Utah, Wasatch Fault  
*Chen et al.* [2013]—southeastern Taiwan, Longitudinal Valley  
*Ching et al.* [2011]—Taiwan  
*Ching et al.* [2007]—southwestern Taiwan  
*Chiu* [2010]—northern Taiwan, Taipei  
*Chlieh et al.* [2011]—Bolivia, southern Peru, northern Chile, central Andes, Altiplano  
*Chousianitis et al.* [2013]—central Greece, Corinth Gulf  
*Cisneros and Nocquet* [2011]—Ecuador  
*Clarke et al.* [1998]—north central Greece  
*Cocard et al.* [1999]—southern Greece, Crete, Peloponnese  
*Correa-Mora et al.* [2009]—El Salvador, Honduras, Nicaragua  
*Crowell et al.* [2013]—San Andreas Fault, Salton Trough  
*D'Agostino et al.* [2008]—Italy, Alpes, Dinarides  
*D'Agostino et al.* [2011a, 2011b]—southern Italy, southern Apennines, Calabria, Sicily  
*D'Agostino* [2014]—Italy, Apennines  
*Darby and Beavan* [2001]—southernmost North Island, New Zealand  
*Denys et al.* [2014]—southeast South Island, New Zealand  
*Devoti et al.* [2011]—Italy  
*Dietrich et al.* [2004]—Antarctic Peninsula  
*Djamour et al.* [2010]—northern Iran, Alborz Mountains  
*Djamour et al.* [2011]—northwest Iran  
*Dogru et al.* [2014]—western Turkey, Karaburun Peninsula  
*Drewes and Heidbach* [2012]—South America  
*Duquesnoy et al.* [1994]—central Philippines, central Philippine Fault  
*Echeverria et al.* [2013]—southern Spain, eastern Betics  
*Elliott et al.* [2010]—southeast Alaska  
*Elliott et al.* [2013]—southeast Alaska  
*Feng et al.* [2012]—Costa Rica, Nicoya Peninsula  
*Fernandes et al.* [2004]—Azores  
*Fernandes et al.* [2013]—East African Rift, Victoria micro-plate  
*Floyd et al.* [2010]—western Turkey  
*Franco et al.* [2012]—Guatemala, El Salvador, Mexico  
*Freymueller et al.* [1999]—northern California, San Andreas Fault  
*Freymueller et al.* [2008]—Alaska  
*Gahalaut et al.* [2013]—northeast India, Indo-Burmese Range  
*Galgana et al.* [2007]—northern Philippines, Luzon  
*Galvani et al.* [2012]—central Italy, central Apennines  
*Genrich et al.* [2000]—Sumatra, Indonesia  
*Gomez et al.* [2007]—Lebabon, Dead Sea Fault  
*Hammond and Thatcher* [2004]—Basin and Range, USA  
*Hammond and Thatcher* [2005]—northwest Basin and Range, USA  
*Hammond and Thatcher* [2007]—western Basin and Range, Walker Lane, USA  
*Hashimoto et al.* [2009]—northern Japan, northern Honshu, Hokkaido  
*He et al.* [2013]—China, Altyn Tagh Fault  
*Hessami et al.* [2006]—southern Iran, Zagros Mountains  
*Hilley et al.* [2009]—China, Altyn Tagh Fault  
A. Holland (personal communication, 2012)—Arizona, USA  
*Hollenstein et al.* [2003]—Sicily  
*Hreinsdóttir et al.* [2001]—southwest Iceland, Reykjanes Peninsula

- Hsu et al.* [2009]—southern Taiwan  
*Hsu et al.* [2012]—eastern Taiwan  
*Hu et al.* [2007]—southwestern Taiwan  
*Ihemedu* [2012]—Puerto Rico, Virgin Islands  
*Iinuma et al.* [2004]—Costa Rica, Nicoya Peninsula  
*Ischuk et al.* [2013]—Pamir, Hindu Kush  
*Jade et al.* [2004]—southern Tibet, northwest India  
*Jade et al.* [2007]—northeast India, Shillong Plateau, Indo-Burmese Range  
*Jansma and Mattioli* [2005]—Puerto Rico, Virgin Islands  
*Jiang et al.* [2009]—Antarctic Peninsula  
*Jin et al.* [2006]—South Korea  
*Jouanne et al.* [2011]—northern Venezuela, El Pilar Fault  
*Jouanne et al.* [2012]—Albania  
*Kadirov et al.* [2012]—Azerbaijan, eastern Caucasus  
*Karakhanian et al.* [2013]—Armenia, lesser Caucasus  
*Kato et al.* [2003]—Mariana Islands  
*Keiding et al.* [2008]—southwest Iceland, Reykjanes Peninsula  
*Kendrick et al.* [2003]—Galapagos Islands  
*Kierulf et al.* [2013]—Norway  
*Klotz et al.* [2001]—Chile, Argentina, central and southern Andes  
*Kogan et al.* [2012]—Ethiopia, Afar, East African Rift  
*Kotzev et al.* [2006]—Bulgaria, Rhodope Mountains  
*Koulali et al.* [2011]—Spain, Morocco, Betics Mountains, Rif Mountains  
*Kuo et al.* [2008]—Taiwan  
*LaFemina et al.* [2005]—south-central Iceland  
*LaFemina et al.* [2009]—Nicaragua, Costa Rica, Panama  
*Le Beon et al.* [2008]—Israel, Jordan, Dead Sea Fault  
*Liang et al.* [2013]—China, Tibet  
*Lidberg et al.* [2010]—Sweden, Scandinavia  
*Liu et al.* [2010]—southern Japan  
*López et al.* [2006]—Caribbean Plate, Lesser Antilles  
*Lukhnev et al.* [2010]—Western Mongolia, southern Siberia, Baikal Rift  
*Mahanta et al.* [2012]—north-east India, Kopili Fault  
*Mahesh et al.* [2012]—Indian plate  
*Mahmoud et al.* [2013]—eastern Turkey, Eastern Anatolia Fault, Dead Sea Fault  
*Manaker et al.* [2008]—Hispaniola, Puerto Rico, Lesser Antilles  
*Marjanović et al.* [2012]—Croatia, Slovenia, Italy, Adriatic Sea  
*Marques et al.* [2013]—Azores  
*Márquez-Azúa and DeMets* [2003]—Mexico  
*Márquez-Azúa and DeMets* [2009]—Mexico  
*Matev* [2011]—southwest Bulgaria, northern Greece, Albania, Macedonia  
*Mattia et al.* [2009]—Italy, northeastern Sicily, Aeolian Islands  
*Maurin et al.* [2010]—Myanmar, Sagaing Fault  
*Mazzotti et al.* [2011]—western Canada  
*Mazzotti et al.* [2005]—eastern Canada, St. Lawrence Valley  
*McCaffrey et al.* [2013]—Pacific Northwest, USA  
*McClusky et al.* [2010]—Eritrea, Ethiopia, Yemen, Saudi Arabia, Afar  
*Medak and Pribicevic* [2006]—Croatia, Zagreb  
*Meilano et al.* [2012]—Indonesia, west Java, Lembang Fault  
*Mendes et al.* [2013]—Azores, São Jorge Island  
*Mendoza et al.* [2011]—southern Chile, Tierra del Fuego, Magallanes-Fagnano Fault system  
*Meng et al.* [2009]—Russia, eastern Siberia, Kamchatka  
*Métois et al.* [2013]—north-central Chile  
*Metzger et al.* [2013]—north Iceland, Tjörnes Fracture Zone

- Miranda et al.* [2012]—Azores, Terceira Island  
*H. Mora* (personal communication, 2012)—Colombia  
*Moreno et al.* [2011]—south-central Chile  
*Mousavi et al.* [2013]—north-east Iran, Kopeh Dagh  
*Mukul et al.* [2010]—northeast India, Shillong Plateau, Indo-Burmese Range  
*Müller et al.* [2013]—Greece, Aegean  
*Mullick et al.* [2009]—north-east India, eastern Himalayas  
*Nguyen et al.* [2013]—Vietnam, Red Sea Fault  
*Nishimura* [2011]—southern Japan, Ryukyu Islands  
*Nugroho et al.* [2009]—Indonesia, Banda Arc  
*Ohzono et al.* [2011]—central Japan, Atotsugawa fault system  
*Ozener et al.* [2013a]—Turkey, North Anatolian Fault Zone  
*Ozener et al.* [2013b]—Turkey, North Anatolian Fault Zone  
*Palano et al.* [2012]—southern Italy, Calabria, Sicily, Aeolian Islands  
*Paul et al.* [2001]—India, Himalayas, Andaman Islands  
*Pérez et al.* [2001]—Venezuela, El Pilar Fault  
*Pérez et al.* [2011]—Venezuela, Bocono Fault  
*Pérez-Peña et al.* [2010]—southern Spain, Betics Mountains  
*Pesci et al.* [2010]—central Italy, central Apennines  
*Peyret et al.* [2009]—southern Iran, Minab-Zendan-Palami fault system  
*Phillips* [2003]—Tonga, Vanuatu, Solomon Islands  
*Plattner et al.* [2007]—Baja California  
*Poland et al.* [2006]—northeast California  
*Ponraj et al.* [2010]—northern India, central Lesser Himalayas  
*Prawirodirdjo et al.* [2010]—Indonesia, Sumatra  
*Protti et al.* [2012]—Cocos Plate  
*Reilinger and McClusky* [2011]—eastern Mediterranean, Middle East, Persia, Arabia, Afar  
*Reilinger et al.* [2006]—eastern Mediterranean, Middle East, Persia, Arabia  
*Rodriguez* [2007]—Trinidad and Tobago  
*Rodriguez et al.* [2009]—Honduras  
*Rontogianni* [2010]—northern Greece  
*Ruegg et al.* [2009]—central Chile  
*Sadeh et al.* [2012]—Israel, Dead Sea Fault  
*Sagiya et al.* [2000]—Japan  
*Saleh and Becker* [2014]—Egypt  
*Saria et al.* [2013]—African and Somalian Plate, East African Rift  
*Sato et al.* [2013]—Japan, offshore Honshu  
*Scheiber-Enslin et al.* [2011]—south-central Iceland  
*Schiffman et al.* [2013]—Pakistan  
*Serpelloni et al.* [2007]—western Mediterranean, Italy, Algeria, Iberia, Morocco  
*Serpelloni et al.* [2010]—southern Italy, Sicily, Aeolian Islands, Calabrian Arc  
*Shen et al.* [2011]—southwestern United States, southern San Andreas Fault System  
Z.-K. Shen (personal communication, 2012)—China, Tibet  
*Shestakov et al.* [2011]—eastern Siberia, Sakhalin Island  
*Shin et al.* [2011]—Taiwan  
*Simons et al.* [2007]—Southeast Asia, Indonesia, Malaysia, Thailand, Philippines  
*Smalley et al.* [2003]—southern Chile, southern Argentina, Tierra del Fuego  
*Smalley et al.* [2007]—Scotia Plate and surroundings  
*Socquet et al.* [2006]—Sulawesi, Indonesia, Palu Fault  
*Sol et al.* [2007]—Eastern Himalaya Syntaxis  
*Spinler et al.* [2010]—southern California, Mojave Desert, USA  
*Stamps et al.* [2008]—East African Rift  
M. Steckler (personal communication, 2012)—Bangladesh  
*Stevens et al.* [2002]—Indonesia, western New Guinea

- C. Subarya (personal communication, 2012)—Indonesia  
*Svarc et al.* [2002]—western Nevada, Walker Lane, USA  
*Szeliga et al.* [2012]—Pakistan, Chaman Fault  
*Tadokoro et al.* [2012]—Japan, offshore Kii Peninsula  
*Tarazi et al.* [2011]—Dead Sea Fault, Jordan, Israel  
*Tatar et al.* [2012]—Turkey, eastern North Anatolia Fault  
*Tavakoli et al.* [2008]—southern Iran, Zagros Mountains  
*Taylor et al.* [2008]—Antarctic Peninsula, South Shetland Islands  
*Tesauro et al.* [2006]—Switzerland  
*Tiryakioğlu et al.* [2013]—southwest Turkey, Isparta Angle  
*Titus et al.* [2011]—Central San Andreas Fault, USA  
*Tran et al.* [2013]—Vietnam, Red Sea Fault  
*Tregoning et al.* [1998a]—Papua New Guinea, Woodlark Plate, South Bismarck Plate  
*Tregoning et al.* [1998b]—Solomon Islands  
*Tregoning* [2002]—Australia, Papua New Guinea  
*Trenkamp et al.* [2002]—Colombia, Ecuador, Panama, Venezuela, north Andes  
*Trenkamp et al.* [2004]—south Colombia  
*Tsai et al.* [2012]—southwest Taiwan  
*Tserolas et al.* [2013]—Greece, western Crete  
*van der Hoeven et al.* [2005]—Romania, southeastern Carpathians  
*Vernant et al.* [2010]—Morocco, Rif Mountains  
*Vigny et al.* [2007]—Djibouti, Afar  
*Wallace et al.* [2004a]—Papua New Guinea  
*Walpersdorf et al.* [2006b]—southern Iran, Zagros Mountains  
*Walpersdorf et al.* [2014]—eastern Iran  
*Wang et al.* [2007]—southern Chile, Nazca Plate  
*Weber et al.* [2001]—Caribbean Plate, Lesser Antilles  
*Weber et al.* [2010]—northeast Italy, Istria Peninsula  
*Weber et al.* [2011]—Trinidad and Tobago  
*Williams et al.* [2006]—northwest California, northernmost San Andreas Fault system, USA  
*Yang et al.* [2008]—Tien Shan Mountains, Pamir, Tarim Basin  
*Yavaşoğlu et al.* [2011]—Turkey, North Anatolian Fault  
*Yoshioka et al.* [2004]—Mexico, Guerrero  
*Yoshioka and Matsuoka* [2013]—southwest Japan  
*Yu and Kuo* [2001]—eastern Taiwan, Longitudinal Valley Fault  
*Yu et al.* [2013]—Philippines, Luzon, Philippine Fault  
*Zubovich et al.* [2010]—Tien Shan Mountains, Pamir, Tarim Basin

## Appendix B

To model the strain rate field as a continuous model, we explicitly assume that the crustal thickness over which the strain rates apply is relatively small compared to the horizontal dimension. We actually model the velocity gradient tensor field, which comprises both strain rates and vorticity. For this, we relate the velocity gradient tensor field to a three-dimensional rotation rate vector  $\dot{W}$  (which intercepts the Earth's center and surface). A continuous velocity field  $v(\hat{x})$  can then be written as:

$$v(\hat{x}) = R[\dot{W}(\hat{x}) \times \hat{x}] \quad (B1)$$

where  $R$  is the Earth's radius, and  $\hat{x}$  is a three-dimensional unit vector for any point on the Earth's surface with latitude  $\theta$  and longitude  $\phi$ :

$$\hat{x} = (\cos\theta\cos\phi, \cos\theta\sin\phi, \sin\theta) \quad (B2)$$

If  $\dot{W}$  is constant over a given area, then (B1) gives the well-known formulation for a rigid body rotation. In fact, we define a rigid plate by enforcing  $\dot{W}$  to be constant (i.e., its spatial derivatives are zero) for part of the grid. For the new GSRM,  $\dot{W}$  is set *a priori* for each plate, using the results in Table 2.

The horizontal strain rates on a sphere can be written using the spatial derivatives of  $\dot{W}$ :

$$\dot{\varepsilon}_{\varphi\varphi} = \frac{\hat{\Theta}}{\cos \theta} \frac{\partial \dot{W}}{\partial \varphi} \quad (B3)$$

$$\dot{\varepsilon}_{\theta\theta} = -\hat{\Phi} \frac{\partial \dot{W}}{\partial \theta} \quad (B4)$$

$$\dot{\varepsilon}_{\varphi\theta} = \frac{1}{2} \left( \hat{\Theta} \frac{\partial \dot{W}}{\partial \theta} - \frac{\hat{\Phi}}{\cos \theta} \frac{\partial \dot{W}}{\partial \varphi} \right) \quad (B5)$$

where  $\Theta$  and  $\Phi$  are the unit vectors in the North and East directions, respectively. In these definitions the contribution of any gradient in vertical velocities is omitted, because it is small.

The rotation rate about a local vertical axis (i.e., vorticity) can be written as:

$$\dot{\omega}_r = \hat{x} \cdot \dot{W} - \frac{1}{2} \left( \frac{\hat{\Phi}}{\cos \theta} \frac{\partial \dot{W}}{\partial \varphi} + \hat{\Theta} \frac{\partial \dot{W}}{\partial \theta} \right) \quad (B6)$$

The rotation vector function ( $\dot{W}$ ) is expanded spatially using bicubic Bessel functions.

The objective function that is minimized in the inversion is:

$$\sum_1^N \left( \dot{\varepsilon}_{ij}^{fit} - \dot{\varepsilon}_{ij}^{obs} \right) \left( \dot{\varepsilon}_{pq}^{fit} - \dot{\varepsilon}_{pq}^{obs} \right) V_{ij,pq}^{-1} + \sum_1^M \left( u_i^{fit} - u_i^{obs} \right) \left( u_j^{fit} - u_j^{obs} \right) C_{ij}^{-1} \quad (B7)$$

where  $ij$ , and  $pq$  denote tensor components of the strain rate tensor. The above equation suggest that “observed” strain rates can also be input, as was done in the previous GSRM, but this option was not used for the current GSRM. In any case, the strain rate variance covariance matrix  $V$  needs to be set. One could set the off-diagonal components of  $V$  such that preferred strain rate direction/style is imposed (as was done in the previous GSRM using earthquake focal mechanisms). However, for the new GSRM we only set the diagonal components of  $V$ , i.e., variances of the three strain rate components (see section 6.1). The second part of (7) pertains to the fit of the  $M$  geodetic velocities, with the data covariance matrix given by  $C$ .

## Acknowledgments

This work was funded by the Global Earthquake Model Foundation, with additional support from the National Science Foundation (EAR-0911754 to CK and EAR-1252210 to GB) and NASA (NNX12AK26G to GB and CA-NCA-NNX10AF07A-S1 to CK and GB). We thank D. Argus and an anonymous reviewer for suggestions that greatly improved the paper. D. Argus is also thanked for help in comparing 3-D covariance ellipses, and Z. Altamimi is thanked for providing the ITRF2008 covariance matrix. The GPS analysis would not have been possible without the efforts of the International GNSS Service and all GPS network investigators for network maintenance and for, together with the data archives, making data freely available. In particular, we thank the following networks/archives: AFREF; Alabama Department of Transportation (DOT) CORS network, USA; Albuquerque Real Time GNSS Network, USA; Arpa Piemonte, Italy; Asia Pacific Crustal Monitoring System; AZGPS, USA; BANIAN, New Caledonia; BARD, USA; Bureau of Meteorology, Australia; Canary GNSS Center; CDDIS, USA;

## References

- Ader, T., et al. (2012), Convergence rate across the Nepal Himalaya and interseismic coupling on the Main Himalayan Thrust: Implications for seismic hazard, *J. Geophys. Res.*, 117, B04403, doi:10.1029/2011JB009071.
- Aktuğ, B., and A. Kılıçoğlu (2006), Recent crustal deformation of İzmir, Western Anatolia and surrounding regions as deduced from repeated GPS measurements and strain field, *J. Geodyn.*, 41(5), 471–484, doi:10.1016/j.jog.2006.01.004.
- Aktuğ, B., et al. (2009), Deformation of western Turkey from a combination of permanent and campaign GPS data: Limits to block-like behavior, *J. Geophys. Res.*, 114, B10404, doi:10.1029/2008JB006000.
- Aktuğ, B., E. Parmaksız, M. Kurt, O. Lenk, A. Kılıçoğlu, M. A. Gürdal, and S. Özdemir (2013a), Deformation of Central Anatolia: GPS implications, *J. Geodyn.*, 67, 78–96, doi:10.1016/j.jog.2012.05.008.
- Aktuğ, B., E. Meherremov, M. Kurt, S. Özdemir, N. Esedov, and O. Lenk (2013b), GPS constraints on the deformation of Azerbaijan and surrounding regions, *J. Geodyn.*, 67, 40–45, doi:10.1016/j.jog.2012.05.007.
- Aktuğ, B., U. Dikmen, A. Dogru, and H. Ozener (2013c), Seismicity and strain accumulation around Karliova Triple Junction (Turkey), *J. Geodyn.*, 67, 21–29, doi:10.1016/j.jog.2012.04.008.
- Alisic, L., M. Gurnis, G. Stadler, C. Burstedde, and O. Ghattas (2012), Multi-scale dynamics and rheology of mantle flow with plates, *J. Geophys. Res.*, 117, B10402, doi:10.1029/2012JB009234.
- Allmendinger, R. W., R. Smalley, M. Bevis, H. Caprio, and B. Brooks (2005), Bending the Bolivian orocline in real time, *Geology*, 33(11), 905–908, doi:10.1130/G21779.1.
- Almuselmani, B., F. Teferle, R. M. Bingley, and T. Moore (2008), New estimates of present-day Arabia plate motion and deformation from a dense GPS network in Saudi Arabia, *Eos Trans. AGU*, 89(53), Fall Meet. Suppl., Abstract G34A-02.
- Altamimi, Z., X. Collilieux, J. Legrand, B. Garayt, and C. Boucher (2007), ITRF2005: A new release of the International Terrestrial Reference Frame based on time series of station positions and Earth Orientation Parameters, *J. Geophys. Res.*, 112, B09401, doi:10.1029/2007JB004949.
- Altamimi, Z., X. Collilieux, and L. Métivier (2011), ITRF2008: An improved solution of the international terrestrial reference frame, *J. Geod.*, 85(8), 457–473, doi:10.1007/s00190-011-0444-4.
- Altamimi, Z., L. Métivier, and X. Collilieux (2012), ITRF2008 plate motion model, *J. Geophys. Res.*, 117, B07402, doi:10.1029/2011JB008930.
- al Tarazi, E., J. A. Rajab, F. Gomez, W. Cochran, R. Jaafar, and M. Ferry (2011), GPS measurements of near-field deformation along the southern Dead Sea Fault System, *Geochem. Geophys. Geosyst.*, 12, Q12021, doi:10.1029/2011GC003736.
- Alvarado, A., et al. (2014), Active tectonics in Quito, Ecuador, assessed by geomorphological studies, GPS data, and crustal seismicity, *Tectonics*, 33, 67–83, doi:10.1002/2012TC003224.

CORS-NGS, USA; Danish GPS Center; DPGA-TUDELF, The Netherlands; EarthScope Plate Boundary Observatory, USA; ERVA Instituto Geográfico Valencia, Spain; EUREF; FLEPOS, Belgium; FREDNET, Italy; GEODAF, Italy; Geodetic Observatory Pecny, Czech Republic; GeoNet, New Zealand; Geosciences Australia; Gobierno de la Rioja, Spain; GREF-BKG; GSSCOPE-INSU; HEMUNET, Bulgaria; Idaho National Laboratory, USA; Indiana DOT CORS network, USA; Indiana DOT CORS network, USA; Institut Teknologi Bandung, Indonesia; Instituto Geográfico Nacional, Spain; Instituto Geográfico Nacional, Tommy Guardia, Panama; Instituto Geográfico Portugués, Portugal; Instituto Tecnológico Agrario, Castilla y León, Spain; Institut Cartogràfic de Catalunya, Spain; Iowa DOT CORS network, USA; KARA, USA; Laboratorio di Topografia, Università degli Studi di Perugia, Italy; LATPOS, Latvia; Leica Kazachstan; Leica SmartnetUSA, USA and Canada; Lower Colorado River Authority, USA; MAGNA-ECO, Colombia; Maine DOT CORS network, USA; Mesa county, Colorado, USA; Missouri DOT CORS network, USA; Minnesota DOT CORS network, USA; Natural Resources Canada; NEGAR, California Institute of Technology, USA; MAGNET/NEARNET, University of Nevada, Reno, USA; NOANET, Greece; Norwegian Mapping Authority; OLGGPS, Austria; Pacific Geoscience Centre, Canada; Pacific GPS Facility, Hawaii, USA; Panamá Canal Authority, Panama; PANGA, USA; Provincia di Milano, Italy; RAMSAM, Argentina; RBMC Brasil; Red Andaluza de Posicionamiento, Spain; Red de Estaciones de Referencia GNSS de Euskadi, Spain; Red Extremeña de Posicionamiento, Spain; Red de Geodesia Activa de Navarra, Spain; Regione Autonoma Friuli Venezia Giulia, Italy; Regione Campania, Italy; Regione Emilia Romagna, Italy; Regione Liguria, Italy; Región de Murcia, Spain; REMOS, Venezuela; RENAG, France; Réseau GNSS Permanent, France; Rete GPS Veneto, Italy; RING-INGV, Italy; SCIGN, USA; Seiler Instrument Company, USA; SONEL, France; SOPAC, USA; South Carolina DOT CORS network, USA; STPOS Bolzano, Italy; SUGAR-NTU, Singapore; Survey of Israel; TAZNET, Arizona, USA; Texas DOT CORS network, USA; TGRef, Romania; TRIGNET, South Africa; UNAVCO, USA; Universidad de Cantabria; Universidad Politécnica de Madrid, Spain; University of Western Ontario, Canada; Washoe County, Nevada, U.S.; and West Virginia DOT CORS network, USA. We also thank all Principal Investigators for making data available from the following NSF-funded networks or regions: Africa Array, Andes (CAP),

- Alvarado, D., C. DeMets, B. Tikoff, D. Hernández, T. F. Wawrzyniec, C. Pullinger, G. Mattioli, H. L. Turner, M. Rodriguez, and F. Correa-Mora (2011), Forearc motion and deformation between El Salvador and Nicaragua: GPS, seismic, structural, and paleomagnetic observations, *Lithosphere*, 3(1), 3–21, doi:10.1130/L108.1.
- Amiri-Simkooei, A. R., C. C. J. M. Tiberius, and P. J. G. Teunissen (2007), Assessment of noise in GPS coordinate time series: Methodology and results, *J. Geophys. Res.*, 112, B07413, doi:10.1029/2006JB004913.
- Anderson, H., and J. Jackson (1987), Active tectonics of the Adriatic Region, *Geophys. J. Int.*, 91(3), 937–983, doi:10.1111/j.1365-246X.1987.tb01675.x.
- Antonelis, K., D. J. Johnson, M. M. Miller, and R. Palmer (1999), GPS determination of current Pacific–North American plate motion, *Geology*, 27(4), 299–302, doi:10.1130/0091-7613(1999)027<0299:GDOCPN>2.3.CO;2.
- Apel, E. V., R. Bürgmann, G. Steblow, N. Vasilenko, R. King, and A. Prytkov (2006), Independent active microplate tectonics of northeast Asia from GPS velocities and block modeling, *Geophys. Res. Lett.*, 33, L11303, doi:10.1029/2006GL026077.
- Argus, D. F. (2007), Defining the translational velocity of the reference frame of Earth, *Geophys. J. Int.*, 169(3), 830–838, doi:10.1111/j.1365-246X.2007.03344.x.
- Argus, D. F., and R. G. Gordon (1991a), Current Sierra Nevada–North America motion from very long baseline interferometry: Implications for the kinematics of the western United States, *Geology*, 19(11), 1085–1088, doi:10.1130/0091-7613(1991)019<1085:CSNNAM>2.3.CO;2.
- Argus, D. F., and R. G. Gordon (1991b), No-net-rotation model of current plate velocities incorporating plate motion model NUVEL-1, *Geophys. Res. Lett.*, 18(11), 2039–2042, doi:10.1029/91GL01532.
- Argus, D. F., and R. G. Gordon (1996), Tests of the rigid-plate hypothesis and bounds on intraplate deformation using geodetic data from very long baseline interferometry, *J. Geophys. Res.*, 101(B6), 13,555–13,572, doi:10.1029/95JB03775.
- Argus, D. F., R. G. Gordon, M. B. Heflin, C. Ma, R. J. Eanes, P. Willis, W. R. Peltier, and S. E. Owen (2010), The angular velocities of the plates and the velocity of Earth's centre from space geodesy, *Geophys. J. Int.*, 180(3), 913–960, doi:10.1111/j.1365-246X.2009.04463.x.
- Argus, D. F., R. G. Gordon, and C. DeMets (2011), Geologically current motion of 56 plates relative to the no-net-rotation reference frame, *Geochem. Geophys. Geosyst.*, 12, Q11001, doi:10.1029/2011GC003751.
- Árnadóttir, T., W. Jiang, K. L. Feigl, H. Geirsson, and E. Sturkell (2006), Kinematic models of plate boundary deformation in southwest Iceland derived from GPS observations, *J. Geophys. Res.*, 111, B07402, doi:10.1029/2005JB003907.
- Árnadóttir, T., B. Lund, W. Jiang, H. Geirsson, H. Björnsson, P. Einarsson, and T. Sigurdsson (2009), Glacial rebound and plate spreading: Results from the first countrywide GPS observations in Iceland, *Geophys. J. Int.*, 177(2), 691–716, doi:10.1111/j.1365-246X.2008.04059.x.
- Asensio, E., G. Khazaradze, A. Echeverría, R. W. King, and I. Vilajosana (2012), GPS studies of active deformation in the Pyrenees, *Geophys. J. Int.*, 190(2), 913–921, doi:10.1111/j.1365-246X.2012.05525.x.
- Ashurkov, S. V., V. A. San'kov, A. I. Miroshnichenko, A. V. Lukhnev, A. P. Sorokin, M. A. Serov, and L. M. Byzov (2011), GPS geodetic constraints on the kinematics of the Amurian Plate, *Russ. Geol. Geophys.*, 52(2), 239–249, doi:10.1016/j.rgg.2010.12.017.
- Aurelio, M. A. (2001), GPS velocities in Mindanao Island, *J. Geol. Soc. Philipp.*, 56, 214–224.
- Avallone, A., P. Briole, A. M. Agatza-Balodimou, H. Billiris, O. Charade, C. Mitsakaki, A. Nercessian, K. Papazissi, D. Paradissis, and G. Veis (2004), Analysis of eleven years of deformation measured by GPS in the Corinth Rift Laboratory area, *C. R. Geosci.*, 336(4–5), 301–311, doi:10.1016/j.crte.2003.12.007.
- Avé Lallement, H. G. A., and J. S. Oldow (2000), Active displacement partitioning and arc-parallel extension of the Aleutian volcanic arc based on Global Positioning System geodesy and kinematic analysis, *Geology*, 28(8), 739–742, doi:10.1130/0091-7613(2000)28<739:ADPAAE>2.0.CO;2.
- Avouac, J. P., P. Tappouchnier, M. Bai, H. You, and G. Wang (1993), Active thrusting and folding along the northern Tien Shan and Late Cenozoic rotation of the Tarim relative to Dzungaria and Kazakhstan, *J. Geophys. Res.*, 98(B4), 6755–6804, doi:10.1029/92JB01963.
- Ayhan, M. E., C. Demir, O. Lenk, A. Kılıçoglu, Y. Altiner, A. A. Barka, S. Ergintav, and H. Özener (2002), Interseismic strain accumulation in the Marmara Sea region, *Bull. Seismol. Soc. Am.*, 92(1), 216–229, doi:10.1785/0120000818.
- Bacolcol, T., E. Barrier, T. Duquesnoy, A. Aguilar, R. Jorgio, R. de la Cruz, and M. Lasala (2005), GPS constraints on Philippine Fault slip rate in Masbate Island, central Philippines, *J. Geol. Soc. Philipp.*, 60, 1–7.
- Baek, J., Y.-H. Shin, S.-H. Na, N. V. Shestakov, P.-H. Park, and S. Cho (2012), Coseismic and postseismic crustal deformations of the Korean Peninsula caused by the 2011 Mw 9.0 Tohoku earthquake, Japan, from global positioning system data, *Terra Nova*, 24(4), 295–300, doi:10.1111/j.1365-3121.2012.01062.x.
- Banerjee, P., R. Bürgmann, B. Nagarajan, and E. Apel (2008), Intraplate deformation of the Indian subcontinent, *Geophys. Res. Lett.*, 35, L18301, doi:10.1029/2008GL035468.
- Bar-Sever, Y. E., P. M. Kroger, and J. A. Borjesson (1998), Estimating horizontal gradients of tropospheric path delay with a single GPS receiver, *J. Geophys. Res.*, 103(B3), 5019–5035, doi:10.1029/97JB03534.
- Battaglia, M., M. H. Murray, E. Serpelloni, and R. Bürgmann (2004), The Adriatic region: An independent microplate within the Africa-Eurasia collision zone, *Geophys. Res. Lett.*, 31, L09605, doi:10.1029/2004GL019723.
- Baxter, S. C., S. Kedar, J. W. Parker, F. H. Webb, S. E. Owen, A. Sibthorpe, and D. Dong (2011), Limitations of strain estimation techniques from discrete deformation observations, *Geophys. Res. Lett.*, 38, L01305, doi:10.1029/2010GL046028.
- Bayer, R., J. Chery, M. Tatar, P. Vernant, M. Abbassi, F. Masson, F. Nilforoushan, E. Doerflinger, V. Regard, and O. Bellier (2006), Active deformation in Zagros–Makran transition zone inferred from GPS measurements, *Geophys. J. Int.*, 165(1), 373–381, doi:10.1111/j.1365-246X.2006.02879.x.
- Beavan, J., and J. Haines (2001), Contemporary horizontal velocity and strain rate fields of the Pacific–Australian plate boundary zone through New Zealand, *J. Geophys. Res.*, 106(B1), 741–770, doi:10.1029/2000JB900302.
- Beavan, J., et al. (1999), Crustal deformation during 1994–1998 due to oblique continental collision in the central Southern Alps, New Zealand, and implications for seismic potential of the Alpine fault, *J. Geophys. Res.*, 104(B11), 25,233–25,255, doi:10.1029/1999JB900198.
- Bechtold, M., M. Battaglia, D. C. Tanner, and D. Zuliani (2009), Constraints on the active tectonics of the Friuli/NW Slovenia area from CGPS measurements and three-dimensional kinematic modeling, *J. Geophys. Res.*, 114, B03408, doi:10.1029/2008JB005638.
- Becker, T. W. (2006), On the effect of temperature and strain-rate dependent viscosity on global mantle flow, net rotation, and plate-driving forces, *Geophys. J. Int.*, 167(2), 943–957, doi:10.1111/j.1365-246X.2006.03172.x.
- Béjar-Pizarro, M., A. Socquet, R. Armijo, D. Carrizo, J. Genrich, and M. Simons (2013), Andean structural control on interseismic coupling in the North Chile subduction zone, *Nat. Geosci.*, 6, 462–467, doi:10.1038/ngeo1802.
- Benford, B., C. DeMets, B. Tikoff, P. Williams, L. Brown, and M. Wiggins-Grandison (2012), Seismic hazard along the southern boundary of the Gónave microplate: Block modelling of GPS velocities from Jamaica and nearby islands, northern Caribbean, *Geophys. J. Int.*, 190(1), 59–74, doi:10.1111/j.1365-246X.2012.05493.x.

Antarctica (PoleNet), Bhutan, Calabria, CocoNET, Costa Rica, El Salvador, Eritrea, Ethiopia, Greenland (PoleNet), Hawaii, Iceland, Mediterranean, Mexico, Mid-America (GAMA), New Zealand (SAGE). Pamir Mountains, Puerto Rico, Rio Grande Rift, SUOMI-NET, Tanzania, and Uganda. We thank these Institutions/networks which provided raw RINEX data that are otherwise not available publicly/anonymously: British Columbia Active Control System, Canada; British Isles continuous GNSS Facility (BIGF), U.K.; Central-Asian Institute for Applied Geosciences (CAIAG), Kirghistan; GEONET, GSI, Japan; Instituto Nacional de Estadística y Geografía (INEGI), Mexico; Jeddah Municipality, Saudi Arabia; Las Vegas Valley Water Authority, Nevada, USA; Leica SmartNet, Australia; Leica SmartNet (ITALPOS), Italy; Linz AG, Austria; LITPOS, Lithuania; Low-Latitude Ionospheric Sensor Network (LISN); Provincia Autonoma di Trento, Italy; REGNA, Servicio Geográfico Militar, Uruguay; and WALCORS, Belgium. We very much thank the following individuals who provided unpublished GPS velocity results: R. Bennett, J. Bogusz, A. Holland, H. Mora, Z.-K. Shen, M. Steckler, and C. Subarya. We furthermore thank all investigators who contributed additional information to help us include their published results. We particularly thank N. Teferle for making the results of Almuselmani et al. [2008] available, and M. Sato for sharing results that were, at the time, not yet published. We finally thank the Jet Propulsion Laboratory for the GIPSY-OASIS II software and for clock and orbit parameters. We are grateful to L. Estey, S. Wier, and F. Boler at UNAVCO for maintaining an interactive website that displays the results of GSRS v2.1: <http://gsrm2.unavco.org>.

- Bennett, R. A., et al. (2012), Syn-convergent extension observed using the RETREAT GPS network, northern Apennines, Italy, *J. Geophys. Res.*, 117, B04408, doi:10.1029/2011JB008744.
- Bergeot, N., M. N. Bouin, M. Diament, B. Pelletier, M. Régnier, S. Calmant, and V. Ballu (2009), Horizontal and vertical interseismic velocity fields in the Vanuatu subduction zone from GPS measurements: Evidence for a central Vanuatu locked zone, *J. Geophys. Res.*, 114, B06405, doi:10.1029/2007JB005249.
- Berglund, H. T., A. F. Sheehan, M. H. Murray, M. Roy, A. R. Lowry, R. S. Nerem, and F. Blume (2012), Distributed deformation across the Rio Grande Rift, Great Plains, and Colorado Plateau, *Geology*, 40(1), 23–26, doi:10.1130/G32418.1.
- Bertiger, W., S. D. Desai, B. Haines, N. Harvey, A. W. Moore, S. Owen, and J. P. Weiss (2010), Single receiver phase ambiguity resolution with GPS data, *J. Geod.*, 84(5), 327–337, doi:10.1007/s00190-010-0371-9.
- Bettinelli, P., J.-P. Avouac, M. Flouzat, F. Jouanne, L. Bollinger, P. Willis, and G. Chitrakar (2006), Plate motion of India and interseismic strain in the Nepal Himalaya from GPS and DORIS measurements, *J. Geod.*, 80(8), 567–589, doi:10.1007/s00190-006-0030-3.
- Bird, P. (2003), An updated digital model of plate boundaries, *Geochem. Geophys. Geosyst.*, 4(3), 1027, doi:10.1029/2001GC000252.
- Bird, P., and Y. Y. Kagan (2004), Plate-tectonic analysis of shallow seismicity: Apparent boundary width, beta, corner magnitude, coupled lithosphere thickness, and coupling in seven tectonic settings, *Bull. Seismol. Soc. Am.*, 94(6), 2380–2399, doi:10.1785/0120030107.
- Bird, P., C. Kreemer, and W. E. Holt (2010), A long-term forecast of shallow seismicity based on the global strain rate map, *Seismol. Res. Lett.*, 81(2), 184–194, doi:10.1785/gssrl.81.2.184.
- Blewitt, G. (1989), Carrier phase ambiguity resolution for the Global Positioning System applied to geodetic baselines up to 2000 km, *J. Geophys. Res.*, 94(B8), 10,187–10,203, doi:10.1029/JB094iB08p10187.
- Blewitt, G. (1990), An Automatic Editing Algorithm for GPS data, *Geophys. Res. Lett.*, 17(3), 199–202, doi:10.1029/GL017i003p00199.
- Blewitt, G., and D. Lavallée (2002), Effect of annual signals on geodetic velocity, *J. Geophys. Res.*, 107(B7), 2145, doi:10.1029/2001JB000570.
- Blewitt, G., W. C. Hammond, and C. Kreemer (2009), Geodetic observation of contemporary deformation in the northern Walker Lane: 1. Semipermanent GPS strategy, *Geol. Soc. Am. Spec. Pap.*, 447, 1–15, doi:10.1130/2009.2447(01).
- Blewitt, G., C. Kreemer, W. C. Hammond, and J. M. Goldfarb (2013), Terrestrial reference frame NA12 for crustal deformation studies in North America, *J. Geodyn.*, 72, 11–24, doi:10.1016/j.jog.2013.08.004.
- Bock, Y., L. Prawirodirdjo, J. F. Genrich, C. W. Stevens, R. McCaffrey, C. Subarya, S. S. O. Puntodewo, and E. Calais (2003), Crustal motion in Indonesia from Global Positioning System measurements, *J. Geophys. Res.*, 108(B8), 2367, doi:10.1029/2001JB000324.
- Boehm, J., A. Niell, P. Tregoning, and H. Schuh (2006), Global Mapping Function (GMF): A new empirical mapping function based on numerical weather model data, *Geophys. Res. Lett.*, 33, L07304, doi:10.1029/2005GL025546.
- Brooks, B. A., M. Bevis, R. Smalley Jr., E. Kendrick, R. Manceda, E. Lauria, R. Maturana, and M. Araujo (2003), Crustal motion in the Southern Andes ( $26^{\circ}$ – $36^{\circ}$ S): Do the Andes behave like a microplate?, *Geochem. Geophys. Geosyst.*, 4(10), 1085, doi:10.1029/2003GC000505.
- Brooks, B. A., et al. (2011), Orogenic-wedge deformation and potential for great earthquakes in the central Andean backarc, *Nat. Geosci.*, 4(6), 380–383, doi:10.1038/ngeo1143.
- Bull, W. B., and P. A. Pearthree (1988), Frequency and size of quaternary surface ruptures of the pitayachi fault, northeastern Sonora, Mexico, *Bull. Seismol. Soc. Am.*, 78(2), 956–978.
- Calais, E., J.-M. Nocquet, F. Jouanne, and M. Tardy (2002), Current strain regime in the Western Alps from continuous Global Positioning System measurements, 1996–2001, *Geology*, 30(7), 651–654, doi:10.1130/0091-7613(2002)030<0651:CSRTW>2.0.CO;2.
- Calais, E., L. Dong, M. Wang, Z. Shen, and M. Vergnolle (2006a), Continental deformation in Asia from a combined GPS solution, *Geophys. Res. Lett.*, 33, L24319, doi:10.1029/2006GL028433.
- Calais, E., J. Y. Han, C. DeMets, and J. M. Nocquet (2006b), Deformation of the North American plate interior from a decade of continuous GPS measurements, *J. Geophys. Res.*, 111, B06402, doi:10.1029/2005JB004253.
- Calais, E., C. Ebinger, C. Hartnady, and J.-M. Nocquet (2006c), Kinematics of the East African rift from GPS and earthquake slip vector data, in *The Afar Volcanic Province Within the East African Rift System*, vol. 259, edited by C. J. Ebinger, G. Yirgu, and P. K. Maguire, pp. 9–22, Geological Society of London, London, U. K.
- Calais, E., A. Freed, G. Mattioli, F. Amelung, S. Jónsson, P. Jansma, S.-H. Hong, T. Dixon, C. Prépetit, and R. Momplaisir (2010), Transpressional rupture of an unmapped fault during the 2010 Haïti earthquake, *Nat. Geosci.*, 3(11), 794–799, doi:10.1038/ngeo992.
- Calmant, S., B. Pelletier, P. Lebellegard, M. Bevis, F. W. Taylor, and D. A. Phillips (2003), New insights on the tectonics along the New Hebrides subduction zone based on GPS results, *J. Geophys. Res.*, 108(B6), 2319, doi:10.1029/2001JB000644.
- Caporali, A., et al. (2009), Surface kinematics in the Alpine–Carpathian–Dinaric and Balkan region inferred from a new multi-network GPS combination solution, *Tectonophysics*, 474(1–2), 295–321, doi:10.1016/j.tecto.2009.04.035.
- Cardozo, N., and R. W. Allmendinger (2009), SSPX: A program to compute strain from displacement/velocity data, *Comput. Geosci.*, 35(6), 1343–1357, doi:10.1016/j.cageo.2008.05.008.
- Castro, R. R., P. M. Shearer, L. Astiz, M. Suter, C. Jacques-Ayala, and F. Vernon (2010), The long-lasting aftershock series of the 3 May 1887 Mw 7.5 Sonora earthquake in the Mexican Basin and Range Province, *Bull. Seismol. Soc. Am.*, 100(3), 1153–1164, doi:10.1785/0120090180.
- Catherine, J. K., V. K. Gahalaut, N. Srinivas, S. Kumar, and B. Nagarajan (2014), Evidence of strain accumulation in the Andaman Region for the Giant 2004 Sumatra Andaman Earthquake, *Bull. Seismol. Soc. Am.*, 104(1), 587–591, doi:10.1785/0120130141.
- Cenni, N., E. Mantovani, P. Baldi, and M. Viti (2012), Present kinematics of Central and Northern Italy from continuous GPS measurements, *J. Geodyn.*, 58, 62–72, doi:10.1016/j.jog.2012.02.004.
- Chalouan, A., A. J. Gil, J. Galindo-Zaldívar, M. Ahmamou, P. Ruano, M. C. de Lacy, A. M. Ruiz-Armenteros, M. Benmakhoul, and F. Riguzzi (2014), Active faulting in the frontal Rif Cordillera (Fes region, Morocco): Constraints from GPS data, *J. Geodyn.*, 78, 110–122, doi:10.1016/j.jog.2014.01.002.
- Chamot-Rooke, N., and A. Rabaute (2006), Plate tectonics from space, in Commission for the Geological Map of the World, scale 1:50000000. Commission for the Geological Map of the World, Paris, France.
- Chang, W.-L., R. B. Smith, C. M. Meertens, and R. A. Harris (2006), Contemporary deformation of the Wasatch Fault, Utah, from GPS measurements with implications for interseismic fault behavior and earthquake hazard: Observations and kinematic analysis, *J. Geophys. Res.*, 111, B11405, doi:10.1029/2006JB004326.
- Chen, H.-Y., J.-C. Lee, H. Tung, S.-B. Yu, Y.-J. Hsu, and H. Lee (2013), A new velocity field from a dense GPS array in the southernmost Longitudinal Valley, southeastern Taiwan, *Terrestrial Atmos. Oceanic Sci.*, 24(5), 837, doi:10.3319/TAO.2013.06.18.01(T).
- Ching, K.-E., R.-J. Rau, J.-C. Lee, and J.-C. Hu (2007), Contemporary deformation of tectonic escape in SW Taiwan from GPS observations, 1995–2005, *Earth Planet. Sci. Lett.*, 262(3–4), 601–619, doi:10.1016/j.epsl.2007.08.017.
- Ching, K.-E., R.-J. Rau, K. M. Johnson, J.-C. Lee, and J.-C. Hu (2011), Present-day kinematics of active mountain building in Taiwan from GPS observations during 1995–2005, *J. Geophys. Res.*, 116, B09405, doi:10.1029/2010JB008058.

- Chiu, C.-Y. (2010), Crustal deformation of Taipei region from continuous GPS observations, MS thesis, Natl. Cent. Univ., Jhongli City, Taiwan.
- Chlieh, M., H. Perfettini, H. Tavera, J.-P. Avouac, D. Remy, J.-M. Nocquet, F. Rolandone, F. Bondoux, G. Gabalda, and S. Bonvalot (2011), Interseismic coupling and seismic potential along the Central Andes subduction zone, *J. Geophys. Res.*, 116, B12405, doi:10.1029/2010JB008166.
- Chousianitis, K., A. Ganas, and M. Giannou (2013), Kinematic interpretation of present-day crustal deformation in central Greece from continuous GPS measurements, *J. Geodyn.*, 71, 1–13, doi:10.1016/j.jog.2013.06.004.
- Cisneros, D., and J. M. Nocquet (2011), *Campo de velocidades del Ecuador, obtenido a través de mediciones de campañas GPS de los últimos 15 años y medidas de una red GPS permanente*, Technical Report, Instituto Geográfica Militar, Quito, Ecuador.
- Clarke, P. J., et al. (1998), Crustal strain in central Greece from repeated GPS measurements in the interval 1989–1997, *Geophys. J. Int.*, 135(1), 195–214, doi:10.1046/j.1365-246X.1998.00633.x.
- Cocard, M., H.-G. Kahle, Y. Peter, A. Geiger, G. Veis, S. Feleksis, D. Paradissis, and H. Billiris (1999), New constraints on the rapid crustal motion of the Aegean region: Recent results inferred from GPS measurements (1993–1998) across the West Hellenic Arc, Greece, *Earth Planet. Sci. Lett.*, 172(1–2), 39–47, doi:10.1016/S0012-821X(99)00185-5.
- Cohen, S. C., and J. T. Freymueller (2004), Crustal deformation in the Southcentral Alaska Subduction Zone, *Adv. Geophys.*, 47, 1–63.
- Conder, J. A., and D. W. Forsyth (2001), Seafloor spreading on the Southeast Indian Ridge over the last one million years: A test of the Capricorn plate hypothesis, *Earth Planet. Sci. Lett.*, 188(1), 91–105, doi:10.1016/S0012-821X(01)00326-0.
- Cook, D. B., K. Fujita, and C. A. McMullen (1986), Present-day plate interactions in Northeast Asia: North American, Eurasian, and Okhotsk plates, *J. Geodyn.*, 6(1–4), 33–51, doi:10.1016/0264-3707(86)90031-1.
- Correa-Mora, F., C. DeMets, D. Alvarado, H. L. Turner, G. Mattioli, D. Hernandez, C. Pullinger, M. Rodriguez, and C. Tenorio (2009), GPS-derived coupling estimates for the Central America subduction zone and volcanic arc faults: El Salvador, Honduras and Nicaragua, *Geophys. J. Int.*, 179(3), 1279–1291, doi:10.1111/j.1365-246X.2009.04371.x.
- Cross, R. S., and J. T. Freymueller (2008), Evidence for and implications of a Bering plate based on geodetic measurements from the Aleutians and western Alaska, *J. Geophys. Res.*, 113, B07405, doi:10.1029/2007JB005136.
- Cowell, B. W., Y. Bock, D. T. Sandwell, and Y. Fialko (2013), Geodetic investigation into the deformation of the Salton Trough, *J. Geophys. Res. Solid Earth*, 118, 5030–5039, doi:10.1002/jgrb.50347.
- D'Agostino, N. (2014), Complete seismic release of tectonic strain and earthquake recurrence in the Apennines (Italy), *Geophys. Res. Lett.*, 41, 1155–1162, doi:10.1002/2014GL059230.
- D'Agostino, N., and G. Selvaggi (2004), Crustal motion along the Eurasia-Nubia plate boundary in the Calabrian Arc and Sicily and active extension in the Messina Straits from GPS measurements, *J. Geophys. Res.*, 109, B11402, doi:10.1029/2004JB002998.
- D'Agostino, N., A. Avallone, D. Cheloni, E. D'Anastasio, S. Mantentuto, and G. Selvaggi (2008), Active tectonics of the Adriatic region from GPS and earthquake slip vectors, *J. Geophys. Res.*, 113, B12413, doi:10.1029/2008JB005860.
- D'Agostino, N., S. Mantentuto, E. D'Anastasio, R. Giuliani, M. Mattone, S. Calcaterra, P. Gambino, and L. Bonci (2011a), Evidence for localized active extension in the central Apennines (Italy) from global positioning system observations, *Geology*, 39(4), 291–294, doi:10.1130/G31796.1.
- D'Agostino, N., E. D'Anastasio, A. Gervasi, I. Guerra, M. R. Nedimović, L. Seeber, and M. Steckler (2011b), Forearc extension and slow rollback of the Calabrian Arc from GPS measurements, *Geophys. Res. Lett.*, 38, L17304, doi:10.1029/2011GL048270.
- Darby, D., and J. Beavan (2001), Evidence from GPS measurements for contemporary interplate coupling on the southern Hikurangi subduction thrust and for partitioning of strain in the upper plate, *J. Geophys. Res.*, 106(B12), 30,881–30,891, doi:10.1029/2000JB000023.
- Dawson, J., G. Luton, and R. Govind (2004), *Permanent Committee for GIS Infrastructure for Asia and the Pacific, 1997, 1998, 1999, 2000, 2001, 2002 GPS Campaign Analysis*, Geosci. Aust., Canberra, Australia.
- de Lis Mancilla, F., D. Stich, M. Berrocoso, R. Martín, J. Morales, A. Fernandez-Ros, R. Pérez, and A. Pérez-Peña (2013), Delamination in the Betic Range: Deep structure, seismicity, and GPS motion, *Geology*, 41(3), 307–310, doi:10.1130/G33733.1.
- DeMets, C., R. G. Gordon, D. F. Argus, and S. Stein (1990), Current plate motions, *Geophys. J. Int.*, 101(2), 425–478, doi:10.1111/j.1365-246X.1990.tb06579.x.
- DeMets, C., R. G. Gordon, D. F. Argus, and S. Stein (1994), Effect of recent revisions to the geomagnetic reversal time scale on estimates of current plate motions, *Geophys. Res. Lett.*, 21(20), 2191–2194, doi:10.1029/94GL02118.
- DeMets, C., R. G. Gordon, and D. F. Argus (2010), Geologically current plate motions, *Geophys. J. Int.*, 181(1), 1–80, doi:10.1111/j.1365-246X.2009.04491.x.
- Denys, P., R. Norris, C. Pearson, and M. Denham (2014), A geodetic study of the Otago fault system of the South Island of New Zealand, in *Earth on the Edge: Science for a Sustainable Planet*, edited by C. Rizos and P. Willis, pp. 151–158, Springer, Berlin.
- Devoti, R., A. Esposito, G. Pietrantonio, A. R. Pisani, and F. Riguzzi (2011), Evidence of large scale deformation patterns from GPS data in the Italian subduction boundary, *Earth Planet. Sci. Lett.*, 311(3–4), 230–241, doi:10.1016/j.epsl.2011.09.034.
- Dietrich, R., A. Rülke, J. Ihde, K. Lindner, H. Miller, W. Niemeier, H.-W. Schenke, and G. Seeber (2004), Plate kinematics and deformation status of the Antarctic Peninsula based on GPS, *Global Planet. Change*, 42(1–4), 313–321, doi:10.1016/j.gloplacha.2003.12.003.
- Dixon, T. H., M. Miller, F. Farina, H. Wang, and D. Johnson (2000), Present-day motion of the Sierra Nevada block and some tectonic implications for the Basin and Range province, North American Cordillera, *Tectonics*, 19(1), 1–24, doi:10.1029/1998TC001088.
- Djamour, Y., et al. (2010), GPS and gravity constraints on continental deformation in the Alborz mountain range, Iran, *Geophys. J. Int.*, 183(3), 1287–1301, doi:10.1111/j.1365-246X.2010.04811.x.
- Djamour, Y., P. Vernant, H. R. Nankali, and F. Tavakoli (2011), NW Iran-eastern Turkey present-day kinematics: Results from the Iranian permanent GPS network, *Earth Planet. Sci. Lett.*, 307(1–2), 27–34, doi:10.1016/j.epsl.2011.04.029.
- Dogru, A., E. Gorgun, H. Ozener, and B. Aktug (2014), Geodetic and seismological investigation of crustal deformation near Izmir (western Anatolia), *J. Asian Earth Sci.*, 82, 21–31, doi:10.1016/j.jseas.2013.12.008.
- Drewes, H., and O. Heidbach (2012), The 2009 horizontal velocity field for South America and the Caribbean, in *Geodesy for Planet Earth*, vol. 136, edited by S. Kenyon, M. C. Pacino, and U. Marti, pp. 657–664, Springer, Berlin.
- Duermeijer, C. E., M. Nyst, P. T. Meijer, C. G. Langereis, and W. Spakman (2000), Neogene evolution of the Aegean arc: Paleomagnetic and geodetic evidence for a rapid and young rotation phase, *Earth Planet. Sci. Lett.*, 176(3–4), 509–525, doi:10.1016/S0012-821X(00)00023-6.
- Duquesnoy, T., M. Kasser, M. Aurelio, R. Gaulon, R. S. Punongbayan, and C. Rangin (1994), Detection of creep along the Philippine Fault: First results of geodetic measurements on Leyte Island, central Philippine, *Geophys. Res. Lett.*, 21(11), 975–978, doi:10.1029/94GL00640.
- Echeverria, A., G. Khazaradze, E. Asensio, J. Gárate, J. M. Dávila, and E. Suriñach (2013), Crustal deformation in eastern Betics from CuTeNeo GPS network, *Tectonophysics*, 608, 600–612, doi:10.1016/j.tecto.2013.08.020.
- Elliott, J., J. T. Freymueller, and C. F. Larsen (2013), Active tectonics of the St. Elias Orogen, Alaska, observed with GPS measurements, *J. Geophys. Res. Solid Earth*, 118, 5625–5642, doi:10.1002/jgrb.50341.

- Elliott, J. L., C. F. Larsen, J. T. Freymueller, and R. J. Motyka (2010), Tectonic block motion and glacial isostatic adjustment in southeast Alaska and adjacent Canada constrained by GPS measurements, *J. Geophys. Res.*, 115, B09407, doi:10.1029/2009JB007139.
- Feng, L., A. V. Newman, M. Protti, V. González, Y. Jiang, and T. H. Dixon (2012), Active deformation near the Nicoya Peninsula, northwestern Costa Rica, between 1996 and 2010: Interseismic megathrust coupling, *J. Geophys. Res.*, 117, B06407, doi:10.1029/2012JB009230.
- Fernandes, R. M. S., L. Bastos, B. A. C. Ambrosius, R. Noomen, S. Matheusson, and P. Baptista (2004), Recent geodetic results in the Azores triple junction region, *Pure Appl. Geophys.*, 161(3), 683–699, doi:10.1007/s0024-003-2469-y.
- Fernandes, R. M. S., J. M. Miranda, B. M. L. Meijninger, M. S. Bos, R. Noomen, L. Bastos, B. a. C. Ambrosius, and R. E. M. Riva (2007), Surface velocity field of the Ibero-Maghrebian segment of the Eurasia-Nubia plate boundary, *Geophys. J. Int.*, 169(1), 315–324, doi:10.1111/j.1365-246X.2006.03252.x.
- Fernandes, R. M. S., J. M. Miranda, D. Delvaux, D. S. Stamps, and E. Saria (2013), Re-evaluation of the kinematics of Victoria Block using continuous GNSS data, *Geophys. J. Int.*, 193(1), 1–10, doi:10.1093/gji/ggs071.
- Floyd, M. A., et al. (2010), A new velocity field for Greece: Implications for the kinematics and dynamics of the Aegean, *J. Geophys. Res.*, 115, B10403, doi:10.1029/2009JB007040.
- Franco, A., et al. (2012), Fault kinematics in northern Central America and coupling along the subduction interface of the Cocos Plate, from GPS data in Chiapas (Mexico), Guatemala and El Salvador, *Geophys. J. Int.*, 189(3), 1223–1236, doi:10.1111/j.1365-246X.2012.05390.x.
- French, S., V. Lekic, and B. Romanowicz (2013), Waveform tomography reveals channeled flow at the base of the oceanic asthenosphere, *Science*, 342(6155), 227–230, doi:10.1126/science.1241514.
- Freymueller, J. T., M. H. Murray, P. Segall, and D. Castillo (1999), Kinematics of the Pacific-North America plate boundary zone, northern California, *J. Geophys. Res.*, 104(B4), 7419–7441, doi:10.1029/1998JB900118.
- Freymueller, J. T., H. Woodard, S. C. Cohen, R. Cross, J. Elliott, C. F. Larsen, S. Hreinsdóttir, and C. Zweck (2008), Active deformation processes in Alaska, based on 15 years of GPS measurements, in *Active Tectonics and Seismic Potential of Alaska*, AGU Monogr. Ser. 179, edited by J. T. Freymueller et al., pp. 1–42, AGU, Washington, D. C.
- Gagnon, K., C. D. Chadwell, and E. Norabuena (2005), Measuring the onset of locking in the Peru-Chile trench with GPS and acoustic measurements, *Nature*, 434(7030), 205–208, doi:10.1038/nature03412.
- Gahalaut, V. K., et al. (2013), Aseismic plate boundary in the Indo-Burmese wedge, northwest Sunda Arc, *Geology*, 41(2), 235–238, doi:10.1130/G33771.1.
- Galgana, G., M. Hamburger, R. McCaffrey, E. Corpuz, and Q. Chen (2007), Analysis of crustal deformation in Luzon, Philippines using geodetic observations and earthquake focal mechanisms, *Tectonophysics*, 432(1–4), 63–87, doi:10.1016/j.tecto.2006.12.001.
- Galvani, A., M. Anzidei, R. Devoti, A. Esposito, G. Pietrantonio, A. R. Pisani, F. Riguzzi, and E. Serpelloni (2012), The interseismic velocity field of the central Apennines from a dense GPS network, *Ann. Geophys.*, 55(5), 1039–1049, doi:10.4401/ag-5634.
- Gan, W., P. Zhang, Z.-K. Shen, Z. Niu, M. Wang, Y. Wan, D. Zhou, and J. Cheng (2007), Present-day crustal motion within the Tibetan Plateau inferred from GPS measurements, *J. Geophys. Res.*, 112, B08416, doi:10.1029/2005JB004120.
- Ganas, A., A. Marinou, D. Anastasiou, D. Paradissis, K. Papazissi, P. Tzavaras, and G. Drakatos (2013), GPS-derived estimates of crustal deformation in the central and north Ionian Sea, Greece: 3-yr results from NOANET continuous network data, *J. Geodyn.*, 67, 62–71, doi:10.1016/j.jog.2012.05.010.
- Genrich, J. F., Y. Bock, R. McCaffrey, L. Prawirodirjo, C. W. Stevens, S. S. O. Puntodewo, C. Subarya, and S. Wdowinski (2000), Distribution of slip at the northern Sumatran fault system, *J. Geophys. Res.*, 105(B12), 28,327–28,341, doi:10.1029/2000JB900158.
- Ghosh, A., and W. E. Holt (2012), Plate motions and stresses from global dynamic models, *Science*, 335(6070), 838–843, doi:10.1126/science.1214209.
- Ghosh, A., W. E. Holt, and L. M. Flesch (2009), Contribution of gravitational potential energy differences to the global stress field, *Geophys. J. Int.*, 179(2), 787–812, doi:10.1111/j.1365-246X.2009.04326.x.
- Gomez, F., G. Karam, M. Khawlie, S. McClusky, P. Vernant, R. Reilinger, R. Jaafar, C. Tabet, K. Khair, and M. Barazangi (2007), Global Positioning System measurements of strain accumulation and slip transfer through the restraining bend along the Dead Sea fault system in Lebanon, *Geophys. J. Int.*, 168(3), 1021–1028, doi:10.1111/j.1365-246X.2006.03328.x.
- Gordon, R. G., and S. Stein (1992), Global tectonics and space geodesy, *Science*, 256(5055), 333–342, doi:10.1126/science.256.5055.333.
- Gourmelen, N., and F. Amelung (2005), Post-seismic mantle relaxation in the Central Nevada seismic belt, *Science*, 310, 1473–1476.
- Hackl, M., R. Malservisi, and S. Wdowinski (2009), Strain rate patterns from dense GPS networks, *Nat. Hazards Earth Syst. Sci.*, 9(4), 1177–1187, doi:10.5194/nhess-9-1177-2009.
- Haines, A. J., and W. E. Holt (1993), A procedure for obtaining the complete horizontal motions within zones of distributed deformation from the inversion of strain rate data, *J. Geophys. Res.*, 98(B7), 12,057–12,082, doi:10.1029/93JB00892.
- Hammond, J. O. S., J.-M. Kendall, G. Rümpker, J. Wookey, N. Teanby, P. Joseph, T. Ryberg, and G. Stuart (2005), Upper mantle anisotropy beneath the Seychelles microcontinent, *J. Geophys. Res.*, 110, B11401, doi:10.1029/2005JB003757.
- Hammond, W. C., and W. Thatcher (2004), Contemporary tectonic deformation of the Basin and Range province, western United States: 10 years of observation with the Global Positioning System, *J. Geophys. Res.*, 109, B08403, doi:10.1029/2003JB002746.
- Hammond, W. C., and W. Thatcher (2005), Northwest Basin and Range tectonic deformation observed with the Global Positioning System, 1999–2003, *J. Geophys. Res.*, 110, B10405, doi:10.1029/2005JB003678.
- Hammond, W. C., and W. Thatcher (2007), Crustal deformation across the Sierra Nevada, northern Walker Lane, Basin and Range transition, western United States measured with GPS, 2000–2004, *J. Geophys. Res.*, 112, B05411, doi:10.1029/2006JB004625.
- Hammond, W. C., C. Kreemer, and G. Blewitt (2009), Geodetic constraints on contemporary deformation in the northern Walker Lane; 3, Central Nevada seismic belt postseismic relaxation, vol. 447, edited by J. S. Oldow, and P. H. Cashman, pp. 33–54, Geological Society of America Special Paper, Boulder, Colo.
- Hammond, W. C., G. Blewitt, and C. Kreemer (2011), Block modeling of crustal deformation of the northern Walker Lane and Basin and Range from GPS velocities, *J. Geophys. Res.*, 116, B04402, doi:10.1029/2010JB007817.
- Hammond, W. C., G. Blewitt, Z. Li, H.-P. Plag, and C. Kreemer (2012), Contemporary uplift of the Sierra Nevada, western United States, from GPS and InSAR measurements, *Geology*, 40, 667–670, doi:10.1130/G32968.1.
- Harada, Y. (2000), The motion of the Pacific plate determined by a GPS network of Pacific Islands, *Bull. Geogr. Surv. Inst.*, 46, 11–15.
- Hartnady, C. J. H. (2002), Earthquake hazard in Africa: Perspectives on the Nubia-Somalia boundary, *S. Afr. J. Sci.*, 98(9–10), 425–428.
- Hashimoto, C., A. Noda, T. Sagiya, and M. Matsu'ura (2009), Interplate seismogenic zones along the Kuril–Japan trench inferred from GPS data inversion, *Nat. Geosci.*, 2(2), 141–144, doi:10.1038/ngeo421.
- He, J., P. Vernant, J. Chéry, W. Wang, S. Lu, W. Ku, W. Xia, and R. Bilham (2013), Nailing down the slip rate of the Altyn Tagh fault, *Geophys. Res. Lett.*, 40, 5382–5386, doi:10.1002/2013GL057497.

- Henton, J. A., M. R. Craymer, R. Ferland, H. Dragert, S. Mazzotti, and D. L. Forbes (2006), Crustal motion and deformation monitoring of the Canadian landmass, *Geomatica*, 60(2), 173–191.
- Hessami, K., F. Nilforoushan, and C. J. Talbot (2006), Active deformation within the Zagros Mountains deduced from GPS measurements, *J. Geol. Soc.*, 163(1), 143–148, doi:10.1144/0016-764905-031.
- Hetland, E. A., and B. H. Hager (2003), Postseismic relaxation across the Central Nevada Seismic Belt, *J. Geophys. Res.*, 108(B8), 2394, doi:10.1029/2002JB002257.
- Hill, E. M., and G. Blewitt (2006), Testing for fault activity at Yucca Mountain, Nevada, using independent GPS results from the BARGEN network, *Geophys. Res. Lett.*, 33, L14302, doi:10.1029/2006GL026140.
- Hilley, G. E., K. M. Johnson, M. Wang, Z.-K. Shen, and R. Bürgmann (2009), Earthquake-cycle deformation and fault slip rates in northern Tibet, *Geology*, 37(1), 31–34, doi:10.1130/G25157A.1.
- Hollenstein, C., H.-G. Kahle, A. Geiger, S. Jenny, S. Goes, and D. Giardini (2003), New GPS constraints on the Africa-Eurasia plate boundary zone in southern Italy, *Geophys. Res. Lett.*, 30(18), 1935, doi:10.1029/2003GL017554.
- Holt, W. E., and A. J. Haines (1993), Velocity fields in deforming Asia from the inversion of earthquake-released strains, *Tectonics*, 12(1), 1–20, doi:10.1029/92TC00658.
- Holt, W. E., B. Shen-Tu, J. Haines, and J. Jackson (2000), On the determination of self-consistent strain rate fields within zones of distributed continental deformation, in *The History and Dynamics of Global Plate Motions*, *Geophys. Monogr. Ser.* 121, edited by M. A. Richards, R. G. Gordon, and R. D. van der Hilst, pp. 113–141, AGU, Washington, D. C.
- Holt, W. E., C. Kreemer, A. J. Haines, L. Estey, C. Meertens, G. Blewitt, and D. Lavallée (2005), Project helps constrain continental dynamics and seismic hazards, *Eos Trans. AGU*, 86(41), 383–387, doi:10.1029/2005EO410002.
- Horner-Johnson, B. C., R. G. Gordon, and D. F. Argus (2007), Plate kinematic evidence for the existence of a distinct plate between the Nubian and Somalian plates along the Southwest Indian Ridge, *J. Geophys. Res.*, 112, B05418, doi:10.1029/2006JB004519.
- Hreinsson, S., P. Einarsson, and F. Sigmundsson (2001), Crustal deformation at the oblique spreading Reykjanes Peninsula, SW Iceland: GPS measurements from 1993 to 1998, *J. Geophys. Res.*, 106(B7), 13803–13,816, doi:10.1029/2001JB000428.
- Hsu, Y.-J., S.-B. Yu, M. Simons, L.-C. Kuo, and H.-Y. Chen (2009), Interseismic crustal deformation in the Taiwan plate boundary zone revealed by GPS observations, seismicity, and earthquake focal mechanisms, *Tectonophysics*, 479(1–2), 4–18, doi:10.1016/j.tecto.2008.11.016.
- Hsu, Y.-J., M. Ando, S.-B. Yu, and M. Simons (2012), The potential for a great earthquake along the southernmost Ryukyu subduction zone, *Geophys. Res. Lett.*, 39, L14302, doi:10.1029/2012GL052764.
- Hu, J.-C., et al. (2007), Fault activity and lateral extrusion inferred from velocity field revealed by GPS measurements in the Pingtung area of southwestern Taiwan, *J. Asian Earth Sci.*, 31(3), 287–302, doi:10.1016/j.jseas.2006.07.020.
- Husson, L. (2012), Trench migration and upper plate strain over a convecting mantle, *Phys. Earth Planet. Inter.*, 212–213, 32–43, doi:10.1016/j.pepi.2012.09.006.
- Iaffaldano, G. (2014), A geodynamical view on the steadiness of geodetically derived rigid plate motions over geological time, *Geochem. Geophys. Geosystems*, 15(1), 238–254, doi:10.1002/2013GC005088.
- Ihemedu, D. K. (2012), An updated GPS velocity field for Puerto Rico and Virgin Islands: Constraints on tectonic setting and internal deformation, MS thesis, Univ. of Tex., Arlington.
- Imuma, T., M. Protti, K. Obana, V. González, R. Van der Laat, T. Kato, S. Miyazaki, Y. Kaneda, and E. Hernández (2004), Inter-plate coupling in the Nicoya Peninsula, Costa Rica, as deduced from a trans-peninsula GPS experiment, *Earth Planet. Sci. Lett.*, 223(1–2), 203–212, doi:10.1016/j.epsl.2004.04.016.
- Ischuk, A., et al. (2013), Kinematics of the Pamir and Hindu Kush regions from GPS geodesy, *J. Geophys. Res. Solid Earth*, 118, 2408–2416, doi:10.1002/jgrb.50185.
- Jackson, J., and D. McKenzie (1984), Active tectonics of the Alpine—Himalayan Belt between western Turkey and Pakistan, *Geophys. J. Int.*, 77(1), 185–264, doi:10.1111/j.1365-246X.1984.tb01931.x.
- Jade, S., B. C. Bhatt, Z. Yang, R. Bendick, V. K. Gaur, P. Molnar, M. B. Anand, and D. Kumar (2004), GPS measurements from the Ladakh Himalaya, India: Preliminary tests of plate-like or continuous deformation in Tibet, *Geol. Soc. Am. Bull.*, 116(11–12), 1385–1391, doi:10.1130/B25357.1.
- Jade, S., et al. (2007), Estimates of interseismic deformation in Northeast India from GPS measurements, *Earth Planet. Sci. Lett.*, 263(3–4), 221–234, doi:10.1016/j.epsl.2007.08.031.
- Jansma, P. E., and G. S. Mattioli (2005), GPS results from Puerto Rico and the Virgin Islands: Constraints on tectonic setting and rates of active faulting, edited by P. Mann, *Geol. Soc. Am. Spec. Pap.*, 385, 13–30, doi:10.1130/0-8137-2385-X.13.
- Jansma, P. E., G. S. Mattioli, A. Lopez, C. DeMets, T. H. Dixon, P. Mann, and E. Calais (2000), Neotectonics of Puerto Rico and the Virgin Islands, northeastern Caribbean, from GPS geodesy, *Tectonics*, 19(6), 1021–1037, doi:10.1029/1999TC001170.
- Jiang, W.-P., D.-C. E. B.-W. Zhan, and Y.-W. Liu (2009), New model of Antarctic plate motion and its analysis, *Chin. J. Geophys.*, 52(1), 23–32.
- Jin, S., Z. Li, and P.-H. Park (2006), Seismicity and GPS constraints on crustal deformation in the southern part of the Korean Peninsula, *Geosci. J.*, 10(4), 491–497, doi:10.1007/BF02910442.
- Jouanne, F., F. A. Audemard, C. Beck, A. Van Welden, R. Ollarves, and C. Reinoza (2011), Present-day deformation along the El Pilar Fault in eastern Venezuela: Evidence of creep along a major transform boundary, *J. Geodyn.*, 51(5), 398–410, doi:10.1016/j.jog.2010.11.003.
- Jouanne, F., J. L. Mugnier, R. Koci, S. Bushati, K. Matev, N. Kuka, I. Shinko, S. Kociu, and L. Duni (2012), GPS constraints on current tectonics of Albania, *Tectonophysics*, 554–557, 50–62, doi:10.1016/j.tecto.2012.06.008.
- Kadirov, F., M. Floyd, A. Alizadeh, I. Guliev, R. Reilinger, S. Kuleli, R. King, and M. Toksoz (2012), Kinematics of the eastern Caucasus near Baku, Azerbaijan, *Nat. Hazards*, 63(2), 997–1006, doi:10.1007/s11069-012-0199-0.
- Kahle, H.-G., M. Cocard, Y. Peter, A. Geiger, R. Reilinger, A. Barka, and G. Veis (2000), GPS-derived strain rate field within the boundary zones of the Eurasian, African, and Arabian Plates, *J. Geophys. Res.*, 105(B10), 23,353–23,370, doi:10.1029/2000JB900238.
- Kang, T.-S., and J. S. Shin (2009), Shear-wave splitting beneath southern Korea and its tectonic implication, *Tectonophysics*, 471(3–4), 232–239, doi:10.1016/j.tecto.2009.02.021.
- Karakhanian, A., et al. (2013), GPS constraints on continental deformation in the Armenian region and Lesser Caucasus, *Tectonophysics*, 592, 39–45, doi:10.1016/j.tecto.2013.02.002.
- Karimzadeh, S., Z. Cakir, B. Osmanoğlu, G. Schmalzle, M. Miyajima, R. Amiraslanzadeh, and Y. Djamar (2013), Interseismic strain accumulation across the North Tabriz Fault (NW Iran) deduced from InSAR time series, *J. Geodyn.*, 66, 53–58, doi:10.1016/j.jog.2013.02.003.
- Kato, T., J. Beavan, T. Matsushima, Y. Kotake, J. T. Camacho, and S. Nakao (2003), Geodetic evidence of back-arc spreading in the Mariana Trough, *Geophys. Res. Lett.*, 30(12), 1625, doi:10.1029/2002GL016757.
- Kaviani, A., D. Hatzfeld, A. Paul, M. Tatar, and K. Priestley (2009), Shear-wave splitting, lithospheric anisotropy, and mantle deformation beneath the Arabia-Eurasia collision zone in Iran, *Earth Planet. Sci. Lett.*, 286(3–4), 371–378, doi:10.1016/j.epsl.2009.07.003.

- Keiding, M., T. Árnadóttir, E. Sturkell, H. Geirsson, and B. Lund (2008), Strain accumulation along an oblique plate boundary: The Reykjanes Peninsula, southwest Iceland, *Geophys. J. Int.*, 172(2), 861–872, doi:10.1111/j.1365-246X.2007.03655.x.
- Kendrick, E., M. Bevis, R. Smalley Jr., B. Brooks, R. B. Vargas, E. Lauria, and L. P. S. Fortes (2003), The Nazca–South America Euler vector and its rate of change, *J. South Am. Earth Sci.*, 16(2), 125–131, doi:10.1016/S0895-9811(03)00028-2.
- Kierulf, H. P., M. Ouassou, M. J. R. Simpson, and O. Vestel (2013), A continuous velocity field for Norway, *J. Geod.*, 87(4), 337–349, doi:10.1007/s00190-012-0603-2.
- King, M. A., and S. D. P. Williams (2009), Apparent stability of GPS monumentation from short-baseline time series, *J. Geophys. Res.*, 114, B10403, doi:10.1029/2009JB006319.
- Klotz, J., G. Khazaradze, D. Angermann, C. Reigber, R. Perdomo, and O. Cifuentes (2001), Earthquake cycle dominates contemporary crustal deformation in Central and Southern Andes, *Earth Planet. Sci. Lett.*, 193(3–4), 437–446, doi:10.1016/S0012-821X(01)00532-5.
- Kogan, L., S. Fisseha, R. Bendick, R. Reilinger, S. McClusky, R. King, and T. Solomon (2012), Lithospheric strength and strain localization in continental extension from observations of the East African Rift, *J. Geophys. Res.*, 117, B03402, doi:10.1029/2011JB008516.
- Kogan, M. G., and G. M. Steblow (2008), Current global plate kinematics from GPS (1995–2007) with the plate-consistent reference frame, *J. Geophys. Res.*, 113, B04416, doi:10.1029/2007JB005353.
- Kotzev, V., R. Nakov, T. Georgiev, B. C. Burchfiel, and R. W. King (2006), Crustal motion and strain accumulation in western Bulgaria, *Tectonophysics*, 413(3–4), 127–145, doi:10.1016/j.tecto.2005.10.040.
- Koulali, A., D. Ouazar, A. Tahayt, R. W. King, P. Vernant, R. E. Reilinger, S. McClusky, T. Mourabit, J. M. Davila, and N. Amraoui (2011), New GPS constraints on active deformation along the Africa–Iberia plate boundary, *Earth Planet. Sci. Lett.*, 308(1–2), 211–217, doi:10.1016/j.epsl.2011.05.048.
- Kreemer, C. (2009), Absolute plate motions constrained by shear wave splitting orientations with implications for hot spot motions and mantle flow, *J. Geophys. Res.*, 114, B10405, doi:10.1029/2009JB006416.
- Kreemer, C., and R. G. Gordon (2014), Pacific plate deformation from horizontal thermal contraction, *Geology*, 42(10), 847–850.
- Kreemer, C., and W. E. Holt (2001), A no-net-rotation model of present-day surface motions, *Geophys. Res. Lett.*, 28(23), 4407–4410, doi:10.1029/2001GL013232.
- Kreemer, C., J. Haines, W. Holt, G. Blewitt, and D. Lavallée (2000), On the determination of a global strain rate model, *Geophys. J. Int.*, 52(10), 765–770.
- Kreemer, C., W. E. Holt, and A. J. Haines (2002), The global moment rate distribution within plate boundary zones, in *Plate Boundary Zones*, edited by S. Stein and J. T. Freymueller, pp. 173–190, AGU, Washington, D. C.
- Kreemer, C., W. E. Holt, and A. J. Haines (2003), An integrated global model of present-day plate motions and plate boundary deformation, *Geophys. J. Int.*, 154(1), 8–34, doi:10.1046/j.1365-246X.2003.01917.x.
- Kreemer, C., D. A. Lavallée, G. Blewitt, and W. E. Holt (2006), On the stability of a geodetic no-net-rotation frame and its implication for the International Terrestrial Reference Frame, *Geophys. Res. Lett.*, 33, L17306, doi:10.1029/2006GL027058.
- Kreemer, C., G. Blewitt, and W. C. Hammond (2010a), Evidence for an active shear zone in southern Nevada linking the Wasatch fault to the Eastern California shear zone, *Geology*, 38(5), 475–478, doi:10.1130/G30477.1.
- Kreemer, C., G. Blewitt, and R. A. Bennett (2010b), Present-day motion and deformation of the Colorado Plateau, *Geophys. Res. Lett.*, 37, L10311, doi:10.1029/2010GL043374.
- Kreemer, C., W. C. Hammond, G. Blewitt, A. A. Holland, and R. A. Bennett (2012), A geodetic strain rate model for the Pacific–North American plate boundary, western United States, *Map 178*, scale 1:1,500,000. Nevada Bureau of Mines and Geology, Reno, Nevada.
- Kumar, R. R., and R. G. Gordon (2009), Horizontal thermal contraction of oceanic lithosphere: The ultimate limit to the rigid plate approximation, *J. Geophys. Res.*, 114, B01403, doi:10.1029/2007JB005473.
- Kuo, S.-M., K.-E. Ching, R.-J. Rau, and C.-S. Hou (2008), Contemporary crustal deformation in Tainan area from GPS observation, 1996–2006, *Cent. Geol. Surv. Spec. Publ.*, 20, 1–16.
- LaFemina, P., T. H. Dixon, R. Govers, E. Norabuena, H. Turner, A. Saballo, G. Mattioli, M. Protti, and W. Strauch (2009), Fore-arc motion and Cocos Ridge collision in Central America, *Geochem. Geophys. Geosyst.*, 10, Q05S14, doi:10.1029/2008GC002181.
- LaFemina, P. C., T. H. Dixon, R. Malservisi, T. Árnadóttir, E. Sturkell, F. Sigmundsson, and P. Einarsson (2005), Geodetic GPS measurements in south Iceland: Strain accumulation and partitioning in a propagating ridge system, *J. Geophys. Res.*, 110(B11), B11405, doi:10.1029/2005JB003675.
- Langbein, J. (2012), Estimating rate uncertainty with maximum likelihood: Differences between power-law and flicker-random-walk models, *J. Geod.*, 86(9), 775–783, doi:10.1007/s00190-012-0556-5.
- Langbein, J., and H. Johnson (1997), Correlated errors in geodetic time series: Implications for time-dependent deformation, *J. Geophys. Res.*, 102(B1), 591–603, doi:10.1029/96JB02945.
- Latychev, K., J. X. Mitrovica, J. Tromp, M. E. Tamisiea, D. Komatsitsch, and C. C. Christara (2005), Glacial isostatic adjustment on 3-D Earth models: A finite-volume formulation, *Geophys. J. Int.*, 161(2), 421–444, doi:10.1111/j.1365-246X.2005.02536.x.
- Le Beon, M. L., Y. Klinger, A. Q. Amrat, A. Agnon, L. Dorbath, G. Baer, J.-C. Ruegg, O. Charade, and O. Mayyas (2008), Slip rate and locking depth from GPS profiles across the southern Dead Sea Transform, *J. Geophys. Res.*, 113, B11403, doi:10.1029/2007JB005280.
- Leonard, M. (2010), Earthquake fault scaling: Self-consistent relating of rupture length, width, average displacement, and moment release, *Bull. Seismol. Soc. Am.*, 100, 1971–1988, doi:10.1785/0120090189.
- Le Pichon, X., and C. Kreemer (2010), The Miocene-to-Present kinematic evolution of the eastern Mediterranean and Middle East and its implications for dynamics, *Annu. Rev. Earth Planet. Sci.*, 38(1), 323–351, doi:10.1146/annurev-earth-040809-152419.
- Liang, S., W. Gan, C. Shen, G. Xiao, J. Liu, W. Chen, X. Ding, and D. Zhou (2013), Three-dimensional velocity field of present-day crustal motion of the Tibetan Plateau derived from GPS measurements, *J. Geophys. Res. Solid Earth*, 118, 5722–5732, doi:10.1002/2013JB010503.
- Lidberg, M., J. M. Johansson, H.-G. Scherneck, and G. A. Milne (2010), Recent results based on continuous GPS observations of the GIA process in Fennoscandia from BIFROST, *J. Geodyn.*, 50(1), 8–18, doi:10.1016/j.jog.2009.11.010.
- Liu, Z., S. Owen, D. Dong, P. Lundgren, F. Webb, E. Hetland, and M. Simons (2010), Estimation of interplate coupling in the Nankai trough, Japan using GPS data from 1996 to 2006, *Geophys. J. Int.*, 181(3), 1313–1328, doi:10.1111/j.1365-246X.2010.04600.x.
- Lockridge, J. S., M. J. Fouch, and J. R. Arrowsmith (2012), Seismicity within Arizona during the deployment of the EarthScope USArray transportable array, *Bull. Seismol. Soc. Am.*, 102(4), 1850–1863, doi:10.1785/0120110297.
- Long, M. D., and P. G. Silver (2009), Mantle flow in subduction systems: The subslab flow field and implications for mantle dynamics, *J. Geophys. Res.*, 114, B10312, doi:10.1029/2008JB006200.
- López, A. M., S. Stein, T. Dixon, G. Sella, E. Calais, P. Jansma, J. Weber, and P. LaFemina (2006), Is there a northern Lesser Antilles forearc block?, *Geophys. Res. Lett.*, 33, L07313, doi:10.1029/2005GL025293.

- Lukhnev, A. V., V. A. San'kov, A. I. Miroshnichenko, S. V. Ashurkov, and E. Calais (2010), GPS rotation and strain rates in the Baikal–Mongolia region, *Russ. Geol. Geophys.*, 51(7), 785–793, doi:10.1016/j.rgg.2010.06.006.
- Lyard, F., F. Lefevre, T. Letellier, and O. Francis (2006), Modelling the global ocean tides: Modern insights from FES2004, *Ocean Dyn.*, 56(5–6), 394–415, doi:10.1007/s10236-006-0086-x.
- Mackey, K. G., K. Fujita, L. V. Gunbina, V. N. Kovalev, V. S. Imaev, B. M. Koz'min, and L. P. Imaeva (1997), Seismicity of the Bering Strait region: Evidence for a Bering block, *Geology*, 25(11), 979–982, doi:10.1130/0091-7613(1997)025<0979:SOTBSR>2.3.CO;2.
- Mahanta, K., J. D. Chowdhury, A. Kumar, I. Laskar, S. L. Singh, and P. Barman (2012), Earthquakes and crustal deformation studies of the seismically active Kopili Fault as well as North East India: A scientific field study using Global Positioning System (GPS), *Clarión*, 11(1), 51–58.
- Mahesh, P., et al. (2012), Rigid Indian plate: Constraints from GPS measurements, *Gondwana Res.*, 22(3–4), 1068–1072, doi:10.1016/j.gr.2012.01.011.
- Mahmoud, S., R. Reilinger, S. McClusky, P. Vernant, and A. Tealeb (2005), GPS evidence for northward motion of the Sinai Block: Implications for E. Mediterranean tectonics, *Earth Planet. Sci. Lett.*, 238(1–2), 217–224, doi:10.1016/j.epsl.2005.06.063.
- Mahmoud, Y., F. Masson, M. Meghraoui, Z. Cakir, A. Alchalbi, H. Yavasoglu, O. Yonlu, M. Daoud, S. Ergintav, and S. Inan (2013), Kinematic study at the junction of the East Anatolian fault and the Dead Sea fault from GPS measurements, *J. Geodyn.*, 67, 30–39, doi:10.1016/j.jog.2012.05.006.
- Malservisi, R., U. Hugentobler, R. Wonnacott, and M. Hackl (2013), How rigid is a rigid plate? Geodetic constraint from the TrigNet CGPS network, South Africa, *Geophys. J. Int.*, 192(3), 918–928, doi:10.1093/gji/ggs081.
- Manaker, D. M., E. Calais, A. M. Freed, S. T. Ali, P. Przybylski, G. Mattioli, P. Jansma, C. Petit, and J. B. de Chabalier (2008), Interseismic plate coupling and strain partitioning in the Northeastern Caribbean, *Geophys. J. Int.*, 174(3), 889–903.
- Mann, P., F. W. Taylor, R. L. Edwards, and T.-L. Ku (1995), Actively evolving microplate formation by oblique collision and sideways motion along strike-slip faults: An example from the northeastern Caribbean plate margin, *Tectonophysics*, 246(1–3), 1–69, doi:10.1016/0040-1951(94)00268-E.
- Mao, A., C. G. A. Harrison, and T. H. Dixon (1999), Noise in GPS coordinate time series, *J. Geophys. Res.*, 104(B2), 2797–2816, doi:10.1029/1998JB900033.
- Marjanović, M., Ž. Bačić, and T. Bašić (2012), Determination of horizontal and vertical movements of the Adriatic microplate on the basis of GPS measurements, in *Geodesy for Planet Earth*, vol. 136, edited by S. Kenyon, M. C. Pacino, and U. Marti, pp. 683–688, Springer, Berlin.
- Marques, F. O., J. C. Catalão, C. DeMets, A. C. G. Costa, and A. Hildenbrand (2013), GPS and tectonic evidence for a diffuse plate boundary at the Azores Triple Junction, *Earth Planet. Sci. Lett.*, 381, 177–187, doi:10.1016/j.epsl.2013.08.051.
- Márquez-Azúa, B., and C. DeMets (2003), Crustal velocity field of Mexico from continuous GPS measurements, 1993 to June 2001: Implications for the neotectonics of Mexico, *J. Geophys. Res.*, 108(B9), 2450, doi:10.1029/2002JB002241.
- Márquez-Azúa, B., and C. DeMets (2009), Deformation of Mexico from continuous GPS from 1993 to 2008, *Geochem., Geophys. Geosyst.*, 10, Q02003, doi:10.1029/2008GC002278.
- Mascle, J., J. Benkhelil, G. Bellaiche, T. Zitter, J. Woodside, and L. Loncke (2000), Marine geologic evidence for a Levantine-Sinai plate, a new piece of the Mediterranean puzzle, *Geology*, 28(9), 779–782, doi:10.1130/0091-7613(2000)28<779:MGEFAL>2.0.CO;2.
- Masson, F., M. Anvari, Y. Djamour, A. Walpersdorf, F. Tavakoli, M. Daignières, H. Nankali, and S. Van Gorp (2007), Large-scale velocity field and strain tensor in Iran inferred from GPS measurements: New insight for the present-day deformation pattern within NE Iran, *Geophys. J. Int.*, 170(1), 436–440, doi:10.1111/j.1365-246X.2007.03477.x.
- Masson, F., M. Lehujeur, Y. Ziegler, and C. Doubre (2014), Strain rate tensor in Iran from a new GPS velocity field, *Geophys. J. Int.*, 197(1), 10–21, doi:10.1093/gji/gjt509.
- Matev, K. (2011), GPS constraints on current tectonics of southwest Bulgaria, northern Greece, and Albania, PhD thesis, Univ. de Grenoble.
- Mattia, M., M. Palano, V. Bruno, and F. Cannavò (2009), Crustal motion along the Calabro-Peloritano Arc as imaged by twelve years of measurements on a dense GPS network, *Tectonophysics*, 476(3–4), 528–537, doi:10.1016/j.tecto.2009.06.006.
- Maurin, T., F. Masson, C. Rangin, U. T. Min, and P. Collard (2010), First global positioning system results in northern Myanmar: Constant and localized slip rate along the Sagaing fault, *Geology*, 38(7), 591–594, doi:10.1130/G30872.1.
- Mazzotti, S., T. S. James, J. Henton, and J. Adams (2005), GPS crustal strain, postglacial rebound, and seismic hazard in eastern North America: The Saint Lawrence valley example, *J. Geophys. Res.*, 110, B11301, doi:10.1029/2004JB003590.
- Mazzotti, S., L. J. Leonard, R. D. Hyndman, and J. F. Cassidy (2008), Tectonics, dynamics, and seismic hazard in the Canada-Alaska Cordillera, in *Active Tectonics and Seismic Potential of Alaska*, edited by J. T. Freymueller et al., pp. 297–319, AGU, Washington, D. C.
- Mazzotti, S., L. J. Leonard, J. F. Cassidy, G. C. Rogers, and S. Halchuk (2011), Seismic hazard in western Canada from GPS strain rates versus earthquake catalog, *J. Geophys. Res.*, 116, B12310, doi:10.1029/2011JB008213.
- McCaffrey, R. (2005), Block kinematics of the Pacific–North America plate boundary in the southwestern United States from inversion of GPS, seismological, and geologic data, *J. Geophys. Res.*, 110, B07401, doi:10.1029/2004JB003307.
- McCaffrey, R., R. W. King, S. J. Payne, and M. Lancaster (2013), Active tectonics of northwestern U.S. inferred from GPS-derived surface velocities, *J. Geophys. Res. Solid Earth*, 118, 709–723, doi:10.1029/2012JB009473.
- McCann, W. R. (1985), On the earthquake hazards of Puerto Rico and the Virgin Islands, *Bull. Seismol. Soc. Am.*, 75(1), 251–262.
- McClusky, S., et al. (2000), Global Positioning System constraints on plate kinematics and dynamics in the eastern Mediterranean and Caucasus, *J. Geophys. Res.*, 105(B3), 5695–5719, doi:10.1029/1999JB900351.
- McClusky, S., et al. (2010), Kinematics of the southern Red Sea–Afar Triple Junction and implications for plate dynamics, *Geophys. Res. Lett.*, 37, L05301, doi:10.1029/2009GL041127.
- McKenzie, D. P. (1970), Plate tectonics of the Mediterranean region, *Nature*, 226(5242), 239–243, doi:10.1038/226239a0.
- Meade, B. J. (2007), Present-day kinematics at the India-Asia collision zone, *Geology*, 35(1), 81–84, doi:10.1130/G22924A.1.
- Medak, D., and B. Pribicevic (2006), Processing of geodynamic GPS neworks in Croatia with GAMIT software, in *The Adriatic Microplate: GPS Geodesy, Tectonics and Hazards*, vol. 61, edited by N. Pinter, pp. 247–256, Springer, Dordrecht, Netherlands.
- Meilano, I., et al. (2012), Slip rate estimation of the Lembang Fault West Java from geodetic observation, *J. Disaster Res.*, 7(1), 12–18.
- Mendes, V. B., J. Madeira, A. Brum da Silveira, A. Trota, P. Elosegui, and J. Pagarete (2013), Present-day deformation in São Jorge Island, Azores, from episodic GPS measurements (2001–2011), *Adv. Space Res.*, 51(8), 1581–1592, doi:10.1016/j.asr.2012.10.019.
- Mendoza, L., R. Perdomo, J. L. Hormaechea, D. D. Coglianico, M. Fritsche, A. Richter, and R. Dietrich (2011), Present-day crustal deformation along the Magallanes–Fagnano Fault System in Tierra del Fuego from repeated GPS observations, *Geophys. J. Int.*, 184(3), 1009–1022, doi:10.1111/j.1365-246X.2010.04912.x.
- Meng, G. J., X. H. Shen, S. Vladimir, A. R. Eugene, and J. C. Wu (2009), Research on characteristics of present-day crustal motion and deformation in Kamchatka area, *Chin. J. Geophys.*, 52(3), 720–731.

- Métois, M., C. Vigny, A. Socquet, A. Delorme, S. Morvan, I. Ortega, and C.-M. Valderrama-Bermejo (2013), GPS-derived interseismic coupling on the subduction and seismic hazards in the Atacama region, Chile, *Geophys. J. Int.*, 196(2), 644–655, doi:10.1093/gji/ggt418.
- Metzger, S., S. Jónsson, G. Danielsen, S. Hreinsdóttir, F. Jouanne, D. Giardini, and T. Villemain (2013), Present kinematics of the Tjörnes Fracture Zone, North Iceland, from campaign and continuous GPS measurements, *Geophys. J. Int.*, 192(2), 441–455, doi:10.1093/gji/ggs032.
- Miranda, J. M., A. Navarro, J. Catalão, and R. M. S. Fernandes (2012), Surface displacement field at Terceira island deduced from repeated GPS measurements, *J. Volcanol. Geotherm. Res.*, 217–218, 1–7, doi:10.1016/j.volgeores.2011.10.009.
- Mitchell, B. J., L. Cong, and G. Ekström (2008), A continent-wide map of 1-Hz Lg coda Q variation across Eurasia and its relation to lithospheric evolution, *J. Geophys. Res.*, 113, B04303, doi:10.1029/2007JB005065.
- Mohadjer, S., et al. (2010), Partitioning of India-Eurasia convergence in the Pamir-Hindu Kush from GPS measurements, *Geophys. Res. Lett.*, 37, L04305, doi:10.1029/2009GL041737.
- Moreno, M., et al. (2011), Heterogeneous plate locking in the South-Central Chile subduction zone: Building up the next great earthquake, *Earth Planet. Sci. Lett.*, 305(3–4), 413–424, doi:10.1016/j.epsl.2011.03.025.
- Mousavi, Z., A. Walpersdorf, R. T. Walker, F. Tavakoli, E. Pathier, H. Nankali, F. Nilforoushan, and Y. Djamous (2013), Global Positioning System constraints on the active tectonics of NE Iran and the South Caspian region, *Earth Planet. Sci. Lett.*, 377–378, 287–298, doi:10.1016/j.epsl.2013.07.007.
- Mukul, M., S. Jade, A. Bhattacharyya, and K. Bhusan (2010), Crustal shortening in convergent orogens: Insights from global positioning system (GPS) measurements in northeast India, *J. Geol. Soc. India*, 75(1), 302–312, doi:10.1007/s12594-010-0017-9.
- Müller, M. D., A. Geiger, H.-G. Kahle, G. Veis, H. Billiris, D. Paradissis, and S. Feleki (2013), Velocity and deformation fields in the North Aegean domain, Greece, and implications for fault kinematics, derived from GPS data 1993–2009, *Tectonophysics*, 597–598, 34–49, doi:10.1016/j.tecto.2012.08.003.
- Mullick, M., F. Riguzzi, and D. Mukhopadhyay (2009), Estimates of motion and strain rates across active faults in the frontal part of eastern Himalayas in North Bengal from GPS measurements, *Terra Nova*, 21(5), 410–415, doi:10.1111/j.1365-3121.2009.00898.x.
- Munekane, H., and Y. Fukuzaki (2006), A plate motion model around Japan, *Bull. Geogr. Surv. Inst.*, 35–41, 35.
- Nguyen, A. D., T. Sagiya, F. Kimata, D. T. Tran, Q. H. Vy, C. C. Duong, X. B. Nguyen, and D. X. Nguyen (2013), Contemporary horizontal crustal movement estimation for northwestern Vietnam inferred from repeated GPS measurements, *Earth Planets Space*, 65(12), 1399–1410, doi:10.5047/eps.2013.09.010.
- Niemi, N. A., B. P. Wernicke, A. M. Friedrich, M. Simons, R. A. Bennett, and J. L. Davis (2004), BARGEN continuous GPS data across the eastern Basin and Range province, and implications for fault system dynamics, *Geophys. J. Int.*, 159(3), 842–862, doi:10.1111/j.1365-246X.2004.02454.x.
- Nilforoushan, F., et al. (2003), GPS network monitors the Arabia-Eurasia collision deformation in Iran, *J. Geod.*, 77(7–8), 411–422, doi:10.1007/s00190-003-0326-5.
- Nishimura, S., M. Hashimoto, and M. Ando (2004), A rigid block rotation model for the GPS derived velocity field along the Ryukyu arc, *Phys. Earth Planet. Inter.*, 142(3–4), 185–203, doi:10.1016/j.pepi.2003.12.014.
- Nishimura, T. (2011), Back-arc spreading of the northern Izu-Ogasawara (Bonin) Islands arc clarified by GPS data, *Tectonophysics*, 512(1–4), 60–67, doi:10.1016/j.tecto.2011.09.022.
- Nocquet, J.-M. (2012), Present-day kinematics of the Mediterranean: A comprehensive overview of GPS results, *Tectonophysics*, 579, 220–242, doi:10.1016/j.tecto.2012.03.037.
- Nocquet, J.-M., and E. Calais (2003), Crustal velocity field of western Europe from permanent GPS array solutions, 1996–2001, *Geophys. J. Int.*, 154(1), 72–88, doi:10.1046/j.1365-246X.2003.01935.x.
- Nocquet, J.-M., et al. (2014), Motion of continental slivers and creeping subduction in the northern Andes, *Nat. Geosci.*, 7(4), 287–291, doi:10.1038/ngeo2099.
- Nugroho, H., R. Harris, A. W. Lestariya, and B. Maruf (2009), Plate boundary reorganization in the active Banda Arc-continent collision: Insights from new GPS measurements, *Tectonophysics*, 479(1–2), 52–65, doi:10.1016/j.tecto.2009.01.026.
- Ohzono, M., T. Sagiya, K. Hirahara, M. Hashimoto, A. Takeuchi, Y. Hoso, Y. Wada, K. Onoue, F. Ohya, and R. Doke (2011), Strain accumulation process around the Atotsugawa fault system in the Niigata-Kobe Tectonic Zone, central Japan, *Geophys. J. Int.*, 184(3), 977–990, doi:10.1111/j.1365-246X.2010.04876.x.
- Ozener, H., O. Yilmaz, A. Dogru, B. Turgut, and O. Gurkan (2013a), GPS-derived velocity field of the Iznik-Mekece segment of the North Anatolian Fault Zone, *J. Geodyn.*, 67, 46–52, doi:10.1016/j.jog.2012.07.001.
- Ozener, H., A. Dogru, and B. Turgut (2013b), Quantifying aseismic creep on the Ismetpasa segment of the North Anatolian Fault Zone (Turkey) by 6 years of GPS observations, *J. Geodyn.*, 67, 72–77, doi:10.1016/j.jog.2012.08.002.
- Palano, M., L. Ferranti, C. Monaco, M. Mattia, M. Aloisi, V. Bruno, F. Cannavò, and G. Siligato (2012), GPS velocity and strain fields in Sicily and southern Calabria, Italy: Updated geodetic constraints on tectonic block interaction in the central Mediterranean, *J. Geophys. Res.*, 117, B07401, doi:10.1029/2012JB009254.
- Paul, J., et al. (2001), The motion and active deformation of India, *Geophys. Res. Lett.*, 28(4), 647–650, doi:10.1029/2000GL011832.
- Peltier, W. R., and R. Drummond (2008), Rheological stratification of the lithosphere: A direct inference based upon the geodetically observed pattern of the glacial isostatic adjustment of the North American continent, *Geophys. Res. Lett.*, 35, L16314, doi:10.1029/2008GL034586.
- Pérez, O. J., R. Bilham, R. Bendick, J. R. Velandia, N. Hernández, C. Moncayo, M. Hoyer, and M. Kozuch (2001), Velocity field across the southern Caribbean plate boundary and estimates of Caribbean/South-American plate motion using GPS geodesy 1994–2000, *Geophys. Res. Lett.*, 28(15), 2987–2990, doi:10.1029/2001GL013183.
- Pérez, O. J., et al. (2011), GPS derived velocity field in western Venezuela: Dextral shear component associated to the Bocono fault and convergent component normal to the Andes, *Interciencia*, 36(1), 39–44.
- Pérez-Peña, A., J. Martín-Davila, J. Gárate, M. Berroceno, and E. Buñom (2010), Velocity field and tectonic strain in Southern Spain and surrounding areas derived from GPS episodic measurements, *J. Geodyn.*, 49(3–4), 232–240, doi:10.1016/j.jog.2010.01.015.
- Pesci, A., G. Teza, G. Casula, N. Cenni, and F. Loddo (2010), Non-permanent GPS data for regional-scale kinematics: Reliable deformation rate before the 6 April, 2009, earthquake in the L'Aquila area, *Ann. Geophys.*, 53(2), 55–68, doi:10.4401/ag-4740.
- Peyret, M., et al. (2009), Present-day strain distribution across the Minab-Zendan-Palami fault system from dense GPS transects, *Geophys. J. Int.*, 179(2), 751–762, doi:10.1111/j.1365-246X.2009.04321.x.
- Phillips, D. A. (2003), Crustal motion studies in the Southwest Pacific: Geodetic measurements of plate convergence in Tonga, Vanuatu and the Solomon Islands, PhD thesis, Univ. of Hawaii at Manoa, Honolulu, Hawaii.
- Plattner, C., R. Malaservisi, T. H. Dixon, P. LaFemina, G. F. Sella, J. Fletcher, and F. Suarez-Vidal (2007), New constraints on relative motion between the Pacific Plate and Baja California microplate (Mexico) from GPS measurements, *Geophys. J. Int.*, 170(3), 1373–1380, doi:10.1111/j.1365-246X.2007.03494.x.

- Poland, M., R. Bürgmann, D. Dzurisin, M. Lisowski, T. Masterlark, S. Owen, and J. Fink (2006), Constraints on the mechanism of long-term, steady subsidence at Medicine Lake volcano, northern California, from GPS, leveling, and InSAR, *J. Volcanol. Geotherm. Res.*, **150**, 55–78, doi:10.1016/j.jvolgeores.2005.07.007.
- Pollitz, F. F., P. McCrory, J. Svart, and J. Murray (2008), Dislocation models of interseismic deformation in the western United States, *J. Geophys. Res.*, **113**, B04413, doi:10.1029/2007JB005174.
- Ponraj, M., S. Miura, C. D. Reddy, S. K. Prajapati, S. Amirtharaj, and S. H. Mahajan (2010), Estimation of strain distribution using GPS measurements in the Kumaun region of Lesser Himalaya, *J. Asian Earth Sci.*, **39**(6), 658–667, doi:10.1016/j.jseaes.2010.04.037.
- Prawirodirdjo, L., and Y. Bock (2004), Instantaneous global plate motion model from 12 years of continuous GPS observations, *J. Geophys. Res.*, **109**, B08405, doi:10.1029/2003JB002944.
- Prawirodirdjo, L., R. McCaffrey, C. D. Chadwell, Y. Bock, and C. Subarya (2010), Geodetic observations of an earthquake cycle at the Sumatra subduction zone: Role of interseismic strain segmentation, *J. Geophys. Res.*, **115**, B03414, doi:10.1029/2008JB006139.
- Protti, M., V. González, J. Freymueller, and S. Doelger (2012), Isla del Coco, on Cocos Plate, converges with Isla de San Andrés, on the Caribbean Plate, at 78mm/yr, *Rev. Biol. Trop.*, **60**, 33–41.
- Reischuk, P., J. Griffiths, J. Ray, R. Schmid, X. Collilieux, and B. Garayt (2012), IGS08: The IGS realization of ITRF2008, *GPS Solutions*, **16**(4), 483–494, doi:10.1007/s10291-011-0248-2.
- Reddy, C. D., S. K. Prajapati, and P. S. Sunil (2010), Co and postseismic characteristics of Indian sub-continent in response to the 2004 Sumatra earthquake, *J. Asian Earth Sci.*, **39**(6), 620–626, doi:10.1016/j.jseaes.2010.04.019.
- Reilinger, R., and S. McClusky (2011), Nubia–Arabia–Eurasia plate motions and the dynamics of Mediterranean and Middle East tectonics, *Geophys. J. Int.*, **186**(3), 971–979, doi:10.1111/j.1365-246X.2011.05133.x.
- Reilinger, R., et al. (2006), GPS constraints on continental deformation in the Africa–Arabia–Eurasia continental collision zone and implications for the dynamics of plate interactions, *J. Geophys. Res.*, **111**, B05411, doi:10.1029/2005JB004051.
- Riegel, S. A., K. Fujita, B. M. Koz'min, V. S. Imaev, and D. B. Cook (1993), Extrusion tectonics of the Okhotsk Plate, northeast Asia, *Geophys. Res. Lett.*, **20**(7), 607–610, doi:10.1029/93GL00267.
- Rodriguez, A. (2007), Global Positioning System (GPS) determination of motions, neotectonics, and seismic hazard in Trinidad and Tobago, MS thesis, Grand Valley State Univ, Allendale, Michigan.
- Rodriguez, M., C. DeMets, R. Rogers, C. Tenorio, and D. Hernandez (2009), A GPS and modelling study of deformation in northern Central America, *Geophys. J. Int.*, **178**(3), 1733–1754, doi:10.1111/j.1365-246X.2009.04251.x.
- Rontogianni, S. (2010), Comparison of geodetic and seismic strain rates in Greece by using a uniform processing approach to campaign GPS measurements over the interval 1994–2000, *J. Geodyn.*, **50**(5), 381–399, doi:10.1016/j.jog.2010.04.008.
- Royer, J.-Y., and R. G. Gordon (1997), The motion and boundary between the Capricorn and Australian plates, *Science*, **277**(5330), 1268–1274, doi:10.1126/science.277.5330.1268.
- Ruegg, J. C., A. Rudloff, C. Vigny, R. Madariaga, J. B. de Chabalier, J. Campos, E. Kausel, S. Barrientos, and D. Dimitrov (2009), Interseismic strain accumulation measured by GPS in the seismic gap between Constitución and Concepción in Chile, *Phys. Earth. Planet. Int.*, **175**(1–2), 78–85, doi:10.1016/j.pepi.2008.02.015.
- Sadeh, M., Y. Hamiel, A. Ziv, Y. Bock, P. Fang, and S. Wdowinski (2012), Crustal deformation along the Dead Sea Transform and the Carmel Fault inferred from 12 years of GPS measurements, *J. Geophys. Res.*, **117**, B08410, doi:10.1029/2012JB009241.
- Sagiya, T., S. Miyazaki, and T. Tada (2000), Continuous GPS array and present-day crustal deformation of Japan, *Pure Appl. Geophys.*, **157**(11–12), 2303–2322, doi:10.1007/PL00022507.
- Salamon, A., A. Hofstetter, Z. Garfunkel, and H. Ron (2003), Seismotectonics of the Sinai subplate—The eastern Mediterranean region, *Geophys. J. Int.*, **155**(1), 149–173, doi:10.1046/j.1365-246X.2003.02017.x.
- Saleh, M., and M. Becker (2014), A new velocity field from the analysis of the Egyptian Permanent GPS Network (EPGN), *Arabian J. Geosci.*, **1**–18, doi:10.1007/s12517-013-1132-x, in press.
- Santamaría-Gómez, A., M.-N. Bouin, X. Collilieux, and G. Wöppelmann (2011), Correlated errors in GPS position time series: Implications for velocity estimates, *J. Geophys. Res.*, **116**, B01405, doi:10.1029/2010JB007701.
- Saria, E., E. Calais, Z. Altamimi, P. Willis, and H. Farah (2013), A new velocity field for Africa from combined GPS and DORIS space geodetic solutions: Contribution to the definition of the African Reference Frame (AFREF), *J. Geophys. Res. Solid Earth*, **118**, 1677–1697, doi:10.1002/jgrb.50137.
- Sato, M., M. Fujita, Y. Matsumoto, T. Ishikawa, H. Saito, M. Mochizuki, and A. Asada (2013), Interplate coupling off northeastern Japan before the 2011 Tohoku-oki earthquake, inferred from seafloor geodetic data, *J. Geophys. Res. Solid Earth*, **118**, 3860–3869, doi:10.1002/jgrb.50275.
- Sauber, J., G. Carver, S. Cohen, and R. King (2006), Crustal deformation and the seismic cycle across the Kodiak Islands, Alaska, *J. Geophys. Res.*, **111**, B02403, doi:10.1029/2005JB003626.
- Scheiber-Enslin, S. E., P. C. LaFemina, E. Sturkell, A. J. Hooper, and S. J. Webb (2011), Geodetic investigation of plate spreading along a propagating ridge: The Eastern Volcanic Zone, Iceland, *Geophys. J. Int.*, **187**(3), 1175–1194, doi:10.1111/j.1365-246X.2011.05243.x.
- Schellart, W. P., D. R. Stegman, and J. Freeman (2008), Global trench migration velocities and slab migration induced upper mantle volume fluxes: Constraints to find an Earth reference frame based on minimizing viscous dissipation, *Earth Sci. Rev.*, **88**(1–2), 118–144, doi:10.1016/j.earscirev.2008.01.005.
- Scherneck, H.-G. (1991), A parametrized solid earth tide model and ocean tide loading effects for global geodetic baseline measurements, *Geophys. J. Int.*, **106**(3), 677–694, doi:10.1111/j.1365-246X.1991.tb06339.x.
- Schiffman, C., B. S. Bali, W. Szeliga, and R. Bilham (2013), Seismic slip deficit in the Kashmir Himalaya from GPS observations, *Geophys. Res. Lett.*, **40**(21), 5642–5645, doi:10.1002/2013GL057700.
- Schmid, R., P. Steigenberger, G. Gendt, M. Ge, and M. Rothacher (2007), Generation of a consistent absolute phase-center correction model for GPS receiver and satellite antennas, *J. Geod.*, **81**(12), 781–798, doi:10.1007/s00190-007-0148-y.
- Sella, G. F., T. H. Dixon, and A. Mao (2002), REVEL: A model for Recent plate velocities from space geodesy, *J. Geophys. Res.*, **107**(B4), 2081, doi:10.1029/2000JB000033.
- Sella, G. F., S. Stein, T. H. Dixon, M. Craymer, T. S. James, S. Mazzotti, and R. K. Dokka (2007), Observation of glacial isostatic adjustment in “stable” North America with GPS, *Geophys. Res. Lett.*, **34**, L02306, doi:10.1029/2006GL027081.
- Serpelloni, E., M. Anzidei, P. Baldi, G. Casula, and A. Galvani (2005), Crustal velocity and strain-rate fields in Italy and surrounding regions: New results from the analysis of permanent and non-permanent GPS networks, *Geophys. J. Int.*, **161**(3), 861–880, doi:10.1111/j.1365-246X.2005.02618.x.
- Serpelloni, E., G. Vannucci, S. Pondrelli, A. Argnani, G. Casula, M. Anzidei, P. Baldi, and P. Gasperini (2007), Kinematics of the Western Africa–Eurasia plate boundary from focal mechanisms and GPS data, *Geophys. J. Int.*, **169**(3), 1180–1200, doi:10.1111/j.1365-246X.2007.03367.x.

- Serpelloni, E., R. Bürgmann, M. Anzidei, P. Baldi, B. Mastrolempo Ventura, and E. Boschi (2010), Strain accumulation across the Messina Straits and kinematics of Sicily and Calabria from GPS data and dislocation modeling, *Earth Planet. Sci. Lett.*, 298(3–4), 347–360, doi: 10.1016/j.epsl.2010.08.005.
- Shen, Z.-K., D. D. Jackson, and B. X. Ge (1996), Crustal deformation across and beyond the Los Angeles basin from geodetic measurements, *J. Geophys. Res.*, 101(B12), 27,957–27,980, doi:10.1029/96JB02544.
- Shen, Z.-K., M. Wang, Y. Li, D. D. Jackson, A. Yin, D. Dong, and P. Fang (2001), Crustal deformation along the Altyn Tagh fault system, western China, from GPS, *J. Geophys. Res.*, 106(B12), 30,607–30,621, doi:10.1029/2001JB000349.
- Shen, Z.-K., R. W. King, D. C. Agnew, M. Wang, T. A. Herring, D. Dong, and P. Fang (2011), A unified analysis of crustal motion in Southern California, 1970–2004: The SCEC crustal motion map, *J. Geophys. Res.*, 116, B11402, doi:10.1029/2011JB008549.
- Shestakov, N. V., et al. (2011), Present tectonics of the southeast of Russia as seen from GPS observations, *Geophys. J. Int.*, 184(2), 529–540, doi:10.1111/j.1365-246X.2010.04871.x.
- Shestakov, N. V., et al. (2012), Analysis of the far-field crustal displacements caused by the 2011 Great Tohoku earthquake inferred from continuous GPS observations, *Tectonophysics*, 524–525, 76–86, doi:10.1016/j.tecto.2011.12.019.
- Shin, T.-C., K.-W. Kuo, P.-L. Lee, C.-H. Tsai, and J.-S. Jiang (2011), Continuous CWB GPS array in Taiwan and applications to monitoring seismic activity, *Terr. Atmos. Oceanic Sci.*, 22(5), 521, doi:10.3319/TAO.2011.05.18.01(T).
- Simons, W. J. F., et al. (2007), A decade of GPS in Southeast Asia: Resolving Sundaland motion and boundaries, *J. Geophys. Res.*, 112, B06420, doi:10.1029/2005JB003868.
- Smalley, R., E. Kendrick, M. G. Bevis, I. W. D. Dalziel, F. Taylor, E. Lauria, R. Barriga, G. Casassa, E. Olivero, and E. Piana (2003), Geodetic determination of relative plate motion and crustal deformation across the Scotia-South America plate boundary in eastern Tierra del Fuego, *Geochem. Geophys. Geosyst.*, 4(9), 1070, doi:10.1029/2002GC000446.
- Smalley, R., I. W. D. Dalziel, M. G. Bevis, E. Kendrick, D. S. Stamps, E. C. King, F. W. Taylor, E. Lauria, A. Zakrajsek, and H. Parra (2007), Scotia arc kinematics from GPS geodesy, *Geophys. Res. Lett.*, 34, L21308, doi:10.1029/2007GL031699.
- Socquet, A., W. Simons, C. Vigny, R. McCaffrey, C. Subarya, D. Sarsito, B. Ambrosius, and W. Spakman (2006), Microblock rotations and fault coupling in SE Asia triple junction (Sulawesi, Indonesia) from GPS and earthquake slip vector data, *J. Geophys. Res.*, 111, B08409, doi: 10.1029/2005JB003963.
- Sol, S., et al. (2007), Geodynamics of the southeastern Tibetan Plateau from seismic anisotropy and geodesy, *Geology*, 35(6), 563–566, doi: 10.1130/G23408A.1.
- Spakman, W., and M. C. J. Nyst (2002), Inversion of relative motion data for estimates of the velocity gradient field and fault slip, *Earth Planet. Sci. Lett.*, 203(1), 577–591, doi:10.1016/S0012-821X(02)00844-0.
- Spinler, J. C., R. A. Bennett, M. L. Anderson, S. F. McGill, S. Hreinsdóttir, and A. McCallister (2010), Present-day strain accumulation and slip rates associated with southern San Andreas and eastern California shear zone faults, *J. Geophys. Res.*, 115, B11407, doi:10.1029/2010JB007424.
- Stamps, D. S., E. Calais, E. Sarie, C. Hartnady, J.-M. Nocquet, C. J. Ebinger, and R. M. Fernandes (2008), A kinematic model for the East African Rift, *Geophys. Res. Lett.*, 35, L05304, doi:10.1029/2007GL032781.
- Stevens, C. W., R. McCaffrey, Y. Bock, J. F. Genrich, M. Pubellier, and C. Subarya (2002), Evidence for block rotations and basal shear in the world's fastest slipping continental shear zone in NW New Guinea, *Geodyn. Ser.*, 30, 87–99, doi:10.1029/GD030p0087.
- Stirling, M., T. Goded, K. Berryman, and N. Litchfield (2013), Selection of earthquake scaling relationships for seismic-hazard analysis, *Bull. Seismol. Soc. Am.*, 103(6), 2993–3011, doi:10.1785/0120130052.
- Suito, H., and J. T. Freymueller (2009), A viscoelastic and afterslip postseismic deformation model for the 1964 Alaska earthquake, *J. Geophys. Res.*, 114, B11404, doi:10.1029/2008JB005954.
- Svarc, J. L., J. C. Savage, W. H. Prescott, and A. R. Ramelli (2002), Strain accumulation and rotation in western Nevada, 1993–2000, *J. Geophys. Res.*, 107(B5), 2090, doi:10.1029/2001JB000579.
- Szeliga, W., R. Bilham, D. M. Kakar, and S. H. Lodi (2012), Interseismic strain accumulation along the western boundary of the Indian subcontinent, *J. Geophys. Res.*, 117, B08404, doi:10.1029/2011JB008822.
- Tadokoro, K., R. Ikuta, T. Watanabe, M. Ando, T. Okuda, S. Nagai, K. Yasuda, and T. Sakata (2012), Interseismic seafloor crustal deformation immediately above the source region of anticipated megathrust earthquake along the Nankai Trough, Japan, *Geophys. Res. Lett.*, 39, L10306, doi:10.1029/2012GL051696.
- Tape, C., P. Musé, M. Simons, D. Dong, and F. Webb (2009), Multiscale estimation of GPS velocity fields, *Geophys. J. Int.*, 179(2), 945–971, doi:10.1111/j.1365-246X.2009.04337.x.
- Tatar, M., D. Hatzfeld, J. Martinod, A. Walpersdorf, M. Ghafori-Ashtiani, and J. Chéry (2002), The present-day deformation of the central Zagros from GPS measurements, *Geophys. Res. Lett.*, 29(19), 1927, doi:10.1029/2002GL015427.
- Tatar, O., et al. (2012), Crustal deformation and kinematics of the Eastern Part of the North Anatolian Fault Zone (Turkey) from GPS measurements, *Tectonophysics*, 518–521, 55–62, doi:10.1016/j.tecto.2011.11.010.
- Tavakoli, F., A. Walpersdorf, C. Authemayou, H. R. Nankali, D. Hatzfeld, M. Tatar, Y. Djamour, F. Nilforoushan, and N. Cotte (2008), Distribution of the right-lateral strike-slip motion from the Main Recent Fault to the Kazerun Fault System (Zagros, Iran): Evidence from present-day GPS velocities, *Earth Planet. Sci. Lett.*, 275(3–4), 342–347, doi:10.1016/j.epsl.2008.08.030.
- Taylor, F. W., M. G. Bevis, I. W. D. Dalziel, R. Smalley Jr., C. Frohlich, E. Kendrick, J. Foster, D. Phillips, and K. Gudipati (2008), Kinematics and segmentation of the South Shetland Islands-Bransfield basin system, northern Antarctic Peninsula, *Geochem. Geophys. Geosyst.*, 9, Q04035, doi:10.1029/2007GC001873.
- Teferle, F. N., et al. (2009), Crustal motions in Great Britain: Evidence from continuous GPS, absolute gravity and Holocene sea level data, *Geophys. J. Int.*, 178(1), 23–46, doi:10.1111/j.1365-246X.2009.04185.x.
- ten Brink, U. S., and A. M. López-Venegas (2012), Plate interaction in the NE Caribbean subduction zone from continuous GPS observations, *Geophys. Res. Lett.*, 39, L10304, doi:10.1029/2012GL051485.
- Tesauro, M., C. Hollenstein, R. Egli, A. Geiger, and H.-G. Kahle (2006), Analysis of central western Europe deformation using GPS and seismic data, *J. Geodyn.*, 42(4–5), 194–209, doi:10.1016/j.jog.2006.08.001.
- Tiryakioğlu, İ., M. Floyd, S. Erdoğan, E. Güläl, S. Ergintav, S. McClusky, and R. Reilinger (2013), GPS constraints on active deformation in the Isparta Angle region of SW Turkey, *Geophys. J. Int.*, 195(3), 1455–1463, doi:10.1093/gji/ggt323.
- Titus, S. J., M. Dyson, C. DeMets, B. Tikoff, F. Rolandone, and R. Bürgmann (2011), Geologic versus geodetic deformation adjacent to the San Andreas fault, central California, *Geol. Soc. Am. Bull.*, 123, 794–820, doi:10.1130/B30150.1.
- Tran, D. T., T. Y. Nguyen, C. C. Duong, Q. H. Vy, W. Zuchiewicz, N. Q. Cuong, and N. V. Nghia (2013), Recent crustal movements of northern Vietnam from GPS data, *J. Geodyn.*, 69, 5–10, doi:10.1016/j.jog.2012.02.009.

- Tregoning, P. (2002), Plate kinematics in the western Pacific derived from geodetic observations, *J. Geophys. Res.*, 107(B1), 2020, doi: 10.1029/2001JB000406.
- Tregoning, P., et al. (1998a), Estimation of current plate motions in Papua New Guinea from Global Positioning System observations, *J. Geophys. Res.*, 103(B6), 12,181–12,203, doi:10.1029/97JB03676.
- Tregoning, P., F. Tan, J. Gilliland, H. McQueen, and K. Lambeck (1998b), Present-day crustal motion in the Solomon Islands from GPS observations, *Geophys. Res. Lett.*, 25(19), 3627–3630, doi:10.1029/98GL52761.
- Tregoning, P., R. Burgette, S. C. McClusky, S. Lejeune, C. S. Watson, and H. McQueen (2013), A decade of horizontal deformation from great earthquakes, *J. Geophys. Res. Solid Earth*, 118, 2371–2381, doi:10.1002/jgrb.50154.
- Trenkamp, R., J. N. Kellogg, J. T. Freymueller, and H. P. Mora (2002), Wide plate margin deformation, southern Central America and northwestern South America, CASA GPS observations, *J. South Am. Earth Sci.*, 15(2), 157–171, doi:10.1016/S0895-9811(02)00018-4.
- Trenkamp, R., H. Mora, E. Salcedo, and J. N. Kellogg (2004), Possible rapid strain accumulation rates near Cali, Colombia, determined from GPS measurements (1996–2003), *Earth Sci. Res. J.*, 8(1), 25–33.
- Tsai, M.-C., S.-B. Yu, Y.-J. Hsu, H.-Y. Chen, and H.-W. Chen (2012), Interseismic crustal deformation of frontal thrust fault system in the Chiayi-Tainan area, Taiwan, *Tectonophysics*, 554–557, 169–184, doi:10.1016/j.tecto.2012.05.014.
- Tserolas, V., S. P. Mertikas, and X. Frantzis (2013), The Western Crete geodetic infrastructure: Long-range power-law correlations in GPS time series using Detrended Fluctuation Analysis, *Adv. Space Res.*, 57(8), 1448–1467, doi:10.1016/j.asr.2012.08.002.
- Umhoefer, P. J., and R. J. Dorsey (1997), Translation of terranes: Lessons from central Baja California, Mexico, *Geology*, 25(11), 1007–1010, doi:10.1130/0091-7613(1997)025<1007:TOTLCF>2.3.CO;2.
- van der Hoeven, A. G. A., V. Mocanu, W. Spakman, M. Nutto, A. Nuckelt, L. Matenco, L. Munteanu, C. Marcu, and B. A. C. Ambrosius (2005), Observation of present-day tectonic motions in the Southeastern Carpathians: Results of the ISES/CRC-461 GPS measurements, *Earth Planet. Sci. Lett.*, 239(3–4), 177–184, doi:10.1016/j.epsl.2005.09.018.
- Vernant, P., et al. (2004a), Present-day crustal deformation and plate kinematics in the Middle East constrained by GPS measurements in Iran and northern Oman, *Geophys. J. Int.*, 157(1), 381–398, doi:10.1111/j.1365-246X.2004.02222.x.
- Vernant, P., F. Nilforoushan, J. Chéry, R. Bayer, Y. Djamour, F. Masson, H. Nankali, J.-F. Ritz, M. Sedighi, and F. Tavakoli (2004b), Deciphering oblique shortening of central Alborz in Iran using geodetic data, *Earth Planet. Sci. Lett.*, 223(1–2), 177–185, doi:10.1016/j.epsl.2004.04.017.
- Vernant, P., A. Fadil, T. Mourabit, D. Ouazar, A. Koulali, J. M. Davila, J. Garate, S. McClusky, and R. Reilinger (2010), Geodetic constraints on active tectonics of the Western Mediterranean: Implications for the kinematics and dynamics of the Nubia-Eurasia plate boundary zone, *J. Geodyn.*, 49(3–4), 123–129, doi:10.1016/j.jog.2009.10.007.
- Vigny, C., J.-B. de Chabalier, J.-C. Ruegg, P. Huchon, K. L. Feigl, R. Cattin, L. Asfaw, and K. Kanbari (2007), Twenty-five years of geodetic measurements along the Tadjoura-Asal rift system, Djibouti, East Africa, *J. Geophys. Res.*, 112, B06410, doi:10.1029/2004JB003230.
- Wallace, L. M., C. Stevens, E. Silver, R. McCaffrey, W. Loratung, S. Hasiata, R. Stanaway, R. Curley, R. Rosa, and J. Taugaloidi (2004a), GPS and seismological constraints on active tectonics and arc-continent collision in Papua New Guinea: Implications for mechanics of microplate rotations in a plate boundary zone, *J. Geophys. Res.*, 109, B05404, doi:10.1029/2003JB002481.
- Wallace, L. M., J. Beavan, R. McCaffrey, and D. Darby (2004b), Subduction zone coupling and tectonic block rotations in the North Island, New Zealand, *J. Geophys. Res.*, 109, B12406, doi:10.1029/2004JB003241.
- Walpersdorf, A., S. Baize, E. Calais, P. Tregoning, and J.-M. Nocquet (2006a), Deformation in the Jura Mountains (France): First results from semi-permanent GPS measurements, *Earth Planet. Sci. Lett.*, 245(1–2), 365–372, doi:10.1016/j.epsl.2006.02.037.
- Walpersdorf, A., D. Hatzfeld, H. Nankali, F. Tavakoli, F. Nilforoushan, M. Tatar, P. Vernant, J. Chéry, and F. Masson (2006b), Difference in the GPS deformation pattern of North and Central Zagros (Iran), *Geophys. J. Int.*, 167(3), 1077–1088, doi:10.1111/j.1365-246X.2006.03147.x.
- Walpersdorf, A., et al. (2014), Present-day kinematics and fault slip rates in Eastern Iran, derived from 11 years of GPS data, *J. Geophys. Res. Solid Earth*, 119, 1359–1383, doi:10.1002/2013JB010620.
- Wang, C.-Y., L. M. Flesch, L. Chang, and T. Zheng (2013), Evidence of active mantle flow beneath South China, *Geophys. Res. Lett.*, 40, 5137–5141, doi:10.1002/grl.50987.
- Wang, K., Y. Hu, M. Bevis, E. Kendrick, R. Smalley, R. B. Vargas, and E. Lauría (2007), Crustal motion in the zone of the 1960 Chile earthquake: Detangling earthquake-cycle deformation and forearc-sliver translation, *Geochim. Geophys. Geosyst.*, 8, Q10010, doi:10.1029/2007GC001721.
- Ward, S. N. (1994), Constraints on the seismotectonics of the central Mediterranean from Very Long Baseline Interferometry, *Geophys. J. Int.*, 117(2), 441–452, doi:10.1111/j.1365-246X.1994.tb03943.x.
- Wdowinski, S., Y. Bock, G. Baer, L. Prawirodirdjo, N. Bechor, S. Naaman, R. Knafo, Y. Forrai, and Y. Melzer (2004), GPS measurements of current crustal movements along the Dead Sea Fault, *J. Geophys. Res.*, 109, B05403, doi:10.1029/2003JB002640.
- Weber, J., M. Vrabec, P. Pavlovič-Prešeren, T. Dixon, Y. Jiang, and B. Stopar (2010), GPS-derived motion of the Adriatic microplate from Istria Peninsula and Po Plain sites, and geodynamic implications, *Tectonophysics*, 483(3–4), 214–222, doi:10.1016/j.tecto.2009.09.001.
- Weber, J. C., T. H. Dixon, C. DeMets, W. B. Ambeh, P. Jansma, G. Mattioli, J. Saleh, G. Sella, R. Bilham, and O. Pérez (2001), GPS estimate of relative motion between the Caribbean and South American plates, and geologic implications for Trinidad and Venezuela, *Geology*, 29(1), 75–78, doi:10.1130/0091-7613(2001)029<0075:GEORMB>2.0.CO;2.
- Weber, J. C., J. Saleh, S. Balkaransingh, T. Dixon, W. Ambeh, T. Leong, A. Rodriguez, and K. Miller (2011), Triangulation-to-GPS and GPS-to-GPS geodesy in Trinidad, West Indies: Neotectonics, seismic risk, and geologic implications, *Mar. Pet. Geol.*, 28(1), 200–211.
- Williams, S. D. P. (2008), CATS: GPS coordinate time series analysis software, *GPS Solutions*, 12(2), 147–153, doi:10.1007/s10291-007-0086-4.
- Williams, S. D. P., Y. Bock, P. Fang, P. Jamason, R. M. Nikolaidis, L. Prawirodirdjo, M. Miller, and D. J. Johnson (2004), Error analysis of continuous GPS position time series, *J. Geophys. Res.*, 109, B03412, doi:10.1029/2003JB002741.
- Williams, T. B., H. M. Kelsey, and J. T. Freymueller (2006), GPS-derived strain in northwestern California: Termination of the San Andreas fault system and convergence of the Sierra Nevada–Great Valley block contribute to southern Cascadia forearc contraction, *Tectonophysics*, 413(3–4), 171–184, doi:10.1016/j.tecto.2005.10.047.
- Wu, Y., Z. Jiang, G. Yang, W. Wei, and X. Liu (2011), Comparison of GPS strain rate computing methods and their reliability, *Geophys. J. Int.*, 185(2), 703–717, doi:10.1111/j.1365-246X.2011.04976.x.
- Yang, S., J. Li, and Q. Wang (2008), The deformation pattern and fault rate in the Tianshan Mountains inferred from GPS observations, *Sci. China Ser. D Earth Sci.*, 51(8), 1064–1080, doi:10.1007/s11430-008-0090-8.
- Yavaşoğlu, H., E. Tari, O. Tüysüz, Z. Çakır, and S. Ergintav (2011), Determining and modeling tectonic movements along the central part of the North Anatolian Fault (Turkey) using geodetic measurements, *J. Geodyn.*, 51(5), 339–343, doi:10.1016/j.jog.2010.07.003.

- Yoshida, M. (2010), Preliminary three-dimensional model of mantle convection with deformable, mobile continental lithosphere, *Earth Planet. Sci. Lett.*, 295(1–2), 205–218, doi:10.1016/j.epsl.2010.04.001.
- Yoshioka, S., and Y. Matsuoka (2013), Interplate coupling along the Nankai Trough, southwest Japan, inferred from inversion analyses of GPS data: Effects of subducting plate geometry and spacing of hypothetical ocean-bottom GPS stations, *Tectonophysics*, 600, 165–174, doi:10.1016/j.tecto.2013.01.023.
- Yoshioka, S., T. Mikumo, V. Kostoglodov, K. M. Larson, A. R. Lowry, and S. K. Singh (2004), Interplate coupling and a recent aseismic slow slip event in the Guerrero seismic gap of the Mexican subduction zone, as deduced from GPS data inversion using a Bayesian information criterion, *Phys. Earth Planet. Int.*, 146(3–4), 513–530, doi:10.1016/j.pepi.2004.05.006.
- Yu, S.-B., and L.-C. Kuo (2001), Present-day crustal motion along the Longitudinal Valley Fault, eastern Taiwan, *Tectonophysics*, 333(1–2), 199–217, doi:10.1016/S0040-1951(00)00275-4.
- Yu, S.-B., Y.-J. Hsu, T. Bacolcol, C.-C. Yang, Y.-C. Tsai, and R. Solidum (2013), Present-day crustal deformation along the Philippine Fault in Luzon, Philippines, *J. Asian Earth Sci.*, 65, 64–74, doi:10.1016/j.jseas.2010.12.007.
- Zhang, J., Y. Bock, H. Johnson, P. Fang, S. Williams, J. Genrich, S. Wdowinski, and J. Behr (1997), Southern California permanent GPS geodetic array: Error analysis of daily position estimates and site velocities, *J. Geophys. Res.*, 102(B8), 18,035–18,055, doi:10.1029/97JB01380.
- Zhang, P.-Z., and W. Gan (2008), Combined model of rigid-block motion with continuous deformation: Patterns of present-day deformation in continental China, in *Investigations into the Tectonics of the Tibetan Plateau*, *Geol. Soc. of Am. Spec. Pap.* 444, edited by B. C. Burchfiel and E. Wang, pp. 59–71, Geological Society of America, Boulder, Colo.
- Zhu, H., and J. Tromp (2013), Mapping Tectonic Deformation in the Crust and Upper Mantle Beneath Europe and the North Atlantic Ocean, *Science*, 341(6148), 871–875, doi:10.1126/science.1241335.
- Zhu, S., and Y. Shi (2011), Estimation of GPS strain rate and its error analysis in the Chinese continent, *J. Asian Earth Sci.*, 40(1), 351–362, doi:10.1016/j.jseas.2010.06.007.
- Zhu, S., Y. Cai, and Y. Shi (2006), The contemporary tectonic strain rate field of continental China predicted from GPS measurements and its geodynamic implications, *Pure Appl. Geophys.*, 163(8), 1477–1493, doi:10.1007/s00024-006-0087-1.
- Zubovich, A. V., et al. (2010), GPS velocity field for the Tien Shan and surrounding regions, *Tectonics*, 29, TC6014, doi:10.1029/2010TC002772.
- Zumberge, J. F., M. B. Heflin, D. C. Jefferson, M. M. Watkins, and F. H. Webb (1997), Precise point positioning for the efficient and robust analysis of GPS data from large networks, *J. Geophys. Res.*, 102(B3), 5005–5017, doi:10.1029/96JB03860.
- Zweck, C., J. T. Freymueller, and S. C. Cohen (2002), The 1964 great Alaska earthquake: Present day and cumulative postseismic deformation in the western Kenai Peninsula, *Phys. Earth Planet. Inter.*, 132(1–3), 5–20, doi:10.1016/S0031-9201(02)00041-9.